

**Geochronology and multi-isotope geochemistry
of three Quaternary volcanoes:
Nisyros-Yali (Greece), Monte Vico and Monte Vulture (Italy)**

Inauguraldissertation
der Philosophisch-naturwissenschaftlichen Fakultät
der Universität Bern

vorgelegt von
Annett Büttner
aus Deutschland

Leiter der Arbeit:
Prof. Dr. Igor M. Villa
Institut für Geologie, Gruppe Isotopengeologie, Universität Bern

**Geochronology and multi-isotope geochemistry
of three Quaternary volcanoes:
Nisyros-Yali (Greece), Monte Vico and Monte Vulture (Italy)**

Inauguraldissertation
der Philosophisch-naturwissenschaftlichen Fakultät
der Universität Bern

vorgelegt von
Annett Büttner
aus Deutschland

Leiter der Arbeit:
Prof. Dr. Igor M. Villa
Institut für Geologie, Gruppe Isotopengeologie, Universität Bern

Von der Philosophisch-naturwissenschaftlichen Fakultät angenommen.

Bern, den 2. November 2004

Der Dekan

Prof. Dr. P. Messerli



«Πολυβώτης δὲ διὰ τῆς θαλάσσης διωχθεὶς ὑπὸ τοῦ Ποσειδῶνος ἤκεν εἰς Κῶ· Ποσειδῶν δὲ τῆς νήσου μέρος ἀπορρήξας ἐπέρριπεν αὐτῶ, τὸ λεγόμενον Νίσυρον.»*

*"Poseidon, god of the sea, proved his loyalty to Zeus, master of gods and men, by fighting the Titans. Polybotes, one of the Titans, was haunted over land and sea until he reached the island Kos. Poseidon pulled out a piece of the island with his trident and buried Polybotes underneath.
A new island was born; Nisyros."*

* Apollodorus, Bib. Vol. 1, Ed. Tolidis

Acknowledgments

I particularly want to thank you, Igor, for offering me the opportunity to think and work with you and for opening my eyes for critical scrutinising pretended facts. I really enjoyed these years!

Thank you very much, Jan for many fruitful discussions and critical comments, which were always helpful and improved my work. I am grateful to Johannes C. Hunziker for initiating the work on Nisyros and for guiding through the field. Thanks to Thomas for many scientific and non-scientific discussions.

Gerhard Brey from the University of Frankfurt, Germany, is grateful acknowledged, who honoured the position as Koreferent.

Yann Lahaye, University of Frankfurt, is thanked for the analyses of trace element data. Edwin Gnos, Marco Herwegh and Karl Ramseyer supported the petrological part of this work. I am grateful to Borgi, the good fairy of the laboratory. Jürg Megert, Vreni Jakob, thank you for prompt manufacturing of loads of thin sections. Claude Lavanchy and H.R. Pfeifer from the CAM, Université de Lausanne, Switzerland, is thanked for XRF-analyses.

A special thank belongs to Doro. I enjoyed being your "officemate" and the many times you let me participate to your joyful character. Your warmth and openness encouraged me very often. Good luck to you!

Ilka, thanks for the countless interesting discussions about science, life..., which contributed to the success of the following pages. Thank you for your friendship!

A special thanks goes also to Bärbel. You always had a shoulder for me!

My dear colleges from inside and outside the Institute. I thank you for the good time here in Switzerland, for the numerous intermezzi and evenings. Danke, merci, grazie, sbosibo to Dänu, Reto, Jüre, Ronny, Nicola, Martin, Katja, Franzi, Schorsch and Marek.

Thank you, Elena, for taking care of me beyond science.

My beloved flatmate Xe is grateful thanked here for many things. It was a pleasure to gossip and philosophise with you at the "Chuchitisch" and it was balm for my stressed soul to listen to your acoustic highlights.

Liebe Mama, danke für Deine Geduld, Dein Interesse und die Unterstützung bei allem, was ich tue.

Jens, I thank you very much for being always on my side!

This thesis was supported by the Swiss National Science Foundation (SNSF–grant-numbers 21-63866.00 and 200020-100230) at the Institute of Geological Sciences – Isotope Geology Group – of the University of Bern, Switzerland under supervision of Prof. Dr. Igor M. Villa and Prof. Dr. Jan D. Kramers. The work included several field excursions to the study areas, namely Nisyros island (Greece), Monte Vico and Monte Vulture (Italy) in collaboration with Dr. Claudia Principe from the Istituto di Geoscienze e Georisorse, CNR, via G. Moruzzi 1, 56124 Pisa, Italy.

The thesis is separated into four chapters. Chapter one and two contain geochemical and geochronological investigations of the Nisyros-Yali volcanic system. In the 3rd chapter geochronological and petrological investigations of Monte Vulture are presented. The 4th chapter deals with U-Th systematics of paleosols of all investigated volcanoes (Monte Vico, Monte Vulture and Nisyros-Yali). All tables of samples and analytical results are summarised in the Appendix A.

Chapter one presents a petrological and geochemical study of Nisyros-Yali volcanic units. Petrological investigations were combined with major and trace element data and Lu-Hf, Sm-Nd Sr-, Pb-isotope systematics. This comprehensive data-set allows a detailed reconstruction of the magma genesis of the volcanic system. The volcanic history, subdivided into a pre- and a post-caldera cycle, is mirrored by a change in petrological style. Geochemical data exhibit a compositional gap (lacking intermediate major element concentrations) between these two cycles resulting in distinct petrological and geochemical characteristics.

Chapter two is a continuation of the first chapter and includes ^{39}Ar - ^{40}Ar and U-Th investigations of the Nisyros-Yali volcanic system. All volcanic products are characterised by the absence of K-bearing mineral-phases. Potassium is hosted in the volcanic glasses that contain mantle-gas inclusions with excess Ar. U-Th disequilibrium analyses show that most rocks and minerals plot in a "forbidden zone" due to a two-stage evolution.

Chapter three presents a refined geochronological database of Monte Vulture ejecta. New selected mineral phases and samples from previous works were analysed with ^{39}Ar - ^{40}Ar step heating. The combination of petrological observations and ^{39}Ar - ^{40}Ar systematics reveal mineralogical complications, which were unravelled. The resulting interpretation is based on isochemical steps and refines the volcanostratigraphy. Furthermore, "allochthonous" tephra deposits can now be ascribed to certain eruptions of the Vesuvius area.

Chapter four includes U-Th systematics of paleosols sandwiched by unpedogenised volcanics of all three investigated volcanic systems (Monte Vico, Monte Vulture and Nisyros-Yali). Bulk and sequential extraction procedures were applied to leach distinct soil components (adsorbed cations, authigenic carbonates, metal oxides and hydroxides from the silicate residue). U-Th data of each leach step exhibit laboratory fractionation of U from Th, which is excluded when calculated bulk ratios (summarising steps). Hence, it is evidenced that even supposedly arrested paleosols are open systems.

Chapter 1**1. Magma generation at the easternmost section of the Hellenic Arc: Hf, Nd, Pb and Sr isotope geochemistry of Nisyros and Yali volcanoes (Greece)**

1.1 Introduction.....	2
1.2 Geological setting	2
1.3 Previous studies	3
1.4 Analytical techniques.....	4
1.5 Petrography	5
1.6 Geochemistry	6
1.6.1 Geochemical signatures of fluid addition and fractional crystallisation	7
1.6.1.1 Role of Th and U	10
1.6.2 Geochemical signatures of crustal assimilation.....	11
1.7 The compositional gap.....	15
1.8 Summary and conclusions	17

Chapter 2**2. Geochronology of Nisyros**

2.1 Introduction.....	23
2.2 Analytical techniques.....	24
2.3 Results and discussion	25
2.3.1 ³⁹ Ar- ⁴⁰ Ar.....	25
2.3.2 U-Th data	27
2.4 Conclusion	28

Chapter 3**3. Chronostratigraphy of Monte Vulture Volcano (southern Italy):****³⁹Ar-⁴⁰Ar systematics and the role of secondary processes**

3.1 Introduction.....	32
3.2 Analytical techniques.....	34
3.3 Mineralogy.....	34
3.3.1 Leucite	36
3.3.2 Sanidine	36

3.3.3 Biotite	36
3.3.4 Phlogopite	36
3.3.5 Mineralogy from Ar isotope systematics.....	36
3.4 ³⁹ Ar- ⁴⁰ Ar results	37
3.4.1 Spinoritola subsynthem	37
3.4.2 Fara d'Olivo subsynthem	38
3.4.3 Rionero subsynthem	39
3.4.4 Vulture San Michele subsynthem.....	40
3.4.5 Castello di Melfi subsynthem	42
3.4.6 Case Lopes subsynthem.....	42
3.4.7 Lago Piccolo and Lago Grande subsynthem	43
3.4.8 Serra di Braida subsynthem	44
3.4.9 Allochthonous deposits.....	45
3.5 Conclusions.....	45

Chapter 4

Differential mobility of actinides in soils: U-Th dating of paleosols of known age

4.1 Introduction.....	51
4.2 Geological setting and sample description	52
4.3 Analytical techniques.....	54
4.3.1 ³⁹ Ar- ⁴⁰ Ar analyses	54
4.3.2 Sequential extraction technique	55
4.3.3 SEM analyses.....	56
4.3.4 U and Th separation.....	57
4.3.5 Multi-collector ICP mass spectrometry	57
4.4 Results and discussion	57
4.4.1 ³⁹ Ar- ⁴⁰ Ar ages.....	57
4.4.2 Selectivity of the sequential extraction technique	58
4.4.3 U-Th results	59
4.5 Conclusions.....	64

Appendices

A Data-tables

A-chapter 1	I
A-chapter 2	V
A-chapter 3	IX
A-chapter 4	XIX

B Curriculum Vitae	XXV
---------------------------------	------------

1. Magma generation at the easternmost section of the Hellenic Arc: Hf, Nd, Pb and Sr isotope geochemistry of Nisyros and Yali volcanoes (Greece)

A. Buettner^{1*}, I. C. Kleinhanns¹, D. Rufer¹, J. C. Hunziker² and I. M. Villa¹

¹ *Institut für Geologie, Universität Bern, Erlachstrasse 9a, 3012 Bern, Switzerland*

² *Institute de Minéralogie et Géochemie, BFSH-2, Université Lausanne, Switzerland*

submitted to Lithos

Abstract

Geochemical and petrographical studies of volcanic products from the Quaternary Nisyros-Yali volcanic system in the easternmost part of the Hellenic arc (Greece) reveal insight into magma generating processes. A compositional gap between 61 and 68 wt % SiO₂ is recognized that coincides with the stratigraphic distinction between pre-caldera and post-caldera volcanic units. Trace elements systematics support the subdivision of Nisyros and Yali volcanic units into two distinct suites of rocks. The variation of Nd and Hf present day isotope data and the fact that they are distinct from the isotope compositions of MORB rule out an origin by pure differentiation and instead require assimilation of a crustal component. ²⁰⁶Pb/²⁰⁴Pb, ²⁰⁷Pb/²⁰⁴Pb and ²⁰⁸Pb/²⁰⁴Pb ratios of Nisyros and Yali volcanic rocks support mixing of mantle material with a lower crust equivalent. Abundant hydrous fluids are characterised by extremely mantle-like Sr isotope ratios between 0.703648 – 0.704847 and probably by CO₂-enrichment responsible for transporting Th. The occurrence of hydrated minerals (e.g., amphibole) in the first post-caldera unit with the lowermost ⁸⁷Sr/⁸⁶Sr ratio of 0.703648 can be interpreted as the result of the increased water activity in the source. The presence of two different plagioclase phenocryst generations in the first lava subsequent to the caldera-causing event is indicative for a longer storage time of this magma at a shallower level. A model capable of explaining these observations involves three evolutionary stages. First stage, assimilation of lower crustal material by a primitive magma of mantle origin (as modelled by Nd-Hf isotope systematics). This stage ended by an interruption in replenishment that led to an increase of crystallisation and, hence, an increase in viscosity, suppressing eruption. During this time gap, differentiation by fractional crystallisation led to enrichment of incompatible species, especially aqueous fluids, to silica depolymerisation and to a decrease in viscosity, finally enabling eruption again in the third stage.

1.1 Introduction

The Hellenic volcanic arc originates from the subduction of the African beneath the Aegean micro plate resulting in the formation of numerous Late Quaternary volcanoes, namely Methana, Aegina, Milos, Santorini and the system of Nisyros-Yali (Le Pichon and Angelier 1979). The arc geometry is variable with a mean depth of the Benioff zone of around 100 km being shallower in the western part and deeper in the eastern part of the arc (Keller 1982; Papazachos and Panagiotopoulos 1993). In this study we focus on the volcanic islands Nisyros and Yali, located in the easternmost part of the Hellenic volcanic arc (Fig. 1). These islands were formed during the last 160.000 years (Smith et al. 1996).

Several authors already recognized a gap in SiO_2 content and ascribe this to a polybaric evolution (Wyers and Barton 1989), mixing processes (Seymour and Vlasopoulos 1992) or convection-retention, crystal-liquid segregation processes in the magma source (Francalanci et al. 1995). We present an extensive geochemical dataset in order to refine existing magma-genetic models of the contrasted bimodal suite of volcanic rocks from Nisyros and Yali. Due to the lack of basement rocks exposure on Nisyros-Yali geochemical data of gneisses from the island of Ios are presented as a possible basement proxy as no basement. We further present the first isotope dataset for the Nisyros-Yali system. Firstly, Hf, Nd and Pb isotope signatures allow a quantitative estimation of assimilation processes. Secondly, the different behaviour of Sr isotope ratios stresses the role of fluids for magma genesis and evolution. The combination of major and trace element data, isotope data and petrographic observations enable us to resolve the controversy on the magmatogenesis of the Nisyros-Yali system.

1.2 Geological setting

The volcanism along the Hellenic arc started in the Pliocene reaching its maximum in Quaternary times (e.g., Keller 1982). Calc-alkaline volcanic products relating to the present Hellenic arc are of Pleistocene age (Keller 1969). In the western part of Kos the collapse of a submarine caldera – leading to the formation of a large ignimbrite (the Kos Plateau Tuff or KPT) dated at 161 ± 1 ka (Smith et al. 1996) – introduced the volcanic activity of the easternmost section of the Hellenic arc.

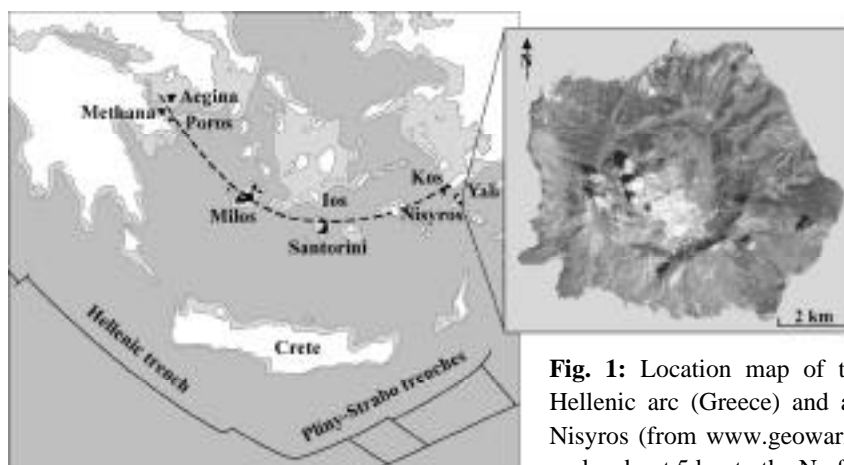


Fig. 1: Location map of the volcanic islands along the Hellenic arc (Greece) and an IKONOS satellite image of Nisyros (from www.geowarn.org). The islet of Yali is off-scale, about 5 km to the N of Nisyros.

The symmetrical stratovolcano of Nisyros has an average diameter of 8 km (based on sealevel niveau) with a caldera (4 km in diameter) formed during the explosive eruption of a large pumice. Pre-volcanic basement is not exposed on Nisyros, although geothermal wells drilled in the Lakki plain inside the caldera (e.g. Marini et al. 1993) indicate a basement of Mesozoic limestones as shallowest part of the underlying crust. Well Nisyros 1 with a total depth of 1816 m crosses a 600 m thick tephra horizon that overlies carbonates and thermometamorphosed marbles of about 750 m thickness. At around 1700 m below sea level, diorites of unknown age were found. A detailed description of the volcanic history of Nisyros is given in Di Paola (1974), Rehren (1988), Limburg and Varekamp (1991), Papanikolaou et al. (1991) and Volentik et al. (2002, 2003). Accordingly, the volcanic activity on Nisyros can be roughly subdivided into the following main phases (Table A-1-1; Appendix A):

- Submarine volcanic activity, which produced mainly basaltic to andesitic hyaloclastic breccia and pillow lavas;
- Extrusion of several subaerial andesitic to dacitic lava flows interbedded with pyroclastics formed the stratovolcano;
- A plinian eruption of the Lower pumice led to the collapse of the present caldera. It was followed by a massive dacitic lava flow (Nikia lava) and the eruption of the Upper pumice.
- Intrusions of dacitic domes along a NE-SW striking axis (following the main fault systems observed for the entire island arc) filled up the main caldera depression.

An additional pumice layer that was deposited inside the caldera originated from the islet of Yali (5 km north of Nisyros). These rhyolitic pumices represent the youngest magmatic event of the Kos-Nisyros-Yali system. The age of Yali was indirectly estimated by Federman and Carey (1980), who proposed an age of ~ 30 ka on the basis of oxygen-isotope stratigraphy, and by Smith et al. (1996), who suggest ~ 35 ka on the basis of interpolation with other submarine layers. The formation of hydrothermal craters inside Nisyros caldera is ascribed to phreatic eruptions, the youngest of which occurred between 1871 and 1887 (Gorceix 1873). Present-day activity is documented by fumarolic degassing of mainly H₂S, CO₂, H₂O, H₂ and CH₄ from the inside of these craters. Intervals of seismic unrest with earthquakes of magnitudes around 5 occur occasionally. The last seismic crisis was recorded between 1996 and 1997 with the majority of epicentres located either in shallow depths down to 10 km or between 31 – 40 km (Papadopoulos et al. 1998).

1.3 Previous studies

A variety of petrogenetic models were proposed for the formation of Nisyros and Yali volcanic system (e.g. Wyers and Barton 1989, Seymour and Vlassopoulos 1992 and Francalanci et al. 1995). Based on petrographical and geochemical observations, Wyers and Barton (1989) divided Nisyros lavas into two series: (i) basaltic andesites and andesites and (ii) dacites. According to these authors, the lavas were produced by assimilation and fractional crystallisation (AFC), although assimilation played a minor role during the evolution of the magma. Wyers and Barton (1989) observed a compositional gap in major element systematics (especially SiO₂-content) between volcanic rocks of andesitic to dacitic composition from Nisyros and attributed this chemical discontinuity to a polybaric evolution. According to these authors, the first group of basaltic-andesites and andesites (SiO₂ ~ 60 wt %) evolved in a shallower magma chamber at depths between 12 and 14 km, whereas the second group of dacites and dacites with SiO₂ contents of more than 66 wt % were generated at depths of around 27 km.

Seymour and Vlasoupoulos (1992) proposed a petrogenetic model involving crustal assimilation and mixing of mafic and felsic magmas. Based on petrographic observations and trace element data, magma mixing becomes a strong argument during the formation of the entire suite of Nisyros magmas. Contrary to the work of Wyers and Barton (1989) these authors suggested a compositionally zoned magma chamber with an underlying, subcrustal mafic and an overlying rhyodacitic layer. Proposed end-member compositions for the suggested mixing were tholeiitic basalts and continental crust. The mixture of these layers resulted in the formation of dacitic magmas with a compositional gap between 60 and 66 wt % SiO₂.

Francalanci et al. (1995) ascribed petrographical and geochemical variations of Nisyros volcanics to convection retention-crystal-liquid-segregation processes. They predict several gaps in the process of magma evolution that are interpreted as the result of liquid segregation from a crystal-rich portion of the magma whenever the point of critical crystallisation was reached. As a consequence more evolved, less porphyric magma separated from the crystal-rich magma.

1.4 Analytical techniques

X-ray fluorescence analyses for major elements were performed at the University of Lausanne, Switzerland, and followed standard procedures. Trace element concentrations were determined at the University of Frankfurt, Germany, using a Thermo-Finnigan Element2 ICP-MS. Analytical details are given at www.rz.uni-frankfurt.de/lahaye. Qualitative and quantitative element distributions and mineral compositions were determined at the Institute of Geological Sciences, University of Bern, Switzerland, using cathodoluminescence (CL) images and electron microprobe (EMP) spot-analyses, respectively.

Sm-Nd and Lu-Hf isotopes were separated from single rock digests following the procedure of Kleinhanns et al. (2002). Due to the young ages (< 160 ka), low mother/daughter ratios of the isotope systems age corrections were not necessary and therefore not performed. The differences between present day ratio and the initial isotope ratio are < 0.2 ppm and therefore negligible. Strontium separation was performed by standard cation exchange chromatography. Sr measurements by multicollector inductively coupled plasma mass spectrometry (MC-ICP-MS) required additional purification step that was achieved by passing samples through Sr-Spec resin (Waight et al. 2002). Lead was separated using anion exchange chromatography in HNO₃-HBr media. Prior to rock digestion mixed ¹⁴⁹Sm-¹⁵⁰Nd, ¹⁷⁶Lu-¹⁸⁰Hf and ⁸⁷Rb-⁸⁴Sr tracers were added to each aliquot. Samples and tracers were homogenised and digested using HF-HNO₃ mixture for 12 hours at 110°C. All measurements were performed on the Nu-Instruments MC-ICP-MS at the University of Bern, Switzerland. During the measuring period 20 analyses of Hf in-house standard solution with a Hf isotopic composition corresponding to the JMC 475 Hf standard have been made and the results obtained were ¹⁷⁶Hf/¹⁷⁷Hf of 0.282143 ± 20, ¹⁷⁸Hf/¹⁷⁷Hf of 1.46727 ± 5 and ¹⁸⁰Hf/¹⁷⁷Hf of 1.8870 ± 5. Nd in-house results of 25 analyses are ¹⁴³Nd/¹⁴⁴Nd of 0.511051 ± 20, ¹⁴⁵Nd/¹⁴⁴Nd of 0.348408 ± 10 and ¹⁵⁰Nd/¹⁴⁴Nd of 0.23642 ± 6, which corresponds to a ¹⁴³Nd/¹⁴⁴Nd La Jolla value of 0.511851. Repeated measurements (n = 6) of reference material NBS SRM 987 Sr standard yielded ⁸⁷Sr/⁸⁶Sr = 0.71028±8. Pb analyte solutions were doped with standard-Tl of known isotope composition to correct for instrumental mass bias. Measurements of NBS SRM 981 Pb standard obtained during the course of this study yielded 16.940 ± 4, 15.495 ± 3 and 36.710 ± 8 for ²⁰⁶Pb/²⁰⁴Pb, ²⁰⁷Pb/²⁰⁴Pb, and ²⁰⁸Pb/²⁰⁴Pb, respectively. Blank levels corresponding for handling 100 mg WR were < 1 ng for Pb, Nd and Hf and thus negligible.

1.5 Petrography

Volcanic rocks of Nisyros and Yali consist of lavas as well as pyroclastics. Table A-1-1 presents the investigated samples in terms of the existing stratigraphical nomenclature given in DiPaola (1974), Vougioukalakis (1993) and Allen et al. (2000). We divided the eruptives of Nisyros and Yali – according to their stratigraphical position from the oldest to the youngest – into pre-caldera, caldera-causing, post-caldera and Yali units. They vary in texture throughout this suites between porphyric basaltic-andesites, andesites and dacites from microphenocryst-bearing to vitrophyric (Lower and Upper pumice of Nisyros) and aphyric (pumices of Yali). Strong porphyric texture is observed in the lavas whereas the contrary is true for the pumices, in accordance with the quantitative values between 55 % and 1% given by Francalanci et al. (1995). In the following the main phenocryst phases are presented according to their abundance.

Plagioclase phenocrysts are generally euhedral to subhedral. Almost all investigated Nisyros units contain plagioclase as a major phenocryst phase; the Nikia lava contains an additional generation (Fig. 2) of plagioclase that exhibits rounded crystals with resorption rims. CL images of phenocrysts from dacitic lavas display zones of different textural habits. EMP analyses of the dacitic, post-caldera Upper Pumice exhibit two different species of plagioclase: firstly, a zoned plagioclase with increasing An-contents and, secondly, a plagioclase showing reverse zoning with An-contents between 67 % and 72 % for An-rich zones. Wyers and Barton (1989) ascribed the presence of two different zoned plagioclase species to different p-T conditions during crystallisation. They explained reverse zoning of phenocrysts with near-adiabatic uprise and normal zoned crystals underwent in their opinion near-isobaric evolution with decreasing temperature.

The presence of an additional generation (marked as generation 2 in Fig. 2) with reaction rims in Nikia lava might be the result of a process that could have affected the parental magma. Near-adiabatic decompression and hence, a longer storage of the magma body at a shallower level could cause incomplete segregation of plagioclase in Nikia magma (Wyers and Barton 1989).

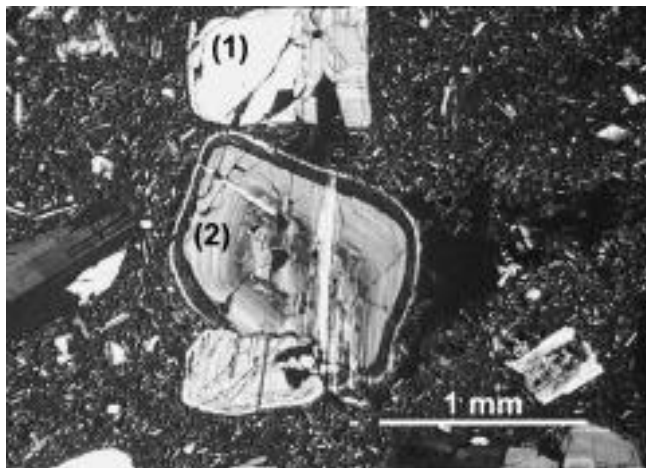


Fig. 2: Photomicrograph of Nikia lava showing two different plagioclase generations: a near euhedral generation (1) and a normal zoned generation with reaction rims (2).

Clinopyroxene is a minor phenocryst phase in the whole suite of Nisyros volcanic rocks. Crystals show euhedral shapes and reach sizes up to 1 mm in the post-caldera volcanic rocks. Cathodoluminescence images reveal apatite inclusions within the clinopyroxene crystal.

Amphibole phenocrysts are elongated and several mm long. They occur in the Nikia lava and in the pre-caldera units. Only in the former we observed variolitic amphibole cumulates of up to 1 m size. Minor abundances of amphibole phenocrysts (below 5 %) were reported by Volentik et al. (2002) in units of the pre-caldera cycle. Subeuhedral crystals exhibit pleochroism from light green to green and are often intergrown with plagioclase needles. Their chemistry varies: Wyers and Barton (1989) described amphiboles of the pre-caldera units as magnesio-hastingsites, whereas post-caldera amphibole phenocrysts were classified as tschermakitic hornblendes.

Orthopyroxene occur in minor abundance in the pre-caldera units. Apatite and zircon are accessory mineral phases in the pre-caldera lavas and are not present in the post-caldera units. *Olivine* is only abundant in pre-caldera basaltic-andesite as a minor phenocryst phase.

1.6 Geochemistry

Based on total alkali-silica contents (Fig. 3) all volcanic units of Nisyros and Yali plot in the subalkaline field. Major and trace element data of the investigated samples are given in Table A-1-2 (Appendix A). Volcanic units found on Nisyros and Yali range from basaltic-andesitic (pre-caldera units) up to dacitic (post-caldera volcanic products) and rhyolitic composition (Yali pumices). The volcanic units describe a calcalkaline differentiation trend in AFM space.

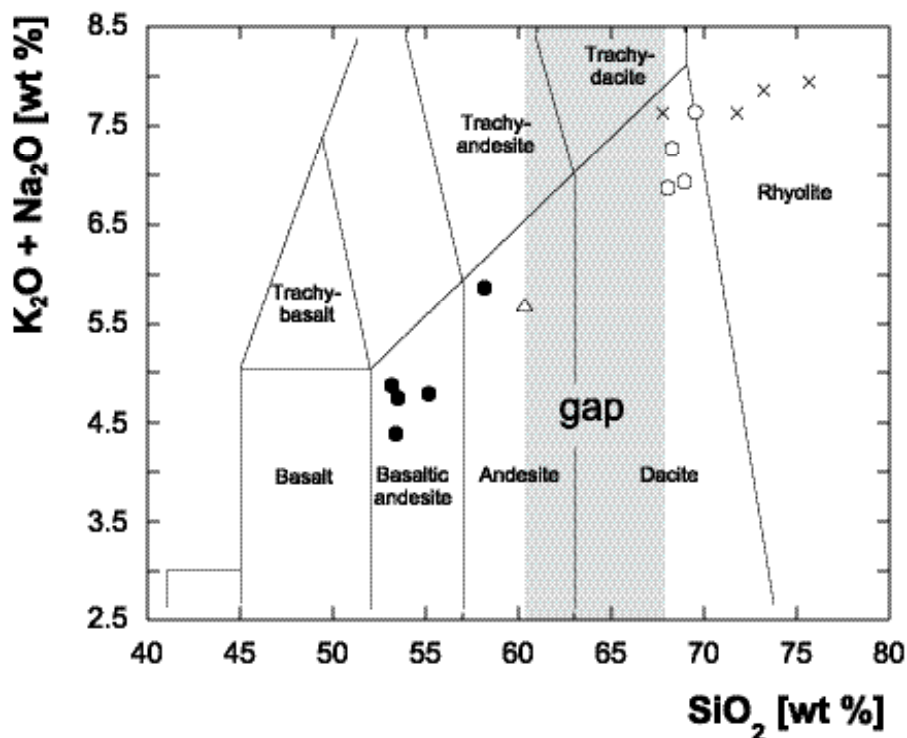


Fig. 3: Total-alkali-silica (TAS) discrimination diagram (Le Maitre 1989) of Nikia-Yali volcanic series. Grey shaded area marks the compositional gap between 61 and 68 wt % SiO_2 . This gap is accompanied by a steeper slope towards the more evolved units. Symbols: ● – mafic, pre-caldera units; ○ – post-caldera, felsic units; △ – gap framing, Lower Pumice; × – Yali units.

A striking feature of Nisyros-Yali volcanics is a compositional gap appearing between 61 – 68 wt % SiO_2 (Fig. 3) also observed by e.g. Wyers and Barton (1989), Seymour and Vlassoupoulos (1992) and DiPaola (1974), Vougioukalakis (1993) and Francalanci (1995), for a total of 225 analysed samples. The caldera-causing Lower Pumice yields around 61 wt % SiO_2 and represents the silica-poor limit of the gap. The silica-rich limit of the gap is represented by the Upper Pumice and Nikia lava with SiO_2 contents of 68 wt %. Al_2O_3 , CaO , FeO and MgO correlate negatively with SiO_2 , whereas Na_2O , K_2O reveal positive correlations (Table A-1-2). The K_2O -content never exceeds 3.1 wt % for volcanics on Nisyros and 4.5 wt % for Yali units. These values are somewhat lower than it is usual for island arc volcanics. P_2O_5 is low (between 0.02 and 0.25 wt %) and decreases towards more felsic magmas.

1.6.1 Geochemical signatures of fluid addition and fractional crystallisation

N-MORB normalised trace element patterns reveal steep negative slopes from incompatible towards more compatible elements for all Nisyros and Yali volcanics (Fig. 4). Enrichment peaks of fluid mobile elements like LILE, Pb and Li in combination with HFSE (e.g., Nb, Ta) depletion can be explained by addition of slab derived fluids into the overlying mantle wedge (e.g., Kamber et al. 2002). The observed high LILE/HFSE ratios are known to be a typical feature of subduction zone derived magmas (e.g., Gill 1981).

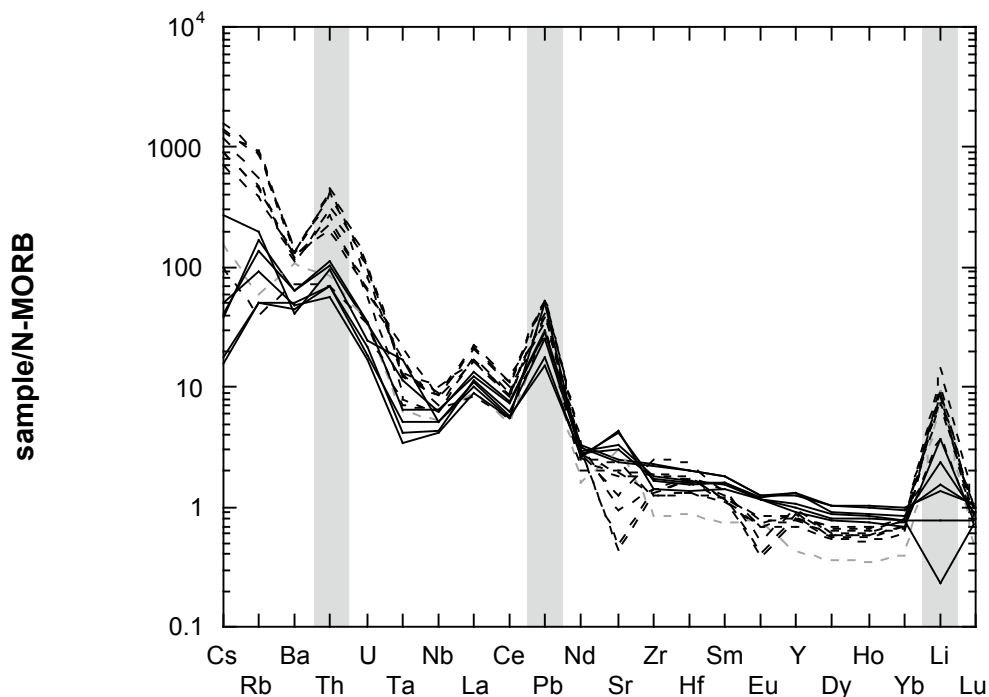


Fig. 4: N-MORB normalised (Sun and McDonough 1989) trace element patterns for pre-caldera (solid lines), first post-caldera eruption (Nikia lava; grey dashed line), post-caldera and Yali units (dashed lines). Grey areas mark enrichment peaks of fluid mobile elements

As it is important to discriminate fractional crystallisation from fluid addition we use Sr and Pb normalised to a HREE, in this case Yb (Fig. 5). Pb and Sr are known to be highly mobile in aqueous fluids. However, changes in the Sr concentration also indicate the presence or the removal of plagioclase. The resulting negative correlation of Sr/Yb vs Pb/Yb (Fig. 5) shows that plagioclase removal (leading to a decrease of the Sr/Yb) was coupled to an increasing influence of fluids towards the post-caldera and Yali units. The presence of the additional plagioclase generation that probably accumulated in the Nikia lava (NIS 1) may be the cause of its very high Sr/Yb ratio (Fig. 2). The other two evolved samples showing a high Sr/Yb ratio are a variolitic amphibole cumulate in the Nikia lava (sample NIS 1b, hereafter Nikia-amph) and a dacite from the post-caldera domes (sample NIS 9c). The enlarged Sr/Yb ratios of these two samples are most likely the result of increasing fluid activity, that is also indicated by the presence of hydrous phases (amphibole). In addition, the Nikia-amph yields the lowest $^{87}\text{Sr}/^{86}\text{Sr}$ ratio (0.703648).

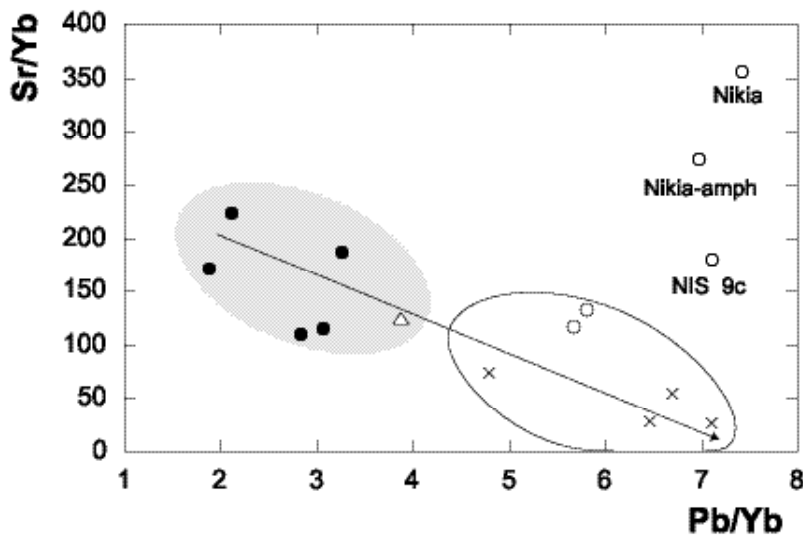


Fig. 5: Pb/Yb vs Sr/Yb diagram. A positive correlation would be expected if only fluid addition influenced both element ratios. The solid arrow is the result of two processes: fluid addition and fractional crystallisation of plagioclase (symbols as in Fig. 3).

Any rising magma undergoes fractional crystallisation in various proportions on its ascent. High degrees of mantle hydration in the source region will lead to primary magmas of basaltic-andesitic to andesitic composition (Baker et al. 1994). The observed decrease in Ni and Co concentrations with increasing degree of differentiation of Nisyros-Yali units is indicative for the progressing influence of olivine fractionation (Table A-1-2, Appendix A). Whilst basaltic-andesites contain olivine as a minor phenocryst phase (reflected in high Ni and Co concentrations up to 40 ppm Ni and 65 ppm Co, see Table A-1-2), andesites and post-caldera units are characterised by low Ni and Co concentrations around 9 and 16 ppm, respectively. Decreasing Cr concentrations from the mafic towards the felsic series express the effect of increasing clinopyroxene fractionation.

To highlight the differences in REE for Nisyros-Yali volcanics, which might be less clearly visible in a spider diagram such as Fig. 4, we follow Haskin's (1990) example and normalise to a representative of the suite. We chose lava NIS 4 for normalisation, because it is the most primitive of the suite (Tables A-1-2 and A-1-3). Accordingly, amphibole fractionation seems to gain importance for post-caldera Nisyros and all Yali units visible in Dy-Ho troughs (Fig. 6). It should be noted that high LREE/HREE ratios are indicative for both amphibole/pyroxene fractionation and fluid contribution to the magma source region. Certainly these two processes can be valid for Nisyros as

they do not contradict each other. The first process requires high amounts of aqueous fluids for amphibole stabilisation, which were available, especially during the evolution of the post-caldera units. Late stages of fractional crystallisation were dominated by some shallow-level fractionation of plagioclase.

A comparison of Eu-anomalies (Eu/Eu^*) and Sr concentrations allows the identification of plagioclase fractionation (Fig. 7). Pre-caldera volcanics show no or only slightly negative Eu/Eu^* and high Sr concentrations. Plagioclase fractionation leads to a decrease of both parameters in the more evolved post-caldera and Yali units. In contrast, Nikia lava (NIS 1) shows a distinct positive Eu/Eu^* of 1.41 accompanied by enhanced Sr concentration that is unrelated to any other Nisyros unit (Fig. 7). Incomplete segregation of plagioclase in the derivative melt may account for this geochemical observation. Plagioclase with resorption rims, indicative for long permanence in the magma, supports such a process. An alternative explanation for the positive Eu/Eu^* could be that Eu in divalent state behaves almost identically to Sr^{2+} and Pb^{2+} and becomes enriched under reducing conditions (Woodhead et al. 1998). However, it is very unlikely that the O_2 -fugacity will change for a single eruption out of a cycle of several in a narrow time interval. We consequently favour the explanation based on multiple plagioclase generations.

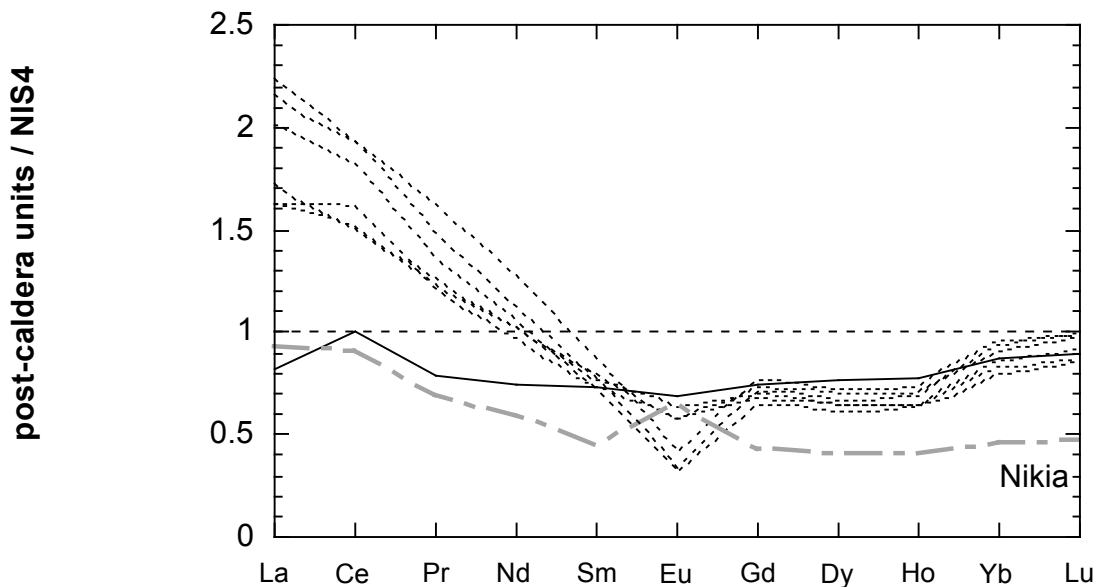


Fig. 6: Rare earth element (REE) patterns of the post-caldera and Yali units relative to NIS 4 (following Haskin 1990), the least evolved lava of the volcanic system. The caldera-causing Lower Pumice pattern (solid line) shows similarities to the Nikia lava (dashed-dotted, grey line). Heavy REE (excluding the Lower Pumice and the Nikia lava) exhibit a trough indicative for amphibole fractionation.

Finally, a comparison of Zr concentrations and SiO_2 contents (Fig. 8) shows that the caldera-causing Lower Pumice and post-caldera units have reached the zircon saturation boundary. In the early stages of fractional crystallisation Zr is a highly incompatible element resulting in positive correlations when plotted against silica content. This characteristic is seen for the pre-caldera samples and for one sample of the Yali units. For the post-caldera samples, however, Zr behaved like a compatible element resulting in a negative correlation with SiO_2 . This is best explained by zircon

saturation (Hanchar and Watson 2003). Saturation of Zr in the melt, leading to fractional crystallisation of zircon, is reached in more differentiated liquids and causes the inflexion in the positive trend observed for dacites of the post-caldera units with more than 68 wt % SiO_2 .

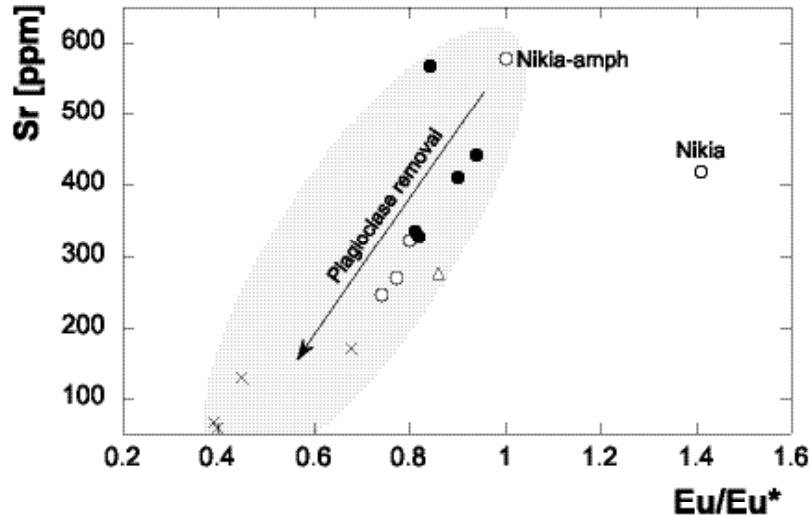


Fig. 7: Eu/Eu^* vs Sr concentration. The positive correlation reveals the increasing role of plagioclase fractionation towards the post-caldera units. The presence of an additional plagioclase generation in the Nikia lava accounts for the positive Eu/Eu^* and the high Sr concentration.

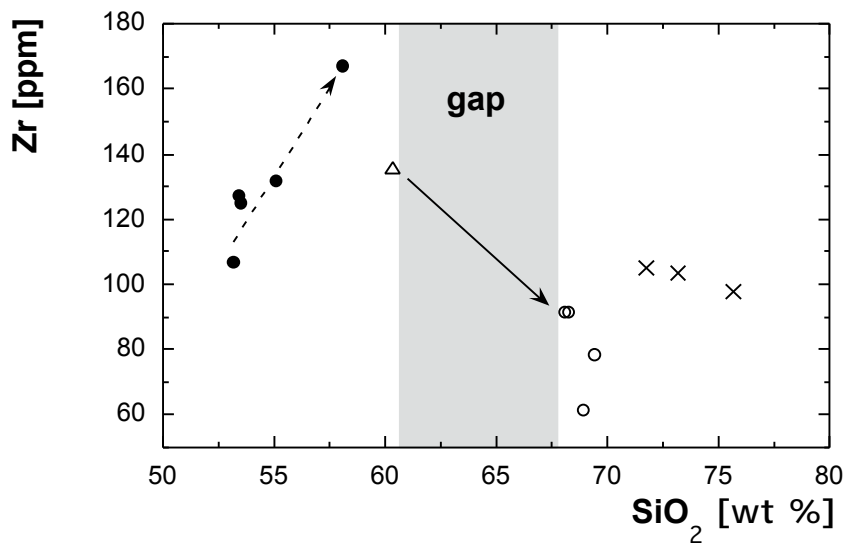


Fig. 8: Bulk Zr-concentration vs differentiation index illustrates the effect of zircon fractionation for the post-caldera units. The dashed arrow marks the increase of Zr and Hf that is accompanied with the presence of zircon as an accessory mineral phase in the pre-caldera units. The solid arrow reflects zircon segregation, which partly occurred during the eruptive stasis (symbols as in Fig.

Fractional crystallisation of olivine, clinopyroxene, amphibole, plagioclase and zircon was the dominant process, increasing towards post-caldera units and reaching its maximum in Yali eruptives. Fluid addition to the source of Nisyros-Yali magma also influenced REE and trace element budget of pre-caldera units and increase from the most primitive lavas towards the caldera-causing Lower Pumice and the post-caldera Nikia lava.

1.6.1.1 Role of Th and U

Thorium shows high incompatibility during mineral-melt partitioning and is generally considered to be a fluid immobile element. The presence of Th in arc magmas is generally explained by melting of pelagic sediments lying on top of the downgoing slab (e.g. Hawkesworth et al. 1997).

The investigated Nisyros and Yali units yield Th concentrations ranging from 8 ppm for some pre-caldera units to ca 30 ppm for the post-caldera units and > 50 ppm for Yali eruptives. Post-caldera and Yali Th concentrations by far exceed that of the Global Subducting Sediment (GLOSS, 6.91 ppm Th, Plank and Langmuir 1998) and those reported for other Hellenic Arc magmas (Milos up to 19 ppm Th; Stewart and McPhie 2003 and Santorini between 15 and 18 ppm Th; Zellmer et al. 2000). Therefore, an involvement of sediments is insufficient to explain our data.

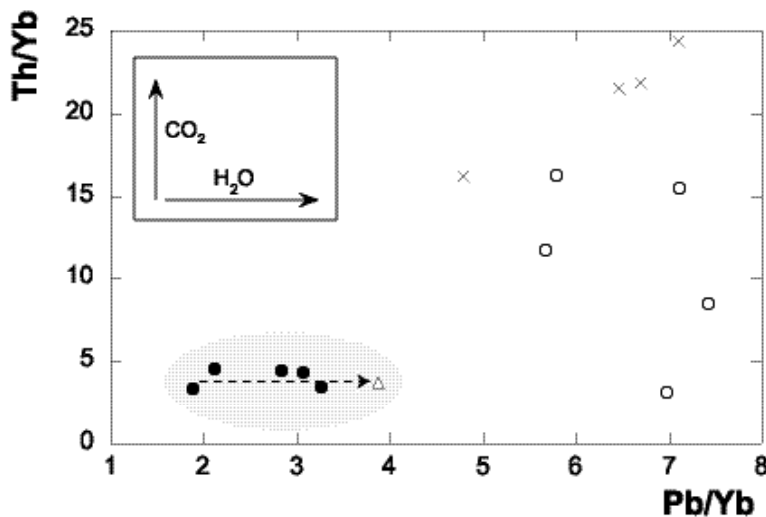


Fig. 9: Pb/Yb vs Th/Yb ratios reflect different fluid-compositions (see inset). Pb/Yb increases monotonic at constant Th/Yb = 4 for the pre-caldera lavas up to the Lower Pumice. The increase of Th/Yb ratios at high Pb/Yb values is not due to Yb decrease; instead, post-caldera lavas and especially Yali pumices have higher Th concentrations than the rest of the Hellenic Arc magmas.

To evaluate the behaviour of Th in the volcanic system we compare it with Pb, which is known to be mobile in aqueous fluids, by normalising both to Yb (Fig. 9). Pb/Yb ratios increase in pre-caldera units up to the caldera-causing Lower Pumice while Th/Yb remains low and constant. Post-caldera units reveal a steep increase of Th/Yb from 4 up to 25 whereas Pb/Yb scatter between 6 and 8 without any trend. We ascribe these to an uncommon fluid chemistry. Chiodini et al. (1993) recorded CO₂-rich fluids in recent fumarolic fluids. The presence of fluids enriched in CO₂ enables a selective transport of Th (Capaldi et al. 1982).

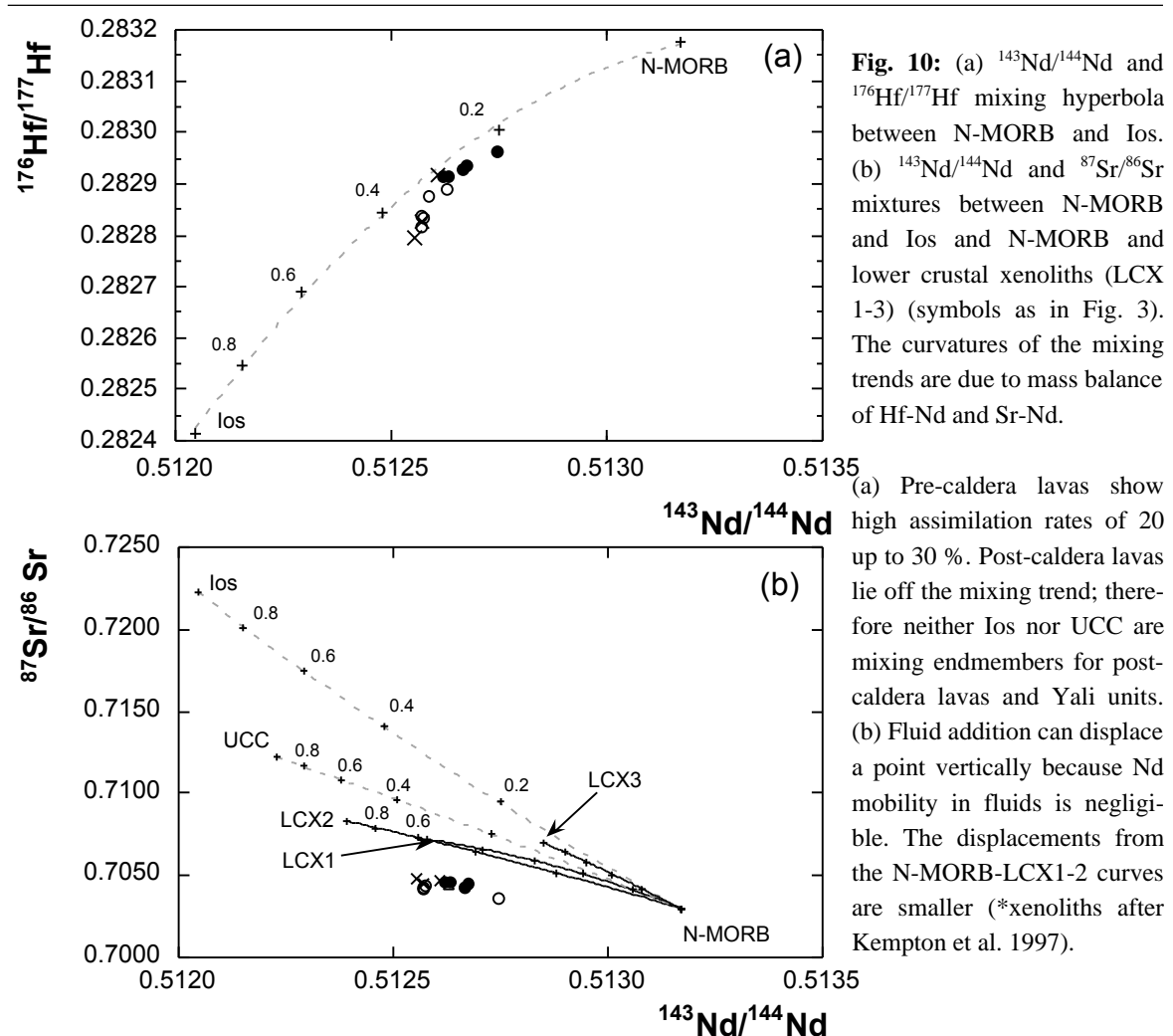
According to Fiebig et al. (2004) CO₂/³He and N₂/³He ratios of recent fumarolic gases average to 4*10⁹ and 6*10⁶, respectively. Such ratios are extremely low for subduction zone settings and are rather close to the range observed for MOR-derived fluids (CO₂/³He = (2±1)*10⁹; N₂/³He = (4±2)*10⁶). The presence of mantle-derived fluids containing CO₂ could, indeed, explain the element distribution pattern presented here: (i) Th behaves as a mobile element in the presence of fluids enriched in CO₂ and (ii) mantle derived fluids carry Sr with a very primitive isotopic signature. In addition to the presence of fluids in the magma chamber, late stage exhalation of volcanic gases could further produce enrichments in porous eruptives after the emplacement.

1.6.2 Geochemical signatures of crustal assimilation

Crustal assimilation is certain to occur to some extent and has in the past already been used to interpret geochemical characteristics of Nisyros units (e.g., Wyers and Barton 1989). A potential assimilation of underlying carbonates as candidate of contaminant is considered unlikely because the carbonate layer directly underlying Nisyros volcanics is only encountered at shallow depths between 600 and 1200 m below sealevel (Marini et al. 1993). More likely basement compositions are either a heterogenous mélange of carbonates, sediments and ophiolites from the Lycian nappe, SW Turkey

(e.g. Oberhänsli et al. 2001) or the Paleozoic gneisses underlying the central part of the Hellenic arc. In order to qualify and quantify crustal assimilation, Nd and Hf isotope measurements were performed. Further, we measured Sr and Pb isotopes, systems that are known to be sensitive indicators for crustal assimilation.

$^{143}\text{Nd}/^{144}\text{Nd}$ ratios of pre-caldera units range between 0.512622 and 0.512675. Post-caldera and Yali units yield $^{143}\text{Nd}/^{144}\text{Nd}$ ratios between 0.512553 and 0.512607 (Table A-1-3; Appendix A). Again, a clear subdivision into a pre-caldera and a post-caldera group is visible. The former group yields values averaging at +0.2 (Nd), whereas the post-caldera and Yali units exhibit (Nd) values averaging around -1.2. However, our Nd isotope data is less radiogenic than the typical (Nd) of N-MORB averaging +10. $^{176}\text{Hf}/^{177}\text{Hf}$ ratios of pre-caldera units range between 0.282914 and 0.282940 that of the post-caldera and Yali units between 0.282794 and 0.282917. Whilst pre-caldera units yield (Hf) values around +5.4, the post-caldera volcanics scatter around less radiogenic (Hf) values of +2.4 compared to typical (Hf) of N-MORB of +17. Thus, both Nd- and Hf-isotope systematics clearly indicate assimilation of crustal material during ascent. This is further visible in calculated Nd- and Hf- mantle extraction ages (t_{Nd} , t_{Hf}) ranging from 750 to 850 Ma. Ios gneisses yield mantle extraction ages > 1.3 Ga (Table A-1-3, Appendix A).

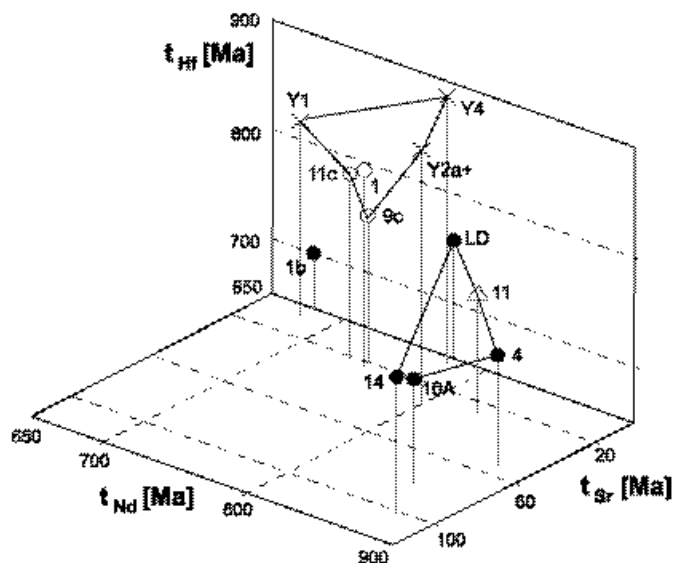


It should be noted that all model ages presented in this study represent the mean crustal age of the magma source (Arndt and Goldstein 1987). All Nisyros and Yali units are characterised by variable but overall unradiogenic $^{87}\text{Sr}/^{86}\text{Sr}$ signatures (0.703648 – 0.704847; Table A-1-3). This is also expressed in the calculated Sr mantle extraction ages (t_{Sr} , between 50 Ma and 100 Ma) that are an order of magnitude lower than Hf and Nd mantle extraction ages.

For a simple two component mixing model, several reservoirs be applicable as end-members. As representative of the melted oceanic crust, N-MORB was chosen. The most likely lower crustal candidate was selected from a large database of xenoliths (Murphy et al. 2002 and references therein); upper crustal candidate as assimilated contaminant is the gneissic basement exposed sporadically along the western Aegean arc (which we sampled in Ios; e.g. Van der Maar and Jansen 1981). Pre-caldera units follow this mixing curve and reveal rather high amounts of assimilated crust of 20 up to 40 % (Fig. 10 a). Post-caldera and Yali units deviate from the mixing curve towards lower $^{176}\text{Hf}/^{177}\text{Hf}$ ratios and/or higher $^{143}\text{Nd}/^{144}\text{Nd}$ ratios; the required assimilation would need to be 40-50 % by mass.

A two-component mixture of $^{143}\text{Nd}/^{144}\text{Nd}$ and $^{87}\text{Sr}/^{86}\text{Sr}$ isotope systematics between N-MORB and Ios gneisses reveals a distinct deviation from the curve (Fig. 10 b). This implies that $^{87}\text{Sr}/^{86}\text{Sr}$ signatures are dominated by either the influence of primitive fluids (probably originated from the altered oceanic crust; e.g. Turner et al. 1996) or due to a contaminant different from UCC. To identify a lower crustal contaminant we have chosen three xenoliths (LCX 1-3) from the SE European continent (Kempton et al. 1997) as endmember. The deviation of our data to the resulting curve is smaller compared to the former mixture. Accordingly, neither UCC nor LCX are representative binary contaminants for Nisyros-Yali magma. To emphasise the role of assimilation in the pre- and post-caldera units we further combine t_{Hf} and t_{Nd} with t_{Sr} in a three-dimensional diagram (Fig. 11). Mantle extraction ages of Hf (t_{Hf}) and Nd (t_{Nd}) are in the same range (750 Ma and 850 Ma) which we have attributed to assimilation of crustal material. Again, a very crude mass balance estimate of the Sm-Nd and Lu-Hf mantle extraction ages require Ios gneisses to have contributed almost half of the Nisyros Nd and Hf budget, and at the same time rules out ophiolitic upper crust as contaminant, as its mantle extraction ages are too young (Permo-Triassic up to Cenozoic times; e.g., Oberhänsli et al. 2001).

Fig. 11: 3-D model ages plot (t_{Sr} , t_{Nd} , t_{Hf}) resulting in two planes defined by the pre-caldera and the post-caldera units. The trajectories of data-points are indicative for different processes: an increasing degree of assimilation towards the post-caldera units and an increasing influence of primitive fluids evidenced by decreasing t_{Sr} (symbols as in Fig. 3).



In stark contrast, t_{Sr} is decoupled from the former two systems. Despite the similarity of t_{Hf} and t_{Nd} , post- and pre-caldera units define two distinct groups. Accordingly, pre-caldera units define a cluster that is characterised high t_{Nd} averaging around 850 Ma, lower t_{Hf} (around 750 Ma) and t_{Sr} ranging from 50 to 100 Ma. Their Sm/Nd values of around 0.2 are higher than that of the post-caldera volcanics averaging 0.15. This latter group, furthermore, spans a plane defined by younger t_{Nd} averaging around 740 Ma and older t_{Hf} of around 800 Ma (Fig. 11). Their t_{Sr} are younger than that of the pre-caldera units and average around 20 Ma.

As UCC (including Ios gneisses) is an unlikely contaminant for Nisyros-Yali volcanics we use Pb-isotope systematics to verify the indication for lower crustal material. Lead isotope compositions $^{206}Pb/^{204}Pb$, $^{207}Pb/^{204}Pb$ and $^{208}Pb/^{204}Pb$ cluster between 18.647 – 18.779, 15.624 – 15.652 and 38.502 – 38.720, respectively. In a $^{206}Pb/^{204}Pb$ vs $^{207}Pb/^{204}Pb$ evolution diagram our data plot to the right of the meteorite isochron and increase towards more felsic volcanic units (Fig. 12). The evolution path for the upper mantle (UM; Kramers and Tolstikhin 1997) and the $^{206}Pb/^{204}Pb$ – $^{207}Pb/^{204}Pb$ compositions of lower-crustal xenoliths (LCX 1-3) allow a mix calculation between N-MORB and one of the xenoliths (LCX 3). Hence, the amount of assimilated lower crust would range between 15 % for the pre-caldera units up to 18 % for post-caldera eruptives. On the contrary Pb isotope signatures of LCX 3 do not account for a correlation of Nd and Sr isotope systematics.

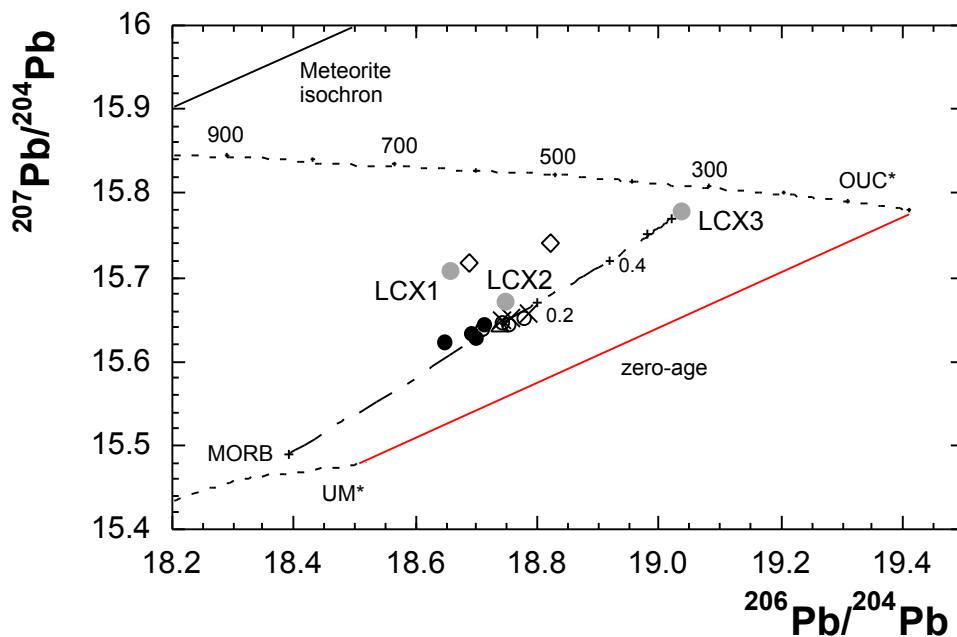


Fig. 12: Lead isotope compositions with modelled evolution paths (Kramers and Tolstikhin 1997) for upper mantle (UM*) and older upper crust (OUC* with model ages in Ma) and Pb isotope compositions for lower crustal xenoliths (LCX1-3; Kempton et al. 1997). $^{206}Pb/^{204}Pb$ – $^{207}Pb/^{204}Pb$ of Nisyros-Yali units increase towards more felsic post-caldera units. The data-points fit on a mixing curve between LCX3 and N-MORB and reveal 15 to 18 % of LCX3 (symbols as in Fig. 3, = Ios).

In summary, Nd- and Hf-isotope systematics are suitable for estimate the increasing role of assimilation of crustal material in the Nisyros-Yali system, whereas Sr-isotope signatures are dominated by primitive fluids. Assimilation rates are not quantifiable as the crustal endmember is unknown. Isotope compositions of lower crustal xenoliths from SE Europe indicate that the

contaminant of Nisyros-Yali magma is similar to lower crustal material. Pb-isotope signatures of volcanics fit on a mix curve between N-MORB and one of the lower crustal xenoliths resulting in a contamination of 15 to 18 %. The same xenolith shows no correlation with our data in the Nd-Sr isotope plot. Hence, there is no confirmation of all parameters and the endmember composition remains uncertain. Because our multi-isotopic data-set allows less degrees of freedom than model input parameters, we can recognise that AFC modelling would not be justified.

1.7 The compositional gap

The compositional gap subdivides Nisyros units into a bimodal volcanic suite. Thompson et al. (2001) & Grove and Donnelly-Nolan (1986) described a similar gap observed for the alkaline volcanic suite from Rarotonga (southern Pacific) lacking intermediate rocks. Peccerillo et al. (2003) recognised a compositional gap in the eruptive units of the Gedemsa volcano (Central Ethiopian Rift). Following Grove & Donnelly-Nolan (1986) development of SiO₂ gaps in volcanic suites occurs as a result of small temperature decreases in the magma chamber, resulting in high degree of crystallisation (60 wt %) and hence, increased viscosity. The interruption of magma replenishment entails closed system behaviour of the magma chamber with continuing crystallisation. Due to the increase of SiO₂ polymerisation, the viscosity of the magma body increased to a critical level suppressing eruption. Subsequently, the enrichment of incompatible elements (especially H₂O) in the residual melt leads to SiO₂ depolymerisation and thus to a decrease in viscosity, whereby the magma becomes able to erupt again, but with a more felsic composition. The compositional gap described by Peccerillo et al. (2003) is the result of (i) the deficiency of intermediate magmas generated by fractional crystallisation and (ii) of a density dependent stratification of the magma chamber leading to the separation of intermediate magma from silicic melts. An essential observation are xenoliths of intermediate composition.

In the present work the following petrological and geochemical features support the explanation given by Thompson et al. (2001): The Nikia lava (first eruption of the post-caldera units with 68 wt % SiO₂) extruded after the explosive eruption of the large caldera-causing pumice layer (Lower Pumice, which frames the gap on the SiO₂-poor side). While Nikia lava contains a hydrous phase, amphibole, both as phenocryst phase and as cumulates, amphibole is lacking in Lower Pumice. Additionally, the Nikia lava is characterised by the presence of two plagioclase generations with and without reaction rims indicative for a longer storage time. This second plagioclase generation is the only indication of a Gedemsa-type cumulate layer. However, no other Nisyros-Yali samples contain intermediate xenoliths, which is an indication that a different process was responsible.

According to Fig. 6 and 13 a distinction based on REE into two groups is evident. Generally, the pre-caldera group REE data exhibit parallel patterns relative to NIS 4 (Fig. 13) only slightly enriched in LREE and HREE. This geochemical feature can be explained with the increasing amount of clinopyroxene phenocrysts through the magma evolution of the pre-caldera units. In contrast to the pre-caldera group, the REE patterns of the post-caldera units (Fig. 6) reveal steep negative slopes for the LREE and MREE relative to NIS 4. Except for Nikia lava all post-caldera units and especially Yali units yield negative Eu/Eu*. Moreover, for the more evolved post-caldera units (excluding Nikia lava as well) a Dy-Ho trough is obvious indicative for amphibole fractionation. Thus, the compositional gap also appears in trace element composition. Furthermore, isotope systematics of Hf, Nd, Sr and Pb stress out that different processes influenced the evolution of the Nisyros-Yali units. While Hf and Nd isotope signatures are mainly controlled by assimilation, Sr isotope systematics

reveal the presence of primitive fluids. Lead isotope signatures in comparison with $^{87}\text{Sr}/^{86}\text{Sr}$ ratios (Fig. 14) enable us to emphasise the change in processes controlling the magma genesis.

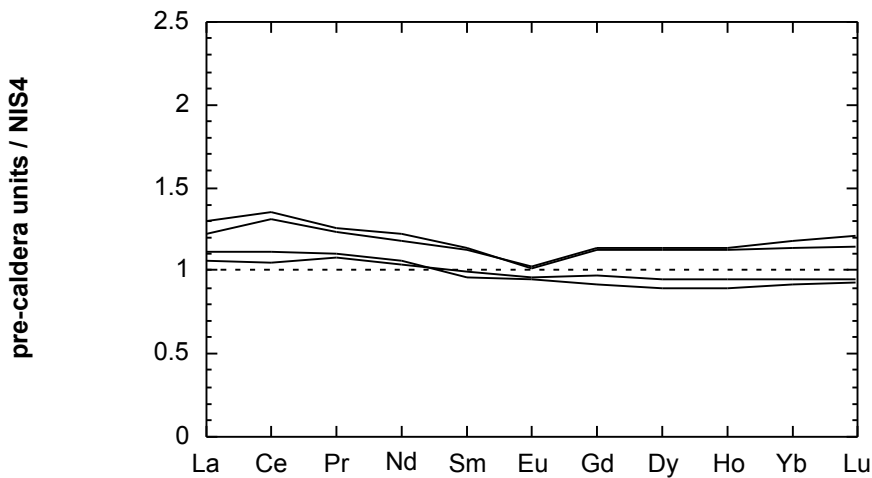


Fig. 13: Rare earth element distributions of the pre-caldera units relative to NIS 4, the least evolved lava of the volcanic system, show near parallel patterns.

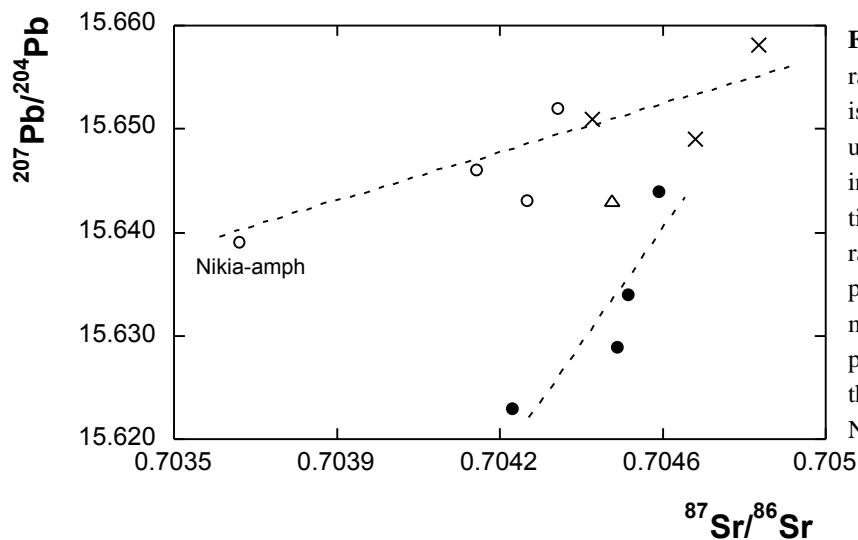


Fig. 14: $^{207}\text{Pb}/^{204}\text{Pb}$ vs $^{87}\text{Sr}/^{86}\text{Sr}$ ratios (errors < symbol size). Lead isotope ratios of the pre-caldera units increase with a steeper slope indicative for increasing assimilation at almost constant $^{87}\text{Sr}/^{86}\text{Sr}$ ratios. A batch of primitive fluid penetrated the first post-caldera magma evidenced by the most primitive Sr isotope signature in the amphibole cumulate of the Nikia lava (symbols as in Fig. 3).

A saltatory change in Pb- and Sr-isotope signatures towards more primitive values for the first post-caldera unit (Nikia lava) is indicative for the presence of a new batch of fluid (with a primitive Sr-isotope signature) during the generation of this magma on the high SiO_2 -side of the compositional gap. Supportingly, the amphibole cumulate within the Nikia lava (sample NIS 1b) is characterised by the highest Sr-content in combination with the most primitive Sr isotope ratio observed for Nisyros-Yali units (581 ppm, $^{87}\text{Sr}/^{86}\text{Sr} = 0.703648$, Tables A-1-2 and A-1-3, Appendix A). Thus, this $^{87}\text{Sr}/^{86}\text{Sr}$ signature is closest to that of the fluid that probably triggered the eruption of the Nikia lava.

1.8 Summary and Conclusions

The geochemistry of Nisyros and Yali volcanics is dominated by the occurrence of a compositional gap. Nisyros and Yali units lack SiO₂-compositions between 61 and 68 wt %. As a typical feature of island arc magma evolution fractional crystallisation, partial mantle melts result in negative slopes in N-MORB normalised trace element pattern. Fluid addition is responsible for positive LILE anomalies and enrichment peaks of other fluid mobile elements as well as for the decoupling of Sr isotope characteristics from Nd, Hf and Pb isotope signatures. Unradiogenic ⁸⁷Sr/⁸⁶Sr ratios reflect the presence of a primitive fluid during the evolution of the whole volcanic suite, with the pre-caldera units being more primitive than the post-caldera units. The exceptional behaviour of the first post-caldera Nikia lava with a very low ⁸⁷Sr/⁸⁶Sr ratio is indicative for the penetration of the magma with a new batch of primitive fluid, as supported by the lowermost ⁸⁷Sr/⁸⁶Sr ratio of the amphibole cumulate from the Nikia lava. As it is inferred from Nd and Hf characteristics assimilation of a crustal reservoir increases in the pre-caldera units from 20 up to 40 % while the post-caldera and Yali units deviate from the mixing of N-MORB and Ios. Nd and Sr isotope data also show a displacement from a N-MORB-Ios mixing trend caused by the addition of primitive fluids to the source. Data approach towards a modelled two-component mixing between N-MORB and lower crustal xenoliths. Hence, a combination of both fluid input and assimilation of a lower crustal reservoir control the Sr isotope budget. Pb-isotope (but not the Nd or Hf) systematics allow a additional qualification of endmembers. Accordingly, a possible mixture between N-MORB and one of the lower crustal xenoliths results in an assimilated mass balance between 15 and 18 %.

Under consideration of petrological and geochemical observations we propose the following magma generation model based on Thompson et al. (2001): After the explosive eruption of the Lower Pumice the magma chamber behaved temporarily as a closed system without replenishment. Continuing crystallisation up to 50 – 60 % led to an increase of viscosity suppressing further eruptions. A batch of primitive fluids penetrates the magma resulting in the crystallisation of hydrated minerals, such as amphibole. The increased water activity furthermore causes a decrease in viscosity and hence, in the eruption of Nikia lava with dacitic composition. Subsequent to this lava flow the less voluminous Upper Pumice erupted. The main volcanic activity on Nisyros ceased with the intrusion of several domes, indicative for low-pressure conditions in the chamber.

Acknowledgements

Thanks are due to H.R. Pfeifer and J.C. Lavanchy at the CAM, Université de Lausanne, Switzerland for XRF analyses and to Yann Lahaye, Universität Frankfurt for trace element analyses. We are indebted to Karl Ramseyer and Edwin Gnos, Universität Bern, Switzerland for supporting at the CL and EMP, respectively. We also thank two anonymous reviewers for critical comments, which helped to improve an earlier version of the manuscript. Claudia Principe is thanked for the helpful guidance in the field. The present work is supported by the Swiss National Science Foundation (grant No21-63866.00).

References

- Allen, S.R., McPhie, J., 2000. Water-settling and re-sedimentation of submarine rhyolitic pumice at Yali, eastern Aegean, Greece. *Journal of Volcanology and Geothermal Research*, 95, 285–307.
- Arndt, N.T., Goldstein, S.L., 1987. Use and abuse of crust-formation ages. *Geology*, 15, 893–895.
- Baker, M.B., Grove, T.L., Price, R., 1994. Primitive basalts and andesites from the Mt. Shasta region, N California – products of varying melt fraction and water-content. *Contributions to Mineralogy and Petrology*, 118(2), 111–129.
- Chiodini, G., Cioni, R., Leonis, C., Marini, L., Raco, B., 1993. Fluid geochemistry of Nisyros island, Dodecanese, Greece. *Journal of Volcanology and Geothermal Research*, 56, 95–112.
- Capaldi, G., Cortini, M., Pece, R., 1982. Th isotopes at Vesuvius: evidence for open-system behaviour of magma-forming processes. *Journal of Volcanology and Geothermal Research*, 14, 247–260.
- DiPaola, G.M., 1974. Volcanology and petrology of Nisyros Island (Dodecanese, Greece). *Bulletin of Volcanology*, 38, 944–987.
- Davidson, J.P., 1987. Crustal contamination versus subduction zone enrichment; examples from the Lesser Antilles and implications for the mantle source composition of island arc volcanic rocks. *Geochimica et Cosmochimica Acta*, 51, 2185–2198.
- Federman, A.N., Carey, S.N., 1980. Electron microprobe correlation of tephra layers from eastern Mediterranean abyssal sediments and the island of Santorini. *Quaternary Research*, 13, 160–171.
- Fiebig, J., Chiodini, G., Caliro, S., Rizzo, A., Spangenberg, J., Hunziker, J.C., 2004. Chemical and isotope equilibrium between CO₂ and CH₄ in fumarolic gas discharges: generation of CH₄ in arc magmatic-hydrothermal systems. *Geochimica et Cosmochimica Acta*, 68 (10), 2321–2334.
- Förster, H.J., 2001. Synchysite-(Y)-synchysite-(Ce) solid solutions from Markersbach, Erzgebirge, Germany: REE and Th mobility during high-T alteration of highly fractionated aluminous A-type granites. *Mineralogy and Petrology*, 72, 259–280.
- Françalanci, L., Varekamp, J.C., Vougioukalakis, G., Defant, M.J., Innocenti, F., Manetti, P., 1995. Crystal retention, fractionation and crustal assimilation in a convecting magma chamber, Nisyros Volcano, Greece. *Bulletin of Volcanology*, 56, 601–620.
- Gorceix, M.H., 1873. Sur l'état du volcan de Nisyros au mois de mars 1873. *C.R. Séances Acad. Sci., Paris*, 77, 597–601.
- Gill, J.B., 1981. *Orogenic Andesites and Plate Tectonics*. Springer Verlag, Berlin, 358 pp.
- Grove, T.L., Donnelly-Nolan, J.M., 1986. The evolution of young silicic lavas at Medicine Lake Volcano, California: Implications for the origin of compositional gaps in calc-alkaline series lavas. *Contributions to Mineralogy and Petrology*, 92, 281–302.
- Grove, T.L., Parman, S.W., Bowring, S.A., Price, R.C., Baker, M.B., 2002. The role of an H₂O-rich fluid component in the generation of primitive basaltic andesites and andesites from the Mt. Shasta region, N California. *Contributions to Mineralogy and Petrology*, 142, 375–396.
- Hanchar, J.M., Watson, E.B., 2003. Zircon saturation thermometry. *Reviews in Mineralogy*, Vol. 53, 89–112.

- Haskin, L.A., 1990. PREEconceptions pREEvent pREEcise pREEdictions. *Geochimica et Cosmochimica Acta*, 54, 2353–2361.
- Hawkesworth, C., Turner, S., Peate, D., McDermott, F., van Calsteren, P., 1997. Elemental U and Th variations in island arc rocks: implications for U-series isotopes. *Chemical Geology*, 139 (1-4), 207–211.
- Kamber, B.S., 2002. Fluid-mobile trace element constraints on the role of slab melting and implications for Archaean crustal growth models. *Contributions to Mineralogy and Petrology*, 144(1), 38–56.
- Keller, J., 1969. Origin of rhyolites by anatectic melting of granitic crustal rocks. The example of rhyolitic pumice from the island of Kos (Aegean Sea). *Bulletin of Volcanology*, 33, 942–959.
- Keller, J., 1982. Mediterranean island arcs. Andesites. Wiley, New York, 307–325 pp.
- Kleinhanns, I.C., Kreissig, K., Kamber, B.S., 2002. Combined chemical separation of Lu, Hf, Sm, Nd and REEs from a single rock digest: Precise and accurate isotope determinations fo Lu-Hf and Sm-Nd using multicollector-ICPMS. *Analytical Chemistry*, 74(1), 67–73.
- Kramers, J.D., Tolstikin, I.N., 1997. Two terrestrial lead isotope paradoxes, forward transport modelling, core formation and the history of the continental crust. *Chemical Geology*, 139, 75–110.
- LeMaitre, R.W., 1989. A classification of igneous rocks and glossary terms. Recommendations of the International Union of Geological Sciences Subcommittee on the Systematics of Igneous Rocks. Blackwell Scientific Publications, Oxford, London, Edingborough, Boston, Melbourne.
- Le Pichon, X., Angelier, J., 1979. The Hellenic arc and trench system: a key to the neotectonic evolution of the Eastern Mediterranean area. *Tectonophysics*, 60, 1–42.
- Limburg, E.M., Varekamp, J.C., 1991. Young pumice deposits on Nisyros, Greece. *Bulletin of Volcanology*, 54(1), 68–77.
- Marini, L., Principe, C., Chiodini, G., Cioni, R., Fytikas, M., Marinelli, G., 1993. Hydrothermal eruptions of Nisyros (Dodecanese, Greece). Past events and present hazard. *Journal of Volcanology and Geothermal Research*, 56, 71–94.
- Murphy, D.T., Kamber, B.S., Collerson, K.D., 2002. A refined solution to the first terrestrial Pb-isotope paradox. *Journal of Petrology*, 44 (1), 39–53.
- Nowell, G.M., Kempton, P.D., Noble, S.R., 1998. High precision Hf isotope measurements of MORB and OIB by thermal ionisation mass spectrometry: insights into the depleted mantle. *Chemical Geology*, 149, 3–4, 211–233.
- Oberhänsli, R., Partzsch, J., Candan, O., Cetinkaplan, M., 2001. First occurrence of Fe-Mg-carpholite documenting a high-pressure metamorphism in metasediments of the Lycian Nappes, SW Turkey. *International Journal of Earth Sciences*, 89, 867–873.
- Papadopoulos, G.A., Sachpazi, M., Panopoulou, G., Stavrakakis, G., 1998. The volcanoseismic crisis of 1996–97 in Nisyros, SE Aegean Sea, Greece. *Terra Nova*, 10, 151–154.
- Papanikolaou, D.J., Lekkas, E.L., Sakelariou, D.T., 1991. Geological structure and evolution of Nisyros volcano. *Bulletin of the Geological Society, Greece*, 25(1), 405–419.

- Papazachos, B.C., Panagiotopoulos, D.G., 1993. Normal faults associated with volcanic activity and deep rupture zones in the southern Aegean volcanic arc. *Tectonophysics*, 220(1-4), 301–308.
- Pearce, J.A., Kempton, P.D., Nowell, G.M., Noble, S.R., 1999. Hf-Nd element and isotope perspective on the nature and provenance of mantle and subduction components in western Pacific arc-basin systems. *Journal of Petrology*, 40, 1579–1611.
- Peccerillo, A., Barberio, M.R., Yirgu, G., Ayalew, D., Barbieri, M., Wu, T.W., 2003. Relationships between mafic and peralkaline silicic magmatism in continental rift settings: a petrological, geochemical and isotopic study of the Gedemsa volcano, Central Ethiopian Rift. *Journal of Petrology*, 44 (11), 2003-2032.
- Plank, T., Langmuir, C.H., 1998. The chemical composition of subducting sediment and its consequences for the crust and mantle. *Chemical Geology*, 145(3-4), 325–394.
- Rehren, T., 1988. *Geochemie und Petrologie von Nisyros (östliche Ägäis)*. Ph.D. Thesis. Univ. Freiburg.
- Saunders, A.D., Norry, M.J., Tarney, J., 1988. Origin of MORB and chemically depleted mantle reservoirs: trace element constraints. *Journal of Petrology*, Special Lithosphere Issue, 415–445.
- Seymour, K.S., Vlassopoulos, D., 1992. Magma mixing at Nisyros volcano, as inferred from incompatible trace-element systematics. *Journal of Volcanology and Geothermal Research*, 50, 273–299.
- Smith, P.E., York, D., Chen, Y., Evensen, N.M., 1996. Single crystal ^{40}Ar - ^{39}Ar dating of a Late Quaternary paroxysm on Kos, Greece: Concordance of terrestrial and marine ages. *Geophysical Research Letters*, 23(21), 3047–3050.
- Stewart, A.L., McPhie, J., (2003). Internal structure and emplacement of an Upper Pliocene dacite cryptodome, Milos island, Greece. *Journal of Volcanology and Geothermal Research*, 124, 129-148.
- Sun, S., Donogh, W.F., 1989. Chemical isotope systematics of oceanic basalts: implications for mantle compositions and processes. *Magmatism in the Ocean Basins*, Special Publication No 42, Geological Society, 313–345.
- Thompson, G.M., Smith, I.E.M., Malpas, J.G., 2001. Origin of oceanic phonolites by crystal fractionation and the problem of the Daly gap: an example from Rarotonga. *Contributions to Mineralogy and Petrology*, 142, 336–346.
- Turner, S., Hawkesworth, Ch., van Calsteren, P., Heath, E., Macdonald, R., Black, S., 1996. U-series isotopes and destructive plate margin magma genesis in the Lesser Antilles. *Earth and Planetary Science Letters*, 142, 191–207.
- Van der Maar, P.A., Jansen, J.B.H., 1981. *Geological Map of Greece, Island of Ios*. 1:50,000 scale. Institute of Geology and Mineral Exploration (I.G.M.E.), Athens.
- Volentik, A., Vanderkluyzen, L. Principe, C., 2002. Stratigraphy of the Caldera walls of Nisyros volcano. *Eclogae geol. Helv.*, 95, 223–235.
- Volentik, A., Vanderkluyzen, L., Rufer, D., Principe, C., Buettner, A., Hougard, L., Hunziker, J.C., 2003. Geological map of Nisyros volcano, Greece. EGS-AGU-EUG Joint Assembly.

- Vougioukalakis, G., 1993. Volcanic stratigraphy and evolution of Nisyros island. *Bulletin of the Geological Society of Greece*, 28(2), 239–258.
- Wagner, G.J., Storzer, D., Keller, J., 1976. Spaltspurendatierungen quaterer Gesteinsgläser aus dem Mittelmeerraum. *N.Jb. Miner. Mh. Jg.*, 84–94.
- Waight, T., Baker, J., Peate, D., 2002. Sr isotope ratio measurements by double-focusing MC-ICPMS: techniques, observation and pitfalls. *International Journal of Mass Spectrometry*, 221, 229–244.
- Woodhead, J.D., Eggins, S.M., Johnson, R.W., 1998. Magma Genesis in the New Britain Island Arc: Further insights into melting and mass transfer processes. *Journal of Petrology*, 39, 1641–1668.
- Woodhead, J.D., Hergt, J.M., Davidson, J.P., Eggins, S.M., 2001. Hafnium isotope evidence for ‘conservative’ element mobility during subduction zone processes. *Earth and Planetary Science Letters*, 192, 331–346.
- Wyers, G.P., Barton, M., 1989. Polybaric evolution of calc-alkaline magmas from Nisyros, southeastern Hellenic Arc, Greece. *Journal of Petrology*, 30(1), 1–37.
- Zellmer, G., Turner, S., Hawkesworth, C., 2000. Timescales of destructive plate margin magmatism: new insights from Santorini, Aegean volcanic arc. *Earth and Planetary Science Letters*, 174, 265–281.

2. Geochronology of Nisyros

Abstract

Geochronological data of Nisyros-Yali volcanic units are scarce and controversial. As the volcanic units are characterised by the absence of potassium-bearing mineral phases and the main portion of K is hosted in the volcanic glasses, ^{39}Ar - ^{40}Ar analyses of both separated glasses and plagioclase phenocrysts failed. Furthermore mineral separates and whole rock aliquots of selected volcanic units have been investigated using the U-Th disequilibrium method. Assuming an initial $^{230}\text{Th}/^{234}\text{U}$ of 0, maximum ages have been calculated. Hence, the majority of the resulting ages are again discordant to the present stratigraphy. Despite intensive and repeating investigations the Nisyros-Yali volcanic system remains undatable.

2.1 Introduction

In the following chapter geochronological experiments on volcanic units from Nisyros (Greece) are presented. The previous chapter provides a geological overview about the investigated Quaternary volcano.

Reliable age information about the easternmost section of the Hellenic arc are not well constrained. Age determinations using ^{14}C -method (e.g. Rehren 1988), fission track (Limburg and Varenkamp 1991; Wagner 1976) and K/Ar whole rock analyses (e.g. Keller et al. 1990) were performed (Table A-2-1). The latter analyses result in large discordances as use of whole rock samples in geochronology leads to discrepancies produced by the mixture of different generations like mineral phases and altered groundmass (Villa 1992). Fission track data of very young volcanic glasses provide very low track densities. It is likely that in young glass samples it is sometimes difficult to distinguish fission tracks from fluid inclusions and dislocations. Therefore, reported ages of 24 ± 10 ka (Wagner 1976) for obsidian glass from Yali (a small islet situated between Kos and Nisyros) and volcanic glasses of the post-caldera Upper pumice unit of Nisyros with an age of > 44 ka (Limburg and Varenkamp 1991) have to be considered with caution. The most reliable age constraint is provided by the ^{39}Ar - ^{40}Ar age of sanidine separates from the Kos Plateau Tuff (KPT) with 161 ± 1 ka (Smith et al. 1996). As no KPT crops out on the island of Nisyros an indirect age determination of < 161 ka for the lower age limit is possible. On the basis of ocean-floor sediment cores, tephra correlations and oxygen isotope stratigraphy, an age around 30 ± 5 ka for Yali is most plausible (Smith et al. 1996).

In the present study we combine electron microprobe analyses (EMPA) with ^{39}Ar - ^{40}Ar analyses on both mineral phases and volcanic glasses. Furthermore, U-Th disequilibrium investigations on selected phenocryst separates, such as plagioclase and magnetite as well as on groundmass separates and whole rock aliquots were performed in attempt to get information about the time interval of volcanic activity in this section of the Hellenic arc.

2.2 Analytical techniques

Plagioclase phenocryst separates (the most abundant mineral phase) and volcanic glasses from Nisyros units were separated and handpicked. The stratigraphic positions and a sample description is given in Table A-1-1 of the Appendix A. Electron microprobe analysis (EMPA) were performed on a CAMECA SX50 micropobe with the an acceleration potential of 15 kV and a beam current of 20 nA. Samples were irradiated at the McMasters research reactor (Canada) without Cd-shielding to allow for correction of additionally produced ^{38}Ar (from ^{37}Cl). The age monitor for determination of the J-value was FCT-Sanidine with an assigned age of 28.02 ± 0.28 Ma (Renne et al. 1998). Ar isotope analyses have been performed using a MAP 215-50B noble gas mass spectrometer. The isotopes of Ar were measured on a Faraday collector. Temperature steps range between 530 and 1415°C.

For U-Th disequilibrium analyses about 100 mg of the handpicked magnetite-separates, plagioclase, volcanic glass and whole rock were spiked with a mixed ^{229}Th - ^{236}U spike solution ($^{232}\text{Th}/^{229}\text{Th} = 0.0013$, $^{238}\text{U}/^{236}\text{U} = 0.001483$). Magnetite was decomposed using 6 M HCl and silicate phases been digested with a mixture of 28 N HF and 14 N HNO₃. U and Th of the diluted samples were separated according to the protocol given in Appendix B-5. Measurements of U and Th isotopes were carried out with a double focusing NU Instruments® multi-collector ICP MS at the University of Bern (Switzerland). The samples are nebulised using an ARIDUS® nebuliser with an uptake rate of 80 µL/min. U and Th analyses are carried out for a mass range from 229 to 238. Th isotopes were measured in two cycles to measure both mass ^{229}Th and ^{230}Th with the electron multiplier that has a WARP filter to reduce ^{232}Th tail to better than 0.01 ppm. Mass fractionation is monitored by adding natural U to the pure Th fraction. U isotopes are analysed separately with ^{234}U and ^{236}U on two electron multipliers. The multiplier gain was calibrated using a NIST U050 standard solution for U. A pristine pre-Pliocene uraninite from Moss (Norway) in radioactive equilibrium has been used as standard solution for the $^{234}\text{U}/^{238}\text{U}$, $^{230}\text{Th}/^{232}\text{Th}$ and $^{230}\text{Th}/^{234}\text{U}$ ratios. Its known $^{230}\text{Th}/^{232}\text{Th}$ of 0.000156 allows to calculate the multiplier gain. $^{230}\text{Th}/^{232}\text{Th}$ varies between 0.000120 and 0.000124 over the time span of several analytical sessions. The external reproducibility of each session ranges between 4 and 320 ‰. Decay constants used in this study for ^{230}Th , ^{234}U and ^{238}U are $9.165 \times 10^{-6}\text{a}^{-1}$, $2.826 \times 10^{-6}\text{a}^{-1}$ and $1.551 \times 10^{-10}\text{a}^{-1}$, respectively (Cheng et al. 2000).

2.3 Results and discussion

2.3.1 ^{39}Ar - ^{40}Ar data

^{39}Ar - ^{40}Ar data of Nisyros and Yali samples are summarised in Appendix A Table A-2-2. Samples of volcanic series of Nisyros volcano never exceed K_2O contents of 3.2 wt % (Table A-1-2; Appendix A). Potassium bearing minerals such as biotite or sanidine are not present. EMPA provide an insight into the distribution of potassium between phenocrysts and volcanic glasses. Thus, less than 0.7 wt % of K_2O is situated in the plagioclase phenocrysts whereas the main portion is concentrated in volcanic glass. The partition coefficient of potassium between feldspar and melt is, therefore, obviously less than one. Furthermore plagioclase phenocrysts can be chemically characterised with cathodoluminescence images (Fig. 1) and corresponding EMPA. Plagioclase phenocrysts of different Nisyros units reveal high anorthite contents of around 70 %. All ^{39}Ar - ^{40}Ar analysis on plagioclase separates and volcanic glass separates yield highly discordant ages (Fig. 2).

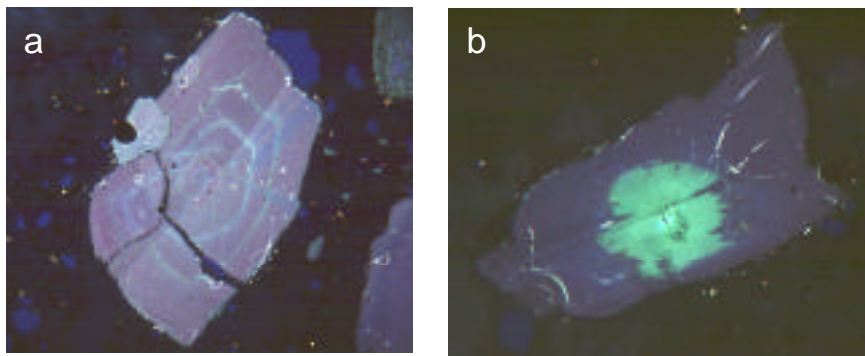


Fig. 1: CL-images of euhedral plagioclase phenocrysts of the pre-caldera (a) and post-caldera (b) pumices. The bright zones are characterised by higher Na contents, dark zones are Ca-rich.

In a three-isotope correlation plot (described in Villa, 2001) the ratios of ^{39}Ar , ^{38}Ar and ^{37}Ar produced during irradiation of K, Cl and Ca, respectively were compared (Fig. 3). As every mineral phase releases their Ar budget at certain temperatures, Ca/K and Cl/K ratios of each step provide information about the mineralogical composition. Low temperature steps are characterised by high Cl/K and low Ca/K ratios, whereas high temperature-steps release the low Cl/K - high Ca/K anorthite-generation. Cl/K and Ca/K ratios of volcanic glasses (sample NIS 19; Fig. 3) follow the same trend.

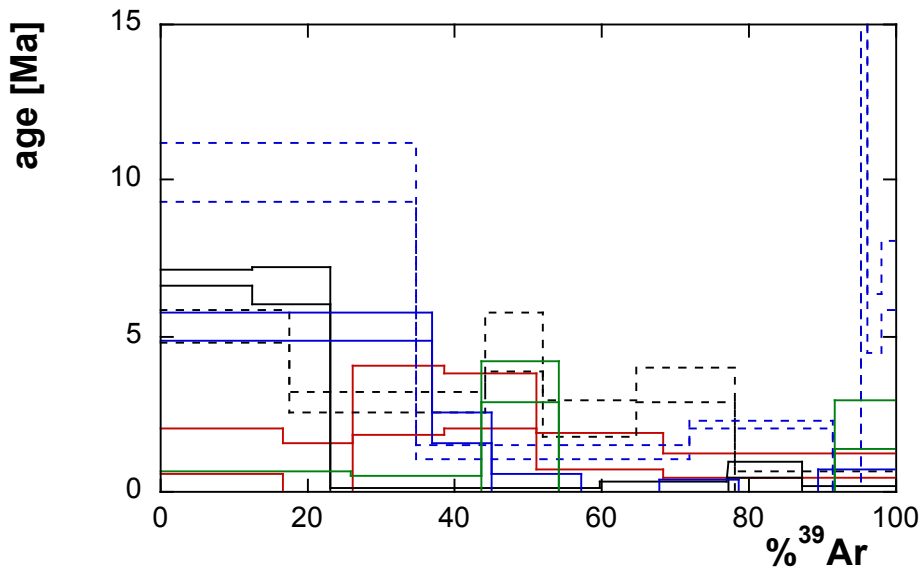


Fig. 2: Selected highly discordant age spectra of phenocryst and volcanic glass separates of Nisyros (blue dashed line = NIS 8-glass, blue solid line = NIS 8-plag., red line = NIS 12, black solid line = NIS 2, black dashed line = NIS 2a, green line = UNT.B.).

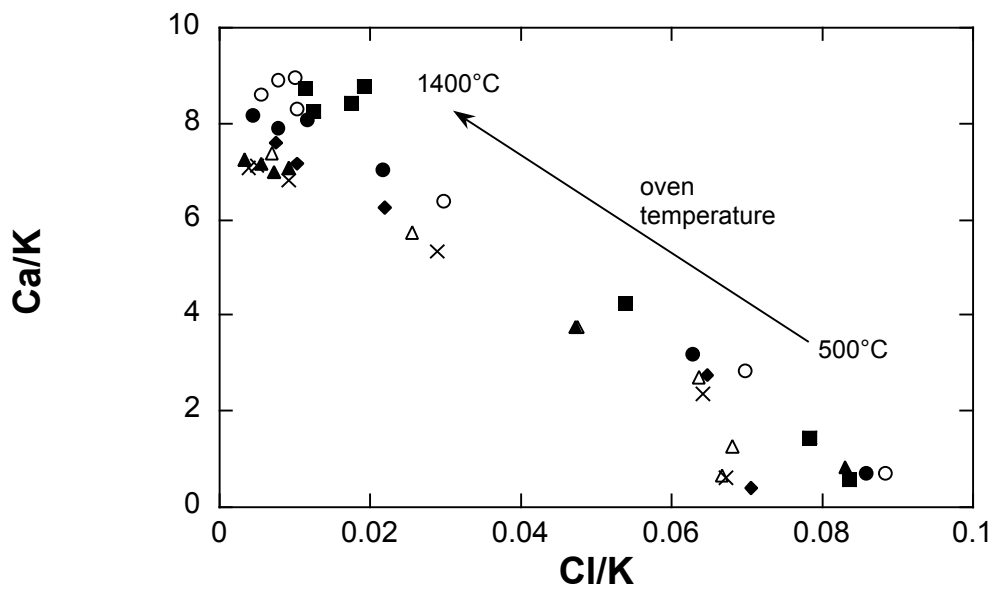


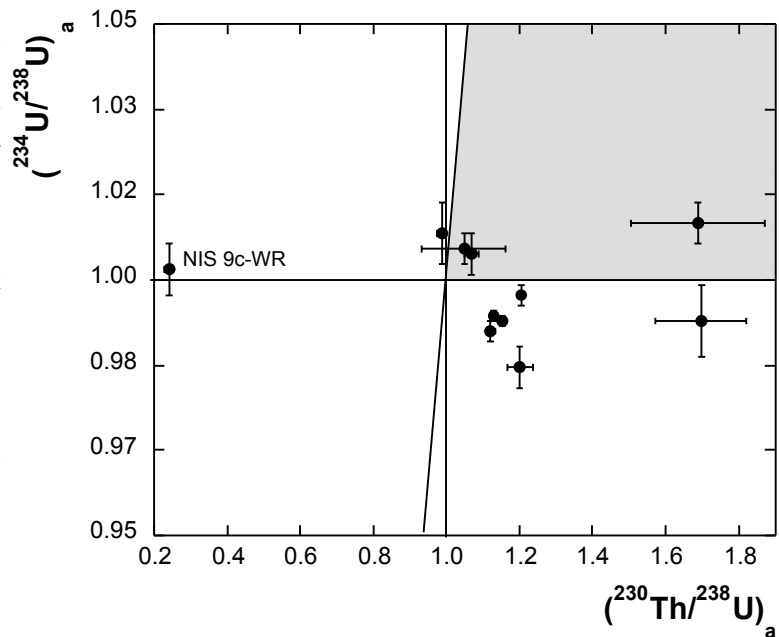
Fig. 3: Three-isotope correlation plot of plagioclase-phenocrysts. With increasing oven-temperature the amount of Ca-derived ^{37}Ar increases significantly (Symbols: \times = NIS 2, \bullet = NIS 19, \square = NIS 2a, open circle = UNT.B., open triangle = NIS 12, solid triangle = NIS 11, quadrangle = NIS 8).

^{39}Ar - ^{40}Ar investigations focussed on volcanic glasses of Nisyros units with the main K-portion have been carried out. Amorphous glasses are characterised by different sized generations of inclusions that release significant amounts of excess Ar over a wide range of temperature. Hence every temperature step is affected by an unknown quantity of excess Ar and the resulting ages are not reliable.

2.3.2 U-Th data

Table A-2-3 of Appendix A summarises all U-Th data. In the following activity ratios are denoted with an “a”. All $(^{234}\text{U}/^{238}\text{U})_a$ show only small variations scattering around equilibrium, whereas the majority of samples is characterised by $(^{230}\text{Th}/^{238}\text{U})_a > 1$ (Fig. 4).

Fig. 4: $(^{230}\text{Th}/^{238}\text{U})_a$ vs $(^{234}\text{U}/^{238}\text{U})_a$ evolution plot. The majority of the data plot in the “forbidden zone”. This is the area into which no point representing a single-stage evolution (e.g., magmatic only) can plot. Points in the forbidden zones require a two-stage history, in which post-magmatic modifications took place (e.g., U loss or Th gain). $(^{230}\text{Th}/^{238}\text{U})_a$ activity ratios vary by an order of magnitude whereas U narrowly scatters around equilibrium. Sample NIS 9c-WR exceptionally plots in the second quadrant i.e. is the only sample compatible with either a single or a two-stage evolution.



The anomalous Th/U ratios disable age calculations. The whole rock of sample NIS 9c (post-caldera dome) shows an exceptional behaviour. In a comparison of U and Th ICP-MS concentration data ($\text{U}/\text{Th} = 0.1$; Table A-1-2) with the U and Th concentrations deriving from the MC ICP-MS analyses ($\text{U}/\text{Th} = 5$), Th concentrations decrease significantly. Hence, laboratory artefacts (possibly related to HF digestion for commercial trace element analyses, with formation of insoluble ThF_4) can lead to U-Th fractionation. Moreover, the maximum age of 30 ± 2 ka for sample NIS9c-WR (calculated for a minimum initial $^{230}\text{Th}/^{234}\text{U}_a$ of 0) is in conflict with the deep-sea sediment chronology.

2.4 Conclusions

Samples from Nisyros and Yali have whole-rock K_2O concentrations up to 3.2%. It turns out that no potassic phase crystallized; phyllosilicates are absent, and feldspars are almost K-free Ca-Na-plagioclases ($K_2O = 0.3\%$, An = 70%). Glass is the only K-bearing phase. This is an extremely surprising observation, because quenched magmatic feldspars should exhibit K concentrations higher than that of the whole rock. The reason for this bizarre petrogenetic behaviour still needs to be understood. The absence of a ternary feldspar has greatly hampered the initial hopes for a straightforward ^{39}Ar - ^{40}Ar dating campaign.

^{39}Ar - ^{40}Ar analyses were performed on plagioclase separates and glasses from pumices. Plagioclases invariably gave discordant age spectra, dominated by recoil artefacts of Ca-produced ^{36}Ar . The Ca interference was predictably minor in the glass analyses; however, these glasses contained very significant amounts of microbubbles containing both chemically active gases (CO_2 , H_2S , CH_4 , etc) and erratic amounts of parentless ^{40}Ar . Parentless ^{40}Ar from Nisyros fumaroles was independently observed by Shimizu et al. (2002) and correlates with mantle $^3He/^4He$ ratios. As a result, the age spectra of the glasses did not provide a reliable chronological framework beyond a vague agreement with the independently known Late Pleistocene assignment. U-Th analyses of magnetite, plagioclase and volcanic glass separates from selected volcanic units are characterised by excessively high ($^{230}Th/^{238}U$) activity ratios caused by secondary processes, and hence are not suitable for U-Th geochronology.

References

- Barberi, F., Navarro, J.M., Rosi, M., Santacroce, R., Sbrana, A., 1988. Explosive interaction of magma with ground water: insights from xenoliths and geothermal drillings. *Rendiconti della Societa Italiana di Mineralogia e Petrologica*, 43: 901-926.
- Chabaux, F., Riotte, J., Dequincey, O. (2003). U-Th-Ra fractionation during weathering and river transport. In: Bourdon, B., Henderson, G.M., Lundstrom, C.C., Turner, S.P., Uranium-series geochemistry. *Reviews in Mineralogy & Geochemistry*, 52, 533-576.
- Cheng, H., Edwards, R.L., Hoff, J., Gallup, C.D., Richards, D.A., Asmerom, Y., 2000. The half-lives of uranium-234 and thorium-230. *Chemical Geology*, 169: 17-33.
- DiPaola, G.M., 1974. Volcanology and petrology of Nisyros Island (Dodecanese, Greece). *Bulletin of Volcanology*, 38: 944-987.
- Federman, A.N., Carey, S.N., 1980. Electron microprobe correlation of tephra layers from eastern Mediterranean abyssal sediments and the island of Santorini. *Quaternary Research*, 13: 160-171.
- Keller, J., Rehren, Th. and Stadlbauer, E., 1990. Explosive volcanism in the Hellenic Arc: a summary and review. In: Hardy, D.A., Keller, J., Galanopoulos, V.P., Flemming, N.C., Druitt, T.H. (Eds.), *Thera and the Aegean World III. Proceedings of the Third International Congress of the Volcano Thera. Santorini*, pp. 13-26.
- Limburg, E.M. and Varekamp, J.C., 1991. Young pumice deposits on Nisyros, Greece. *Bulletin of Volcanology*, 54 (1): 68-77.
- Rehren, T., 1988. *Geochemie und Petrologie von Nisyros (östliche Ägäis)*. PhD Thesis. Univ. Freiburg.
- Renne, P.R., Swisher, C.C., Deino, A.L., Karner, D.B., Owens, T.L., DePaolo, D.J., 1998. Intercalibration of standards, absolute ages and uncertainties in $^{40}\text{Ar}/^{39}\text{Ar}$ dating. *Chemical Geology*, 145: 117-152.
- Shimizu, A., Sumino, H., Nagao, K., Notsu, K., Mitropoulos, P., 2002. Noble gas isotopic compositions of gas samples from the Aegean Arc, Greece. *Geochimica et Cosmochimica Acta*, 66 (15A): A710.
- Smith, P.E., York, D., Chen, Y. and Evensen, N.M., 1996. Single crystal ^{40}Ar - ^{39}Ar dating of a Late Quaternary paroxysm on Kos, Greece: Concordance of terrestrial and marine ages. *Geophysical Research Letters*, 23(21): 3047-3050.
- Villa, I.M., 1992. Datability of Quaternary volcanic rocks: an $^{40}\text{Ar}/^{39}\text{Ar}$ perspective on age conflicts in lavas from the Alban Hills, Italy. *European Journal of Mineralogy*, 4, 369-383.
- Villa, I.M., 2001. Radiogenic isotopes in fluid inclusions. *Lithos*, 55: 115-124.
- Vougioukalakis, G., 1993. Volcanic stratigraphy and evolution of Nisyros island. *Bulletin of the Geological Society of Greece*, 28(2): 239-258.
- Wagner, G.J., Strozer, D. and Keller, J., 1976. Spaltspurendatierungen quartärer Gesteinsgläser aus dem Mittelmeerraum. *N. Jb. Miner. Mh. Jg.* 84-94.

3. Chronostratigraphy of Monte Vulture Volcano (southern Italy): ³⁹Ar-⁴⁰Ar systematics and the role of secondary processes

Annett Buettner¹, Claudia Principe² and Igor M. Villa¹

¹*Institut für Geologie, Isotopengeologie, Universität Bern, Erlachstrasse 9a, 3012 Bern, Switzerland*

²*Istituto di Geoscienze e Georisorse, CNR, via G. Moruzzi 1, 56124 Pisa, Italy*

submitted to Bulletin of Volcanology

Abstract

The eruptive history of Monte Vulture has been the subject of several geochronological investigations during the past decades. We re-analysed samples from previous works and present new data on samples from the main volcano-stratigraphic units of Monte Vulture so as to provide a consistent geochronological database.

Our chronological interpretation is based on isochemical steps, defined as steps for which the Cl/K and/or the Ca/K ratios are constant. Isochemical steps carry the isotopic signature of chemically homogeneous mineral phases and therefore allow a well-constrained age interpretation. Comparison of old and new ³⁹Ar-⁴⁰Ar data proves the analytical reliability of the irradiation and mass spectrometric analyses. Anomalous age spectra are a reproducible property of some specific samples and correlate with mineralogical anomalies. The present data establish the known interval of main volcanic activity from 740 to 600 ka, and additionally allows us to fine-tune the intermediate volcanostratigraphic syntheses of Monte Vulture. The young age of the diatremic activity of Monte Vulture area at

140 ky is confirmed by new analyses on the Lago Piccolo di Monticchio tuffisitic lapilli. Additionally, two “allochthonous” tephra layers deposited in the Ofanto fault system can now be ascribed to the Campanian Ignimbrite (around 40 ka) and to the Pomice di Base plinian eruption of Somma-Vesuvius (around 19 ka) with vent locations

100 km W of Monte Vulture, confirming both the dispersion direction of distal tephra of these eruptions and the activity time-span of the Ofanto fault system.

3.1 Introduction

Monte Vulture is a Quaternary volcano in the southeastern Apennines in southern Italy. Unlike the large Roman Comagmatic Region (RCR) volcanic complexes, which are located west of the Apennines Monte Vulture is located to the east of the main Apenninic chain and it is considered as a part of the Intramontane Ultra-alkaline Province (IUP) defined by Lavecchia and Stoppa (1996). The IUP is located at the outer eastern border of the Tyrrhenian extensional zone, to the east of the Roman Comagmatic Region and comprises the Umbria Latiun Ultra-alkaline District (ULUD) and the Monte Vulture volcano. The IUP rocks include a number of intrusions, diatremes and small volcanic centers that differ markedly from those of the more voluminous RCR. They are characterised by compositions ranging from melilite-bearing rocks, kamafugites and extrusive carbonate-rich volcanics a number of which has been emitted from Monte Vulture volcano (e.g., Stoppa and Woolley, 1997; Stoppa and Principe, 1997 and Peccerillo, 2004). The lithospheric fault system led to the production of ultra-alkaline melts and melilites originated from depths between 90 – 95 km (Lavecchia and Stoppa, 1990 and references therein).

Previous authors (e.g., La Volpe and Principe, 1991, Stoppa and Principe, 1997) divided the volcanic activity into discrete main cycles. Recent studies (Giannandrea et al., 2002; Principe and Giannandrea, 2002; Principe and Giannandrea, 2004) present a refined volcanostratigraphical profile and provide a detailed subdivision into synthem and subsynthem (Fig. 1). The Monte Vulture supersynthem led to the build-up of a strato-volcano was interrupted by an early caldera collapse that results in an overlapping of products emitted from different placed vents. Early meter-sized dykes of this supersynthem directly intruded the basement and are assigned to the Spinoritola subsynthem.

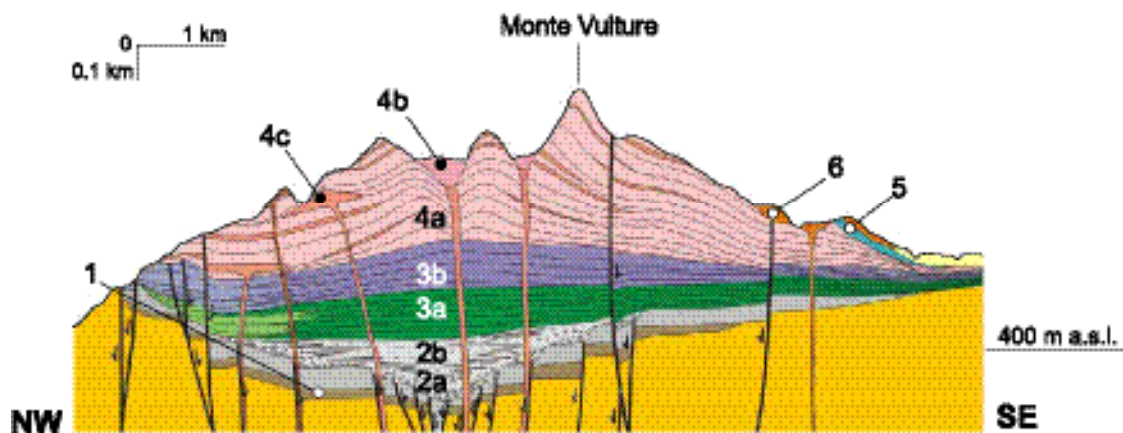


Fig. 1: Geological sketch map of Monte Vulture (simplified from Giannandrea et al., 2004). Monte Vulture supersynthem: (1) Campanile subsynthem; (2) Fara d'Olivo subsynthem, (a) epiclastics, (b) tephra; (3) Rionero subsynthem, (a) Lower series, (b) Upper series; (4) Vulture San Michele subsynthem, (a) tephra, (b) epiclastics, (c) lavas; (5) Ventraruolo Subsynthem; Monticchio supersynthem: (6) Case Lopes subsynthem.

Two large eruptions led to the deposition of the Lower and Upper Ignimbrite, grouped in the Fara d'Olivo subsynthem. The Barile synthem is characterised by the intrusion of the Toppo San Paolo lava dome and by repeated discrete explosive eruptions, which resulted in the cone-building phase. The main volcanic activity ends with the effusion of lavas and pyroclastics (Vulture San Michele subsynthem) and with phreatomagmatic eruptions (Ventaruolo subsynthem). A spatially isolated small lava flow of peculiar composition (Melfi hauynophyre: Hieke Merlin, 1967) is assigned to the Melfi synthem, that concludes the Monte Vulture supersynthem. After a period of quiescence volcanism was re-activated (Lago di Monticchio supersynthem) and resulted in the tectonic dismembering of the previously built volcanic edifice, by means of the scythe-fault system of Valle dei Greggi-Fosso del Corbo. This fault system caused in a sinking of the southern half of the Vulture edifice (La Volpe and Principe, 1991) and in the collapse of its SW portion (Principe and Giannandrea, 2002). During the Lago di Monticchio supersynthem mainly monogenetic eruptions from scattered centres, positioned along the active fault systems (Schiattarella et al., 2004), occurred and led to the formation of diatremic structures, two of them forming the Monticchio Lakes (Fig. 1).

Pyroclastic units and lava flows of Monte Vulture range in composition from trachytes to foiditic trachytes and phonolites (e.g. Melluso et al., 1996). One of the better known mineralogical feature of Monte Vulture volcanics is that they contain peculiar phases like melilite and a number of feldspatoids such as leucite, nepheline and sodalite-group minerals. Final maar-type craters are fed by carbonate-rich, melilitite bearing magma (Stoppa and Principe, 1997). Carbonate globules (Rosatelli et al., 2000) and mantle xenoliths (Solovova et al., *subm.*; Downes et al., 2002; Jones et al., 2000) have been found at different stratigraphical levels interbedded in the deposits related to the explosive activity of Mount Vulture volcano.

During the past three decades several authors present geochronological data (Tab. A-3-1) to provide a chrono-stratigraphy of Monte Vulture. After the K-Ar analyses of Cortini (1975), only ^{39}Ar - ^{40}Ar work was performed (Villa, 1985, 1988, 1991, Brocchini et al., 1994 and Bonadonna et al., 1998). The latter studies broadly constrain the main volcanic activity of Monte Vulture, but with significant discrepancies.

Data presented in Brocchini et al. (1994) and Bonadonna et al. (1998) were calculated using an assumed age of 27.55 Ma for the Fish Canyon biotite monitor; the Renne et al. (1998) value of 28.02 Ma results in an elevation of ages by 2%. Furthermore, ages published by Bonadonna et al. (1998) were expressed as isochron calculations. It should be noted that isochrons (correlation of $^{36}\text{Ar}/^{40}\text{Ar}$ and $^{39}\text{Ar}/^{40}\text{Ar}$) mostly do not consider the possible presence of non-cogenetic generations in a mineral separate (Villa, 1992). An alignment of data points alone does not guarantee that a single, monogenetic phase was analyzed (Villa, 2001), and chemical correlation diagrams are required (see below). We recalculated nine ages published by Brocchini et al. (1994) and Bonadonna et al. (1998) on the basis of the raw data contained in the thesis by Brocchini (1993).

According to petrological investigations by De Fino et al. (1986) Vulture volcanics might be affected by interaction with high-temperature H_2O -rich and/or CO_2 -rich fluids, resulting in partial or complete transformation of primary mineral phases. Hence, most of the analysed minerals represent multiphase systems and are therefore likely to record perturbed ^{39}Ar - ^{40}Ar systematics. Additionally, Ar systematics can likewise be influenced by the complex processes that commonly impact on the generation

of carbonate-rich and melilitolitic magmas which result in zonation and multi-stage phase generation (Solovova et al., *subm.*; Di Muro et al., *subm.*). Finally, expansion of mineral lattices can occur during water-melt interaction, hydrothermal mineral alteration and/or weathering, causing cation exchange and, in particular, analcimization of leucite.

We focus on these mineral heterogeneities and present a combination of mineralogical investigations and ^{39}Ar - ^{40}Ar analyses on different K-bearing phases to address the influence of mineral complexity on ^{39}Ar - ^{40}Ar systematics. Six minerals analyzed in this study were leftover material from previous investigations (**VUT 110, 168, and 251**; **VU 1680, 1813 and 1907**: Tab. A-3-2). A direct comparison with published data allows an assessment of external reproducibility. In some cases, the recalculation of published ages is required, as the irradiation monitor ages have been subsequently revised (Renne et al., 1998). Furthermore, our approach to mixtures of pristine and altered mineral domains led us to a different choice of steps for regression relative to those published by previous authors (see the discussion below). We observe that in most cases this does not greatly change the estimated ages; we also observe a very tight reproducibility both amongst new and old sample preparations, and in the shape of the age spectra.

3.2 Analytical techniques

Rocks were crushed and sieved; selected size fractions (100-150 μm up to 250-350 μm) were all separated using magnetic and density separation at the I.G.G. facilities in Pisa. Separations were performed during three peak activity periods: prior to 1985, in 1992-1993, and in 2002. Separates for the present work were irradiated at the McMasters Research Reactor (Canada) without Cd-shielding. To calculate the J value, Fish Canyon sanidine (FCs) with an assigned age of 28.02 Ma (Renne et al. 1998) was used as irradiation monitor. The ^{39}Ar - ^{40}Ar analyses were performed on a MAPTM 215-50B noble gas mass spectrometer using incremental heating technique. A detailed description is given in Villa et al. (2000). All isotopes were measured on the Faraday collector. Data are shown in Table A-3-3; all errors are given as 1 standard deviation.

Cathodoluminescence (CL) images were performed on both, thin sections and single grain mounts. Element mapping and back-scattered electron (BSE) images were carried out using a Cameca SX-50 electron microprobe (EMP) with an acceleration voltage of 15 kV and a beam current of 50 nA. All facilities are situated at the University of Bern (Switzerland).

3.3 Mineralogy

We focus on K-bearing phases, namely sanidine, leucite, biotite and phlogopite that were separated from numerous volcanic units. Mineralogical observations based on CL and BSE images provide an insight into microchemical and crystallographic characteristics of the mineral. Element mapping provides quantitative information about the distribution of selected elements.

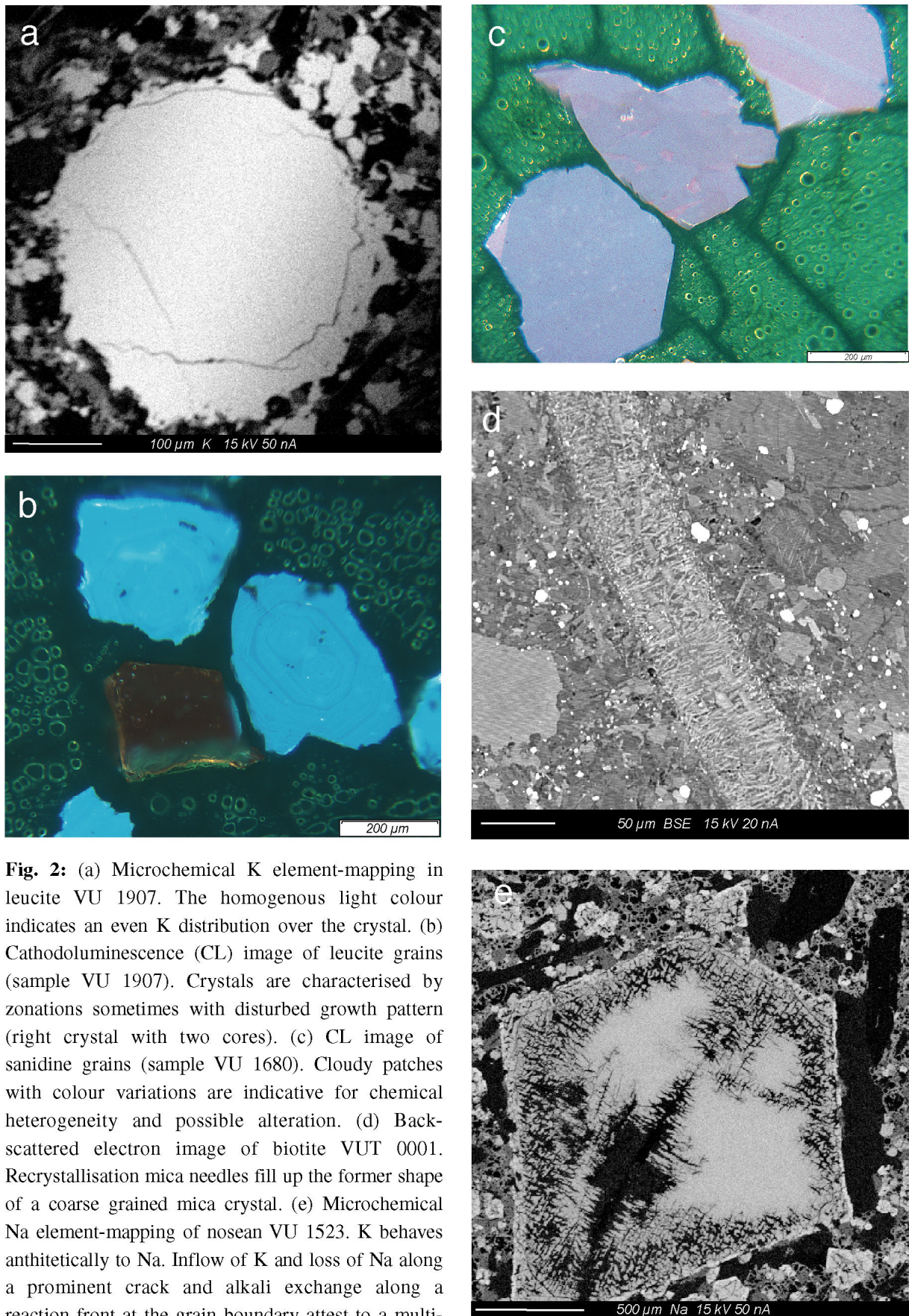


Fig. 2: (a) Microchemical K element-mapping in leucite VU 1907. The homogenous light colour indicates an even K distribution over the crystal. (b) Cathodoluminescence (CL) image of leucite grains (sample VU 1907). Crystals are characterised by zonations sometimes with disturbed growth pattern (right crystal with two cores). (c) CL image of sanidine grains (sample VU 1680). Cloudy patches with colour variations are indicative for chemical heterogeneity and possible alteration. (d) Back-scattered electron image of biotite VUT 0001. Recrystallisation mica needles fill up the former shape of a coarse grained mica crystal. (e) Microchemical Na element-mapping of nosean VU 1523. K behaves antithetically to Na. Inflow of K and loss of Na along a prominent crack and alkali exchange along a reaction front at the grain boundary attest to a multi-stage alteration history.

3.3.1 *Leucite*

Nearly euhedral white leucite crystals were checked for their purity using EMP element mapping and CL images. The phenocrysts of sample **VU 1907** from the Vulture San Michele subsynthem are chemically homogeneous and exhibit a uniform K distribution (Fig. 2a). According to De Fino et al. (1986) the leucites of Vulture are frequently deeply altered and replaced by analcime, evidenced by high Na concentrations. Leucite **VU 1907** has a K₂O content of 20 wt%, i.e. slightly below the expected stoichiometric value of 21.6%. CL shows growth zonation of the crystals and sporadic light blue patches (Fig. 2b), which might be related to the small stoichiometric disturbance. Ca and Cl were below detection limits (ca. 100 ppm).

3.3.2 *Sanidine*

Optical microscope observations of subhedral sanidines that are embedded in a porous rock matrix show mottled textures indicative for secondary reactions. K₂O contents average around 13 wt% and only in one case (sample **VUG 1**) it is below 10 wt%. CL images of sanidine **VU 1680** (Fig. 2c) reveal pink-purple patches that are a likely effect of a disturbance within the lattice of the mineral (Ramseyer pers. com.).

3.3.3 *Biotite*

Biotite phenocrysts are brown to dark brown and generally subhedral. Biotites of sample **VUT 0001** (Fig. 2d) show tiny recrystallization needles pseudomorphosing the former coarse-grained crystal. BSE images of some biotites analysed by ³⁹Ar-⁴⁰Ar show no obvious disturbances, but the K₂O content is between 5 and 8 wt%, clearly non-stoichiometric. The presence of secondary phases like chlorite is probably responsible for low K₂O contents in all investigated samples. These phases are not visible in BSE images but an interlayering of biotite and chlorite has been shown to occur at the nm scale (DiVincenzo et al. 2003), much below the spatial resolution of the EMP.

3.3.4 *Phlogopite*

Phlogopite is present along the whole stratigraphic sequence, frequently associated with biotite. Some phlogopite phenocrysts exhibit opaque rims enriched in Ti (Melluso et al., 1996) indicative of a reaction. Calculated K₂O contents of phlogopite range between 8 and 11wt%, confirming the importance of reactions.

3.3.5 *Mineralogy from Ar isotope systematics*

Our mineralogical observations have documented that several samples consist of mixtures intergrown at the 10 µm scale. In order to unravel the Ar systematics, one can apply three-isotope correlation plots such as described e.g. by Villa (2001). The irradiation of K, Cl and Ca produces isotopes ³⁹Ar, ³⁸Ar and ³⁷Ar, respectively. Because alteration phases and magmatic minerals release Ar at different oven temperatures (Villa et al., 2000), the Cl/K and Ca/K ratios of every step give information on the mineral, which underwent *in vacuo* breakdown during each step. By complementing the Ar-data with CL and BSE images

we can confirm the mineralogical heterogeneity and identify the Ca/K and/or Cl/K ratios of the unaltered phase, which we wish to date.

3.4 ^{39}Ar - ^{40}Ar results

The complete dataset of ^{39}Ar - ^{40}Ar analyses is composed in Table A-3-3. All stratigraphically reliable ages are furthermore summarised in Table A-3-4. As a general remark, it should be noted that the uncertainties of isochrons and averages are larger than that of individual steps. This is an effect of the scatter of the datapoints, itself an effect of the samples' mineralogical complexity. Furthermore the sheet silicates of Monte Vulture (biotites and phlogopites) are characterised by overall non-stoichiometric K contents. Sub-continental phlogopite retain a substantial amount of “parentless ^{40}Ar ” (Wartho and Kelley, 2003). Therefore, the chronological information provided by mantle-derived phlogopites is dubious. We present the Ar analyses of these mineral phases mainly for reasons of completeness. The chronological discussion will be hereafter based on the more reliable results provided by feldspars. The discussions of mica data were omitted when feldspars or foids were available.

Table A-3-3 contains the complete dataset; only those steps that reflect an isochemical reservoir (see discussion below) were used for isochron and average calculations and are marked by an asterisk. In the following we present samples in stratigraphical order.

3.4.1 *Spinoritola subsynthem*

A dyke from this unit, was analyzed a total of three times: an acid-leached sanidine (Villa, unpublished data, 1988, re-evaluated here), Bonadonna et al. (1998) and in this work.

Bonadonna et al. (1998) present an isochron age of 674 ± 7 ka for sample **VUT 110**. The original data (Brocchini, 1993) show some chemical heterogeneity with Ca/K between 0.045 and 0.37 and Cl/K between 0.0014 and 0.0126. This heterogeneity recommends against a regression of different, possibly non-cogenetic phases. We recalculated an isochron only on “isochemical” steps (i.e. steps having constant chemical indicators) and obtained an age of 694 ± 8 ka (1 error), using the updated monitor age (see above).

Villa (unpublished, 1988) rinsed sanidine **VU 110** with diluted HF (hereafter **VU 110L**; presented here in Table A-3-3) to get rid of visible alteration. However, no ^{37}Ar and ^{38}Ar data were acquired, disabling chemical correlations. We, therefore, focus on gas-rich steps, which provide an almost flat spectrum averaging 678 ± 9 ka. We presume that the leached fraction was mostly alteration-free and that its age represents that of the sanidine *sensu stricto*.

Our analysis was performed on **VUT 110 A**, a minute leftover of the same fraction analyzed by Bonadonna (1998). However, the chemical composition of **VUT 110 A** (K = 7.3%, Cl = 96 ppm, Ca = 0.2%) is unlike that of the Bonadonna (1998) analysis (K = 9%, Cl = 202 ppm, Ca = 0.5%). The heterogeneity of two powder aliquots from the same container is a likely electrostatic effect of plastic sample vials. From steps 2 to 8 with low Ca and Cl we calculated an isochron age of 694 ± 48 ka and an initial $^{40}\text{Ar}/^{36}\text{Ar}$ ratio of 339 ± 31 , significantly different from the atmospheric value. Therefore individual step ages are not very reliable.

Sanidine **VUG 1** derives from a further dyke of the Spinoritola subsynthem. This sanidine is low in K_2O with a variable but high Cl content (288 ppm; Tab. A-3-3). Again, the age spectrum shows internally discordances. As the presence of Cl is indicative for alteration phases that affected the sanidine, we chose the chemically most homogeneous, low Cl-steps and provide an average estimate of 698 ± 25 ka for this sample. In summary, the four analyses (VUT 110 and VUG 1) concordantly indicate an age of 687 ± 8 ka.

The mafic dykes intruding the sedimentary basement give reproducibly younger ages than the ignimbrites (see below) containing mafic microenclaves. The lithic microinclusions were not directly dated. It is likely that small volumes of mafic magmas were repeatedly produced – some at the very beginning of Monte Vulture activity, and some about 50 ka later. Thus the duration of the Spinoritola subsynthem overlaps with that of the Fara d’Olivo subsynthem.

3.4.2 Fara d’Olivo subsynthem

This subsynthem contains two large ignimbrite deposits, Lower and Upper Ignimbrite. For the Lower Ignimbrite two sample analyses are available: **VU 1809** (Villa, unpublished data, 1988, reevaluated here) and **PG5** from a different outcrop. Two samples of the Upper Ignimbrite have been analyzed a total of five times: **VU 1813 P** (handpicked single sanidine grains from a pumice), **VU 1813 T** (sanidine from the whole rock), **VU 1813 L** (fraction T leached with diluted HF), **VU 1813 A** (50 mg from fraction T analyzed in this study) and sanidine from sample **VUT 9905** (this work).

The age spectrum of sanidine from sample **VU 1809** exhibits an almost flat spectrum with a slight saddle shape (Villa, 1988). An average of 6 gas-rich steps (containing 72% of the total Ar) provides an age of 738 ± 11 ka. For sanidine **PG5** from the same stratigraphic unit we have chemical information via the Cl/K and Ca/K ratios showing a remarkable inhomogeneity (probably due to the lack of manual separation). The weighted average of “isochemical” steps provides an age of 744 ± 9 ka which is indistinguishable from VU 1809. An isochron of gas-rich steps from both sanidines (justified by their identical magma source) gives an age of 726 ± 11 ka with an atmospheric intercept of 297 ± 2 and an MSWD of 1.7. Therefore, the use of weighted averages of steps is legitimate and we consider 736 ± 10 ka as the best estimate of the sanidine age. The ^{39}Ar - ^{40}Ar analysis of the PG5 phlogopite offers the comparison with the coexisting sanidine. In a Cl/K-age correlation diagram (Fig. 3) a linear trend for gas-rich steps 6-9 shows only a slight ($< 5\%$) chemical heterogeneity of this phlogopite. The average age of steps 4-9, having Cl/K between 0.00235 and 0.00247, is 746 ± 15 ka, correspond to an isochron with atmospheric intercept, and are in excellent agreement with the sanidine age.

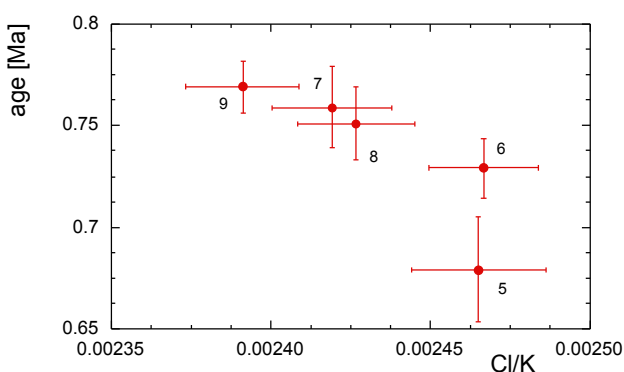
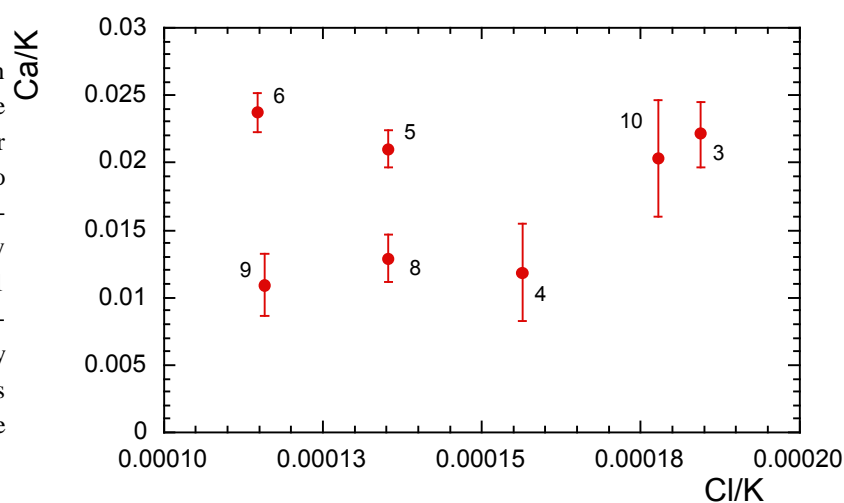


Fig. 3: $^{38}Ar_{Cl}/^{39}Ar_K$ vs $^{40}Ar^*/^{39}Ar_K$ plot of phlogopite PG5 (Lower Ignimbrite, Fara d’Olivo subsynthem). Steps 6 to 9 define an array with negative slope, indicative of a slight chemical heterogeneity. These steps correspond to an isochron with atmospheric intercept; the age of 742 ± 15 ka is close to the more precise sanidine grand average age of 736 ± 10 ka.

In a comparison of the two large ignimbrites of the Fara d'Olivo subsynthem the stratigraphically younger Upper Ignimbrite gives slightly older step ages than the Lower Ignimbrite. According to Villa (1988) the three fractions of sanidine **VU 1813 (P, T, L)** are characterised by the presence of $^{40}\text{Ar}_{\text{xs}}$ and show similar saddle-shaped spectra. A regression through the original data gives no acceptable isochron; as at that time the ^{37}Ar and ^{38}Ar were not acquired, it is impossible to evaluate the chemical identity of reservoirs and thus to calculate an average of "isochemical" steps. Nevertheless, the isochron diagram clearly shows a trapped Ar with an enriched $^{40}\text{Ar}/^{36}\text{Ar}$ ratio and confirms the presence of $^{40}\text{Ar}_{\text{xs}}$.

Sanidine of sample **VUT 9905** was separated from selected pumice pieces. Its age spectrum shows internal discordances. Gas-rich steps seem to be chemically almost uniform (Fig. 4).

Fig. 4: Chemical correlation diagram (Cl/K vs Ca/K) of sanidine **VUT 9905** from the Upper Ignimbrite of the Fara d'Olivo subsynthem. Seven among the gas-rich steps exhibit a chemically uniform composition, with $0.0001 < \text{Cl/K} < 0.0002$. They give an isochron age of 755 ± 21 ka, whereby excess Ar is present. This age is indistinguishable from that of the Lower Ignimbrite.



The isochron with a $^{40}\text{Ar}/^{36}\text{Ar}$ ratio of 348 ± 20 gives an age of 755 ± 21 ka. Sample **VU 1813 A** represents sanidines that were left over from sample VU 1813 T of Villa (1988). An isochron through six gas-rich steps gives 781 ± 29 ka with a non-atmospheric $^{40}\text{Ar}/^{36}\text{Ar}$ initial ratio of 314 ± 18 . It is further possible to plot all analyses of the Upper Ignimbrite in one isochron diagram. The resulting regression has excess scatter, and chemical criteria are not available for the 1988 analyses; however, the evidence for excess Ar is robust, and most fits through arbitrary subsets of the data always produce ages not far from 740 ka. In summary, all sanidines from the Upper Ignimbrite are characterised by significantly non-atmospheric trapped Ar. Isochrons give ages similar to the Lower Ignimbrite.

3.4.3 Rionero subsynthem

Sanidine **VU 1680 A** was a leftover from the sample used by Villa (1988) and Brocchini et al. (1994) and derives from a fallout deposit of the Masseria Boccaglie plinian eruption in the Rionero subsynthem. This sample is characterised by a very high Cl concentration (710ppm). Moreover, the Ar was released between 550 and 820°C, i.e. at much lower temperatures than all other sanidines (Table A-3-3), reproducing the 1988 pattern. Both these observations concordantly indicate that the structure of the **VU 1680** sanidine was heavily damaged during alteration and chlorination. This feature probably results in

the patchy appearance visible in the CL-image (Fig. 2c). Coexisting leucite is analcimized (Villa, 1988) and was not re-analyzed. The age spectrum is discordant. In a Cl/K vs Ca/K graph, a group with lowest amounts of Cl and Ca (steps 3 to 5) can be discriminated from steps having up to 2 orders of magnitude higher Cl/K ratios. The isochron through the three low Cl-steps results in no age as the regression line is horizontal. The step ages suggest an age 720 ± 30 ka, in agreement with the older estimate $t = 650$ ka (Villa, 1988) and $t = 660$ ka (Brocchini et al. 1994).

Two ^{39}Ar - ^{40}Ar analyses of other pyroclastic units of the Rionero subsynthem were published in Bonadonna et al. (1998). Our recalculation based on isochemical steps gives ages of 668 ± 6 ka and 626 ± 20 ka, respectively, bracketing the age of VU 1680 obtained in this study.

Sanidine **VUT 0002** derives from a different position of the same pumice fall deposit as the previous sample of the Rionero subsynthem. It provides an isochemical low Ca/K, low Cl/K group of steps 2 to 5 (containing 63 % of the total gas) with an average of 710 ± 18 ka. This estimate is indistinguishable to the our analysis of VU 1680.

3.4.4 Vulture San Michele subsynthem

We analysed a total of four samples of this subsynthem, phlogopite/biotite **VUT 9919**, **VUT 9923** and **VUT 9918** and leucite **VU 1907 A**. In the following we focus only on one phlogopite (**VUT 9918**) as a representative for this complex mineral group and on the leucite.

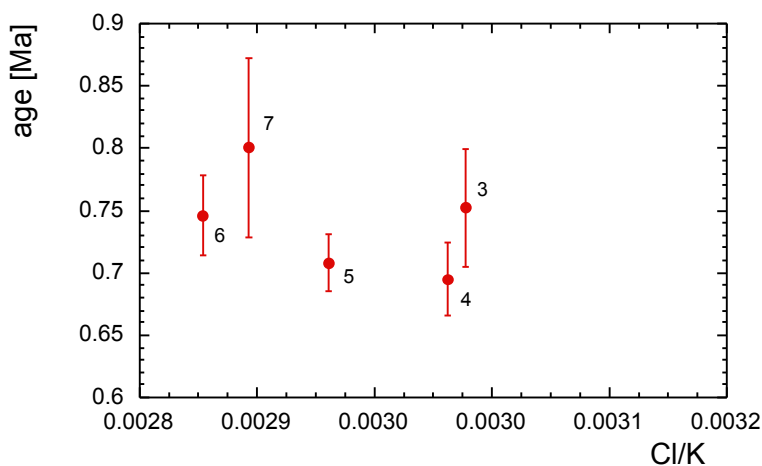


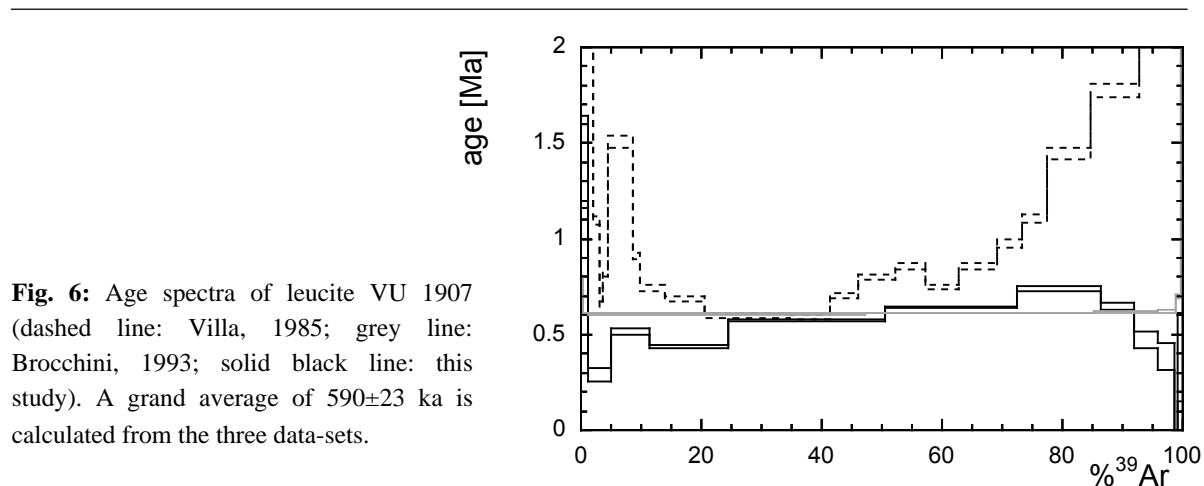
Fig. 5: $^{38}\text{Ar}_{\text{Cl}}/^{39}\text{Ar}_{\text{K}}$ vs $^{40}\text{Ar}^*/^{39}\text{Ar}_{\text{K}}$ diagram of phlogopite **VUT 9918** (Vulture San Michele Subsynchronism) with an anticorrelation between ages and Cl/K ratios. The age information provided by the lowest step age is still affected by excess Ar of possible mantle origin.

Sample **VUT 9918** derives from a small lava flow that represents the final event of an eruptive sequence of a small scoria cone. This cone is situated at the top of the stratigraphical sequence of the Vulture San Michele subsynthem. A phlogopite separate reveals a massively sub-stoichiometric K concentration and accordingly a staircase-shaped ^{39}Ar - ^{40}Ar spectrum. It is important to understand the petrological meaning of such a pattern. Staircase-shaped age spectra are not indicative of a concentric Ar zonation such as could result from diffusive Ar loss, as the combined laser-oven analysis of zoned biotites gave a flat age spectrum (Hodges et al., 1994). Instead, staircases have been documented both in the case of alteration (Hess et al., 1987) and in the case of unaltered mixed generations (Villa et al., 1997).

Focussing on gas rich steps, 4 to 7, an anticorrelation between Cl/K-ratio and corresponding ages is visible (Fig. 5). This implies that ^{39}Ar recoil into chlorite has no influence on this sample. The anticorrelation in Figure 5 indicates the presence of two phases. The calculation of isochron may therefore combine non-cogenetic systems. The lowest step age is 691 ± 25 ka. A mantle origin is very likely for these huge phlogopite xenocrysts (Stoppa and Principe, 1997; Jones et al., 2000; Downes et al., 2002) and hence, it is not surprising that this sample should give so unreliable age.

Leucite of sample **VU 1907** derives from one of the stratigraphically youngest lava flows of the San Michele subsynthem. This sample has been analysed three times (Villa, 1985; Brocchini, 1993; this study, labeled as **VU 1907 A**). Figure 6 presents a combination of all spectra. According to a recalculation of the data by Brocchini (1993), the average of steps 4 to 6 of the near flat spectrum provides an age of 607 ± 6 ka. This age is in agreement with the gas-rich step 11 of the analysis by Villa (1988) yielding a step age of 598 ± 12 ka.

Sample **VU 1907 A** reveals a nearly stoichiometric K_2O content of 20 wt% and shows a discordant, hump-shaped age spectrum (Fig. 6). The Ca/K and Cl/K ratios are linearly correlated, indicative of a binary mixing. The phase with low Ca/K and low Cl/K ratios has the typical chemical signature of leucite; the second phase is not easily identified. The bulk separate has a K concentration close to the stoichiometry of leucite, and a total Cl concentration of 69 ppm. Mass balance implies that “non-leucite” phase is either volumetrically minor (and thus has high Cl and Ca concentrations) or it is itself a high-K phase. Our CL images on few selected grains (Fig. 2a) show no inhomogeneous K distribution, no alteration, and no extraneous phase. Step ages show no correlation to the chemical indicators. We will consider the step with the lowest Cl/K ratio and an age of 571 ± 6 ka to most closely approximate the leucite *sensu stricto*. We further compare it to the minimum age of Villa (1985), 598 ± 12 ka, and the recalculated average age of the low Cl/K and low Ca/K steps of Brocchini (1993), 611 ± 12 ka.



The isochron regression through 27 steps from the three analyses abovementioned shows no significant non-atmospheric intercept; the age of 590 ± 12 ka corresponds to a high MSWD of 18, but because of the atmospheric intercept it is still likely to accurately date the eruption.

3.4.5 *Castello di Melfi subsynthem*

Subsequent to the build up phase of the stratovolcano a small lava flow with a peculiar mineral assemblage (Melfi hauynophyre, Hieke Merlin, 1967) was extruded along a NW-SE trending fault. The original leucite sample (**VU 1523**) analysed by several authors is no longer available. A colourless noseane hardly distinguishable from leucite was, therefore, mistaken for leucite and the texture of the analyzed mineral shows secondary replacement. Hence, the ^{39}Ar - ^{40}Ar analysis failed. According to the geochronological analyses of Villa (1991) this leucite separate of the hauynophyre (**VU 1523**) results in an age of 565 ± 4 ka. After recalculation of the J-value and averaging of the gas rich, isochemical steps from data presented in Bonadonna et al. (1998) the leucite results in a similar age of 573 ± 4 ka.

3.4.6 *Case Lopes subsynthem*

After a period of volcanic quiescence that lasts for several ten thousands years (evidenced in the deposition of a thick paleosol, M18) volcanism was reactivated as a result of an intensive volcano-tectonic activity (Brocchini et al., 1994). Biotite separate of sample **VUT 168** from a scoriae deposit which is related to the volcanic re-activation subsequent to the tectonic event that created the scythe-fault system of Valle dei Greggi-Fosso del Corbo provides a saddle-shaped age spectrum. In a three isotope correlation plot (Fig. 7) the trajectory of datapoints defines two different temperature-dependent regions.

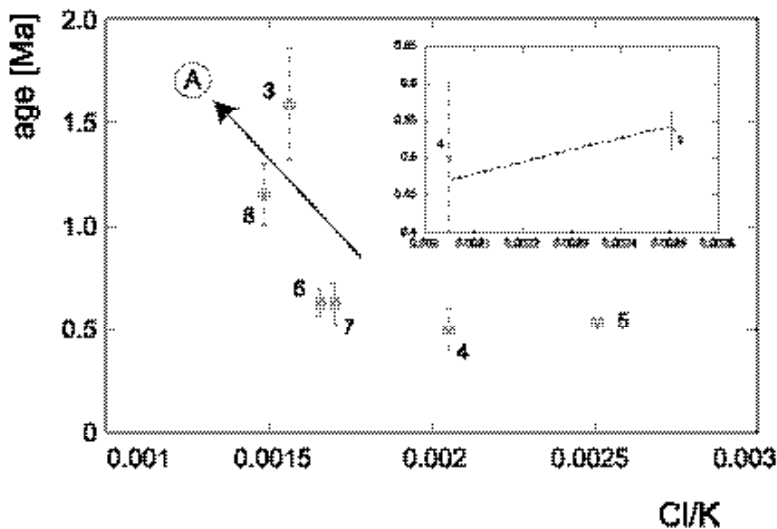


Fig. 7: $^{38}\text{Ar}_{\text{Cl}}/^{39}\text{Ar}_{\text{K}}$ vs $^{40}\text{Ar}^*/^{39}\text{Ar}_{\text{K}}$ plot of biotite **VUT 168** (Case Lopes subsynthem) exhibit a temperature-dependent evolution path (denoted as A) for Cl/K and $^{39}\text{Ar}_{\text{K}}$. It describes the alteration phases with low $^{38}\text{Ar}_{\text{Cl}}$ degassed below 700 and above 900°C. The dashed line shown in the inset is the effect of recoil in sub- μm biotite/chlorite intergrowths. A 15% recoil of ^{39}Ar out of biotite and its reimplantation in chlorite produces a 20% variation range both in the x-values and in the y-values, which simulates a positive correlation. Steps 4 and 5 are compatible with such a biotite-chlorite intergrowth.

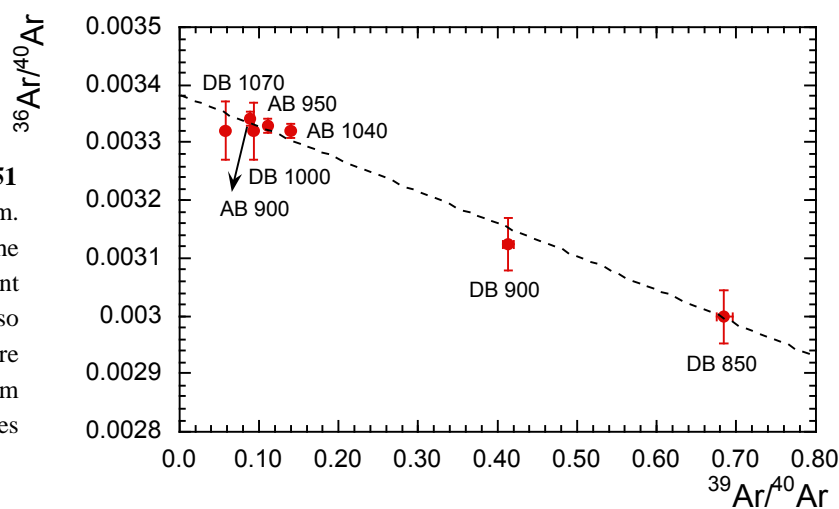
Path A between step 3 and step 5 (corresponding to 715°C – 870°C) results in a negative slope, whereas the path B between step 5 and step 8 (870°C up to 1070°C) provides a positive slope. This pattern might be the result of recoil-dependent redistribution of $^{39}\text{Ar}_{\text{K}}$ and $^{38}\text{Ar}_{\text{Cl}}$ during irradiation of the sample (Di Vincenzo et al., 2003). Path A reflects enrichment in both isotopes while $^{38}\text{Ar}_{\text{Cl}}$ prevails

compared to $^{39}\text{Ar}_K$. Thus, low temperature steps release the chlorite-phase that is enriched in recoil-derived $^{39}\text{Ar}_K$ whilst during high temperatures Cl/K ratios strongly decrease with increasing ages. This path B probably reflects the degassing of the biotite-phase, while its ages have to be considered as maximum estimates. Lo and Onstott (1989) already discussed the disturbance of age spectra of biotite which is randomly intercalated with chlorite. The loss of $^{40}\text{Ar}^*$ as well as K during chloritisation reactions combined with ^{39}Ar recoil deduced from neutron irradiation hamper an age estimation. An age-calculation based on the total amount of $^{40}\text{Ar}^*$ and ^{39}Ar (total fusion age) results in a completely discordant age of 879 ka. However, considering the weighted average of steps 4 and 5 that lie on the “chlorite-biotite line” (the line with a positive slope in the $^{38}\text{Ar}_{\text{Cl}}/^{39}\text{Ar}_K$ vs $^{40}\text{Ar}^*/^{39}\text{Ar}_K$; Fig. 7, inset) suggests a maximum estimate of $530\pm 22\text{ka}$. It must be emphasized that this estimate has a much lower reliability than all other isochron and isochemical ages of the present work, even if it is similar to the recalculated (but not chemical correlatable) estimate of Brocchini (1993) providing an average of gas-rich steps at $494\pm 5\text{ka}$.

3.4.7 Lago Piccolo and Lago Grande subsynthem

After a period of volcanic inactivity a sequence of isolated diatremic events occurred. Two of which led to the formation of the maar-type vents and the eruption of a suite of carbonate-rich, melilitic volcanites (Stoppa and Principe, 1997). Independent age constraints on the formation of the lakes are very scant: they post-date the collapse of the volcanic edifice (ca. 0.53 Ma: preceding section) and pre-date counted varve deposition in the lake sediments (ca. 0.07 Ma: Narcisi, 1993, and references therein).

Fig. 8: Isochron of sample **VUT 251** from the Lago Piccolo subsynthem. Three points labelled AB are the isochemical steps from the present work; oven temperatures are also indicated. Four points labeled DB are the isochemical steps selected from Brocchini (1993); oven temperatures are seen to be coincident.



The mm-sized biotite crystals of sample **VUT 251** derives from the most external shell of the tuffisitic lapilli that represent the juvenile fraction of the Lago Piccolo deposit. Corresponding to the micas of sample VUT 0008 (see below) the biotite is characterised by $^{40}\text{Ar}/^{36}\text{Ar}$ ratios around 300, close to the atmospheric composition. The K concentration, 6.7%, is higher than that of VUT 0008, but still not stoichiometric, indicating a detectable alteration. The absolute ^{36}Ar concentration of $2 \times 10^{-8}\text{ mL/g}$ is

identical to that of VUT 0008 (Table A-3-3), reinforcing the indication that diatreme phlogopites contain an alteration phase rich in trapped Ar. The chemical indicators, Ca/K and Cl/K, identify the degassing of “isochemical” phlogopite *sensu stricto*, corresponding to $\text{Ca/K} < 0.05$ and $0.0021 < \text{Cl/K} < 0.0024$, at oven temperatures between 900 and 1040 °C. Isochron regression of the 900-1040 °C steps gives ca. 100 ka, with an atmospheric intercept.

Brocchini (1993) presents data for a powder aliquot of this sample (hereafter coded as **VUT 251 DB**). Our reanalysis of the original data (Brocchini, 1993) in context with our own data allows a reliability assessment. The K concentration of **VUT 251 DB** can be calculated as 7.8 %, indicating a more thorough separation from alteration than was achieved in **VUT 251 AB**. All measured $^{40}\text{Ar}/^{36}\text{Ar}$ ratios are < 330 , again confirming the dominating role of trapped Ar. The Ca/K vs. Cl/K discrimination identifies the four steps between 850 and 1070 °C as the “true” phlogopite ($\text{Ca/K} < 0.02$, $0.0025 < \text{Cl/K} < 0.0032$). Both the release temperatures and the chemical fingerprint (considering the possible intercalibration uncertainties in reactor production rates of ^{38}Ar from Cl) are identical and support the identity of the principal gas carrier in the two analyzed separates. We therefore feel it is justified to regress the “true” phlogopite steps of both analyses together; this is shown in Fig. 8, with DB referring to Brocchini (1993) and AB to the present work. The isochron age is 146 ± 9 ka. The trapped Ar is calculated as $^{40}\text{Ar}/^{36}\text{Ar} = 295 \pm 1$. The atmospheric intercept can be used to calculate step ages; the weighted average of the seven combined AB and DB steps gives 141 ± 11 ka. This age is the most reliable estimate of the Monticchio phlogopites.

3.4.8 *Serra di Braida subsynthem*

Sample **VUT 0008** are tuffisitic lapilli from deposits of a diatremic eruption (Principe and Giannandrea, 2002; Fig. 1) near the Ripacandida village, east of Monte Vulture edifice. For reasons of comparison three different black-mica fractions were separated: one dark green phlogopite and two dark brown Mg-biotite fractions. The finer grained biotite fraction was obtained by grinding coarse (cm-sized) biotite in the mortar to eliminate altered rims. Firstly, K concentrations range between 3.7 and 5.1 % (Table A-3-3), demonstrating very heavy alteration. Grinding improved the K and Cl concentration, but only to a limited degree. The second observation is that all measured $^{40}\text{Ar}/^{36}\text{Ar}$ ratios are very close to atmospheric composition. The total ^{36}Ar concentration (a measure of the trapped Ar) is one order of magnitude higher in the diatreme micas compared to a typical magmatic phlogopite such as PG5. Calculated isochron ages are, 0.9 ± 1.3 , 0 ± 2 , and 1.1 ± 0.8 Ma for the phlogopite, large biotite and small biotite, respectively. The extreme error enlargement with respect to individual steps is due both to the high MSWD (i.e. to excess scatter) and to the long and unfavourable extrapolation of the very unradiogenic data points. Calculated initial $^{40}\text{Ar}/^{36}\text{Ar}$ ratios are indistinguishable from the atmospheric value, but with a tendency to values around 300. Step ages are therefore meaningless, not only those > 0.5 Ma or < 0 Ma, but all of them.

We interpret the results of these three analyses as follows. A diatreme eruption could contain both a juvenile magmatic mica and a reworked xenocrystic mica entrained from the preexisting volcanic edifice or from an intrusive carbonatitic ring complex below the volcano (Rosatelli et al., 2002, 2004) and mantle xenoliths (Downes et al., 2002; Jones et al., 2000). In any case the high trapped Ar concentration with near-atmospheric $^{40}\text{Ar}/^{36}\text{Ar}$ ratio mirrors extensive alteration during diatreme emplacement. As a result the obtained age is unreliable.

3.4.9 Allochthonous deposits

Sample **VUT 0004** and **PG 3** originate from two tephra sequences deposited in a small lacustrine basin, which was cut by the Ofanto fault in the locality Ripe del Cavallo. The age spectrum of the sanidine (sample **VUT 0004**) shows gas rich steps 3 to 6 that are homogeneous in chemistry with ages between 27 and 50 ka. The weighted average of these steps with an age of 38 ± 9 ka is indistinguishable to the age signature of the Campanian Ignimbrite (39.28 ± 0.11 ka, De Vivo et al., 2001) whose vent is situated in the NW of Naples around 100 km west of Monte Vulture. Finally, sanidine of a pumice fallout (sample **PG3**) deposited directly above the Campanian Ignimbrite provide a dichotomous $^{40}\text{Ar}/^{39}\text{Ar}$ pattern. With respect to Ca/K ratios the sample can be divided into two distinct groups (Fig. 9).

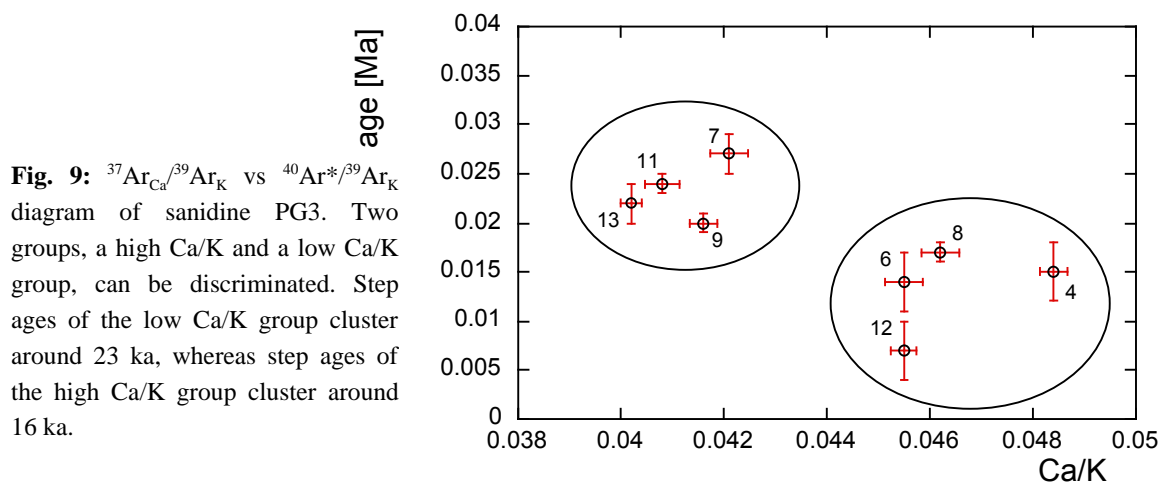


Fig. 9: $^{37}\text{Ar}_{\text{Ca}}/^{39}\text{Ar}_{\text{K}}$ vs $^{40}\text{Ar}^*/^{39}\text{Ar}_{\text{K}}$ diagram of sanidine PG3. Two groups, a high Ca/K and a low Ca/K group, can be discriminated. Step ages of the low Ca/K group cluster around 23 ka, whereas step ages of the high Ca/K group cluster around 16 ka.

The low-Ca group clusters around 23 ka, whereas the average of the high-Ca group yields an age of 16 ka. This latter age signature can be ascribed to the Pomici di Base plinian eruption of Somma-Vesuvius (e.g. Bertagnini et al., 1998). Narcisi (1996) described a 17 cm layer (L9) in a drill core from Lago Grande di Monticchio which can be correlated with this eruption and an 15 cm thick layer (L12) at the depth of 2477 cm which can be ascribed to the Campanian Ignimbrite. Hence, Monte Vulture would be situated within the 0.2 m isopach (at a distance of around 100 km E from the vent) of the Pomici di Base eruption. Field observations (Giannandrea et al., 2004) show that the whole stratigraphic sequence outcropping in the old lacustrine basin has been cut by the Ofanto fault. Thus, the age of the fault system was certainly active more recently than 16 ka ago.

3.5 Conclusions

Our ^{39}Ar - ^{40}Ar investigations on different minerals of Monte Vulture volcanics from several eruptive phases confirm and refine previous geochronological work, and demonstrate the reliability of the whole sample processing and analysis protocol. Internally discordant age spectra, and the attendant increased uncertainties of the age assignments, are the result of mineral heterogeneities. Deep alteration processes,

with the possible involvement of SO_4 typical of many Vulture rocks, lead to transformation of mineral phases; therefore, the loss of LIL elements such as K (and its decay products) is likely to occur. Mineralogical and microchemical investigations demonstrate alteration effects (moderate to strong) in sanidine and phlogopite; leucites are frequently analcimized, but those of the present work have uniform and stoichiometric microchemical K distributions. Since phlogopite has always substoichiometric K concentrations, an appropriate interpretation of Ar systematics needs to consider the effects of chloritisation combined with $^{39}\text{Ar}_K$ recoil deduced from neutron irradiation. Consequently, we generally focussed our geochronological calculations on isochemical steps.

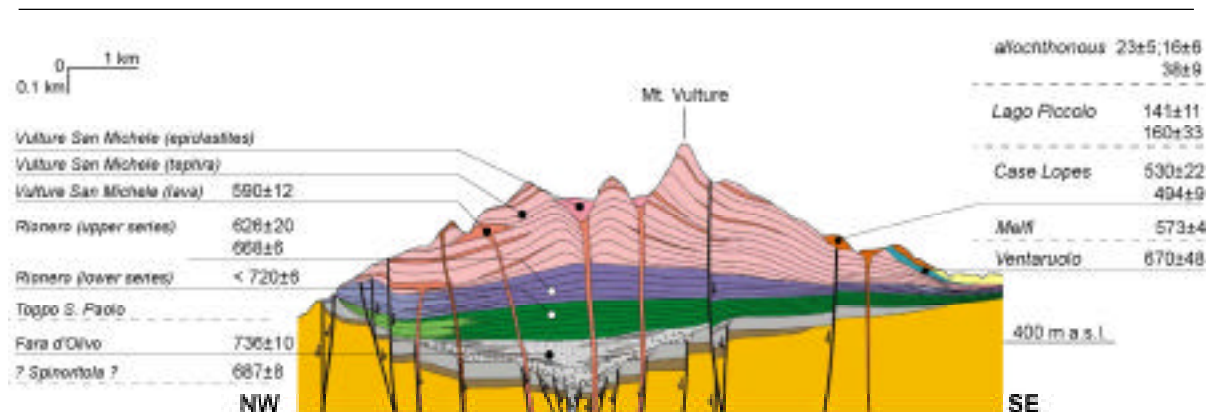


Fig. 10: Stratigraphical sketch of Monte Vulture deposits and corresponding ages. Dashed lines mark subsynthems that are not shown in the profile.

By taking into account chemical heterogeneities of primary and secondary origin, it is possible to derive highly reliable age estimates. These constrain the main volcanic activity to a narrow time interval between 740 ka and 600 ka (Table A-3-4). During this time span the composite stratovolcano was built up (Fig. 10). The definition of the Spinoritola subsynthem as the earliest volcanic manifestation may require a distinction.

Subsequently to the main volcanic activity, the Melfi hauynophyre was extruded at 573 ± 4 ka. In this period only more or less monogenetic centers, aligned along the main active tectonic trends, became active in the Vulture area. After a very long quiescence time gap, final stages of volcanism are characterised by maar-type extrusion of carbonate-rich, melilitic volcanic products; the most voluminous one was dated at 141 ± 11 ka. After the end of volcanic activity at Monte Vulture, allochthonous tephra layers were deposited in a lacustrine basin. According to the ^{39}Ar - ^{40}Ar ages the lower tephra layer can be ascribed to the Campanian Ignimbrite (ca 39 ka) whereas the upper layer probably derives from the Pomici di Base eruption of Somma-Vesuvius (ca 19 ka). Both vents are situated roughly 100 km W of Monte Vulture. As both tephras are cut by the Ofanto fault system, it can be indirectly dated at < 19 ka.

Acknowledgments

This work was supported by SNF grants No. 21-63866.00 and 200020-100230, and by CARG-CNR (R.Polino) and CARG-Regione Basilicata (C.P.) founding. I.M.V. wishes to warmly thank Luigi La Volpe for many discussions and for starting this work a long time ago together with Sergio Borsi and Giorgio Ferrara, who both did not live to see it completed. Edwin Gnos and Karl Ramseyer greatly helped to understand and characterize mineral microtextures. Debora Brocchini provided the analytical data set of her degree thesis and separated mineral phases from new and old samples of IGG Monte Vulture collection.

References

- Beccaluva L, Di Girolamo P, Serri G (1991) Petrogenesis and tectonic setting of the Roman Volcanic Province, Italy. *Lithos* 26(3-4): 191–221
- Bertagnini A, Landi P, Rosi M, Vigliargio A (1998) The Pomici di Base plinian eruption of Somma-Vesuvius. *Journal of Volcanology and Geothermal Research* 83: 219–239
- Bindi L, Cellai D, Melluso L, Conticelli S, Morra V, Menchetti S (1999) Crystal chemistry of clinopyroxene from alkaline undersaturated rocks of Monte Vulture Volcano, Italy. *Lithos* 46: 259–274
- Bonadonna FP, Brocchini D, Laurenzi MA, Principe C, Ferrara G (1998) Stratigraphical and chronological correlations between Monte Vulture volcanics and sedimentary deposits of the Venosa basin. *Quaternary International* 47/48: 87–96
- Brocchini D (1993) Il Vulcano Vulture (Basilicata). Cronologia radiometrica ed evoluzione. Unpublished degree thesis, pp 1-70
- Brocchini D, LaVolpe L, Laurenzi MA, Principe C (1994) Storia evolutiva del Mt. Vulture. *Plinius* 12: 22–25
- Cortini M (1975) Età K-Ar del Monte Vulture (Lucania). *Rivista Italiana di Geofisica e Scienze Affini* 2: 45–46
- De Fino M, La Volpe L, Peccerillo A, Piccarreta G, Poli G (1986) Petrogenesis of Monte Vulture volcano (Italy): inferences from mineral chemistry, major and trace element data. *Contrib Mineral Petrol* 92: 135–145
- De Vivo B, Rolandi G, Gans PB, Calvert A, Bohron WA, Spera FJ, Belkin HE (2001) New constraints on the pyroclastic eruptive history of the Campanian volcanic Plain (Italy). *Mineralogy and Petrology* 73: 47–65
- DiMuro A, Bonaccorsi E, Principe C (2004) Complex colour and chemical zoning of sodalite-group phases in a hauynophyre lava from Mt. Vulture (Italy): a window on a small-volume magma reservoir. Submitted.
- Di Vincenzo G, Viti C, Rocchi S (2003) The effect of chlorite interlayering on ^{40}Ar - ^{39}Ar biotite dating: a ^{40}Ar - ^{39}Ar laser-probe and TEM investigations of variably chloritised biotites. *Contrib Mineral Petrol* 145: 643–658
- Downes H, Kostula T, Jones AP, Beard AD, Thirlwall MF, Bodinier JL (2002) Geochemistry and Sr-Nd isotopic compositions of mantle xenoliths from the Monte Vulture carbonatite-melilitite volcano, central southern Italy. *Contrib Mineral Petrol* 144: 78–92
- Giannandrea P, LaVolpe L, Principe C, Schiattarella M (2004) Carta Geologica del Monte Vulture. *Soc Geol It*, in press
- Giannandrea P, LaVolpe L, Principe C, Schiattarella M (2002) Carta Geologica del Monte Vulture. 81 riunione estiva Soc Geol It, Torino 10-12 Settembre 2002, abstract

- Hess JC, Lippolt HJ, Wirth R (1987) Interpretation of $^{40}\text{Ar}/^{39}\text{Ar}$ spectra of biotites – evidence from hydrothermal degassing experiments and TEM studies. *Chemical Geology* 66 (1-2): 137–149
- Hieke Merlin O (1967) I prodotti vulcanici del Monte Vulture (Lucania). *Mem. Istituto Geol. Mineral. Univ. Padova* 26: 1–67
- Hodges KV, Hames WE, Bowring SA (1994) $^{40}\text{Ar}/^{39}\text{Ar}$ age gradients in micas from a high-temperature low-pressure metamorphic terrain – evidence for very slow cooling and implications for the interpretation of age spectra. *Geology* 22 (1): 55–58
- Jones AP, Kostoula T, Stoppa F, Wooley AR (2000) Petrography and mineral chemistry of mantle xenoliths in a carbonate-rich melilititic tuff from Mt. Vulture volcano, southern Italy. *Mineralogical Magazine* 64(4): 593–613
- LaVecchia G, Stoppa F (1996) The tectonic significance of Italian magmatism: an alternative view to popular interpretation. *Terra Nova* 8: 435–46
- LaVolpe L, Principe C (1991) Comments on “Monte Vulture Volcano (Basilicata, Italy): an analysis of morphology and volcanoclastic facies” by J.E. Guest, A.M. Duncan, D.K. Chester. *Bull. Volcanol* 53: 222–227
- Lo CH, Onstott TC (1989) ^{39}Ar recoil artifacts in chloritized biotite. *Geochimica and Cosmochimica Acta* 53: 2697–2711
- Locardi E (1988) The origin of the Apenninic arcs. *Tectonophysics* 146: 105–123
- Melluso L, Morra V, Di Girolamo P (1996) The Mt. Vulture volcanic complex (Italy): evidence for distinct parental magmas and for residual melts with melilite. *Mineralogy and Petrology* 56: 225–250
- Narcisi B (1996) Tephrochronology of late Quaternary lacustrine record from the Monticchio maar (Vulture volcano, Southern Italy). *Quaternary Science Reviews* 15: 155–165
- Peccerillo A (2004) Carbonate-rich pyroclastic rocks from central Apennines: carbonatites or carbonated rocks? A commentary. *Per. Mineral.* 73: 165–175
- Principe C, Giannandrea P (2002) Stratigrafia ed evoluzione geologica del vulcano Vulture (Basilicata, Italia) – Rapporti fra vulcanismo ed ambienti sedimentari. 81 riunione estiva Soc Geol It , Torino 10-12 Settembre 2002, abstract
- Principe C, Giannandrea P (2004) Stratigraphy and evolutive history of Monte Vulture volcano (Basilicata, southern Italy). In prep.
- Renne PR, Swisher CC, Deino AL, Karner DB, Owens TL, DePaolo DJ (1998) Intercalibration of standards, absolute ages and uncertainties in $^{40}\text{Ar}/^{39}\text{Ar}$ dating. *Chemical Geology* 145: 117–152
- Rosatelli G, Stoppa F, Jones A (2000) Intrusive caatite occurrence from Mt. Vulture volcano, southern Italy. *Mineralogical magazine* 64: 615–624
- Rosatelli G, Stoppa F, Vichi G, Principe C (2004) Extrusive carbonatites and their meaning: the case of Italy. Field Workshop Guide BW02 17th-19th August 2004 IGC Florence 2004. p 22

- Schiattarella M, Beneduce P, DiLeo P, Giano SI, Giannandrea P, Principe C (2004) Assetto strutturale ed evoluzione morfotettonica quaternaria del Monte Vulture (Appenino Lucano). Subm.
- Solovova IP, Girmis AV, Kogarko LN, Kononkova NN, Stoppa F, Rosatelli G (2004) Compositions of magmas and carbonate-silicate liquid immiscibility in the Vulture alkaline igneous complex Italy. Subm.
- Stoppa F, Woolley AR (1997) The Italian carbonatites: field occurrence, petrology and regional significance. *Mineralogy and Petrology* 59: 43–67
- Stoppa F, Principe C (1997) Eruption style and petrology of a new carbonatitic suite from the Mt. Vulture (Southern Italy): The Monticchio Lakes Formation. *Journal of Volcanology and Geothermal Research* 78: 251–265
- Villa IM (1985) Cronologia $^{39}\text{Ar}/^{40}\text{Ar}$ del complesso vulcanico del Monte Vulture. *Rend. Soc. Ital. Miner. Petrol.* 41: 146–147
- Villa IM (1988) Excess Ar in K-rich volcanites: the role of fluids. *Rend. Soc. Ital. Miner. Petrol.* 43: 95–104
- Villa IM (1991) Excess Ar geochemistry in potassic volcanites. *Schweizer Mineralogische und Petrographische Mitteilungen* 71: 205–219
- Villa IM (1992) Datability of Quaternary volcanic rocks: a ^{39}Ar perspective on age conflicts in lavas from the Alban Hills, Italy. *Eur. J. Mineral.* 4: 369–383
- Villa IM (2001) Radiogenic isotopes in fluid inclusions. *Lithos* 55: 115–124
- Villa IM, Ruggieri G, Puxeddu M (1997) Petrological and geochronological discrimination of two white-mica generations in a granite cored from the Larderello-Travale geothermal field (Italy). *Eur. J. Mineal.* 9: 563–568
- Villa IM, Hermann J, Münterer O, Trommsdorff V (2000) ^{39}Ar - ^{40}Ar dating of multiply zoned amphibole generations (Malenco, Italian Alps). *Contrib. Mineral. Petrol.* 140: 363–381
- Wartho JA, Kelley SP (2003) $^{40}\text{Ar}/^{39}\text{Ar}$ ages in mantle xenolith phlogopites: determining the ages of multiple lithospheric mantle events and diatreme ascent rates in southern Africa and Malaita, Solomon Islands. In: *Geochronology: Vance D, Müller W, Villa IM (eds) Linking the Isotopic Record with Petrology and Textures. Geological Society, London, Special Publications 220, pp 231–248*

4. Differential mobility of actinides in soils: U-Th dating of paleosols of known age

Annett Buettner¹, Igor M. Villa¹ and Jan D. Kramers¹

¹ *Institut für Geologie, Universität Bern, Erlachstrasse 9a, 3012 Bern, Switzerland*

to be submitted

Abstract

U-Th isotope systematics are reported for paleosols between volcanic units of three Quaternary volcanoes (Monte Vico and Monte Vulture, Italy and Nisyros-Yali volcanic system, Greece). The ages of the volcanic units under- and overlying the investigated paleosols of the two Italian volcanoes are well constrained. They range from around 150 ka for Monte Vico up to > 700 ka on Monte Vulture (exceeding the datable range for U-Th disequilibrium).

The extraction using sequential "soft" leaching protocols from the literature (Mg(NO₃)₂-solution, acetic buffer-solution, Tamm's reagent) fails to adequately separate paleosol-components such as adsorbed cations, authigenic carbonates, metal oxides and hydroxides from the silicate residue, which is digested with a mixture of HClO₄ and HF. Nevertheless, in order to overcome laboratory fractionation U-Th bulk calculations of relevant leach-steps reveal open system behaviour of paleosols sandwiched of non-pedogenised volcanic rocks.

4.1 Introduction

The behaviour of U-series radionuclides in weathering profiles has been the subject of numerous studies (e.g., Mathieu et al. 1995; Dequincey et al. 1999, 2002; Reiller et al. 2002; Chabaux et al. 2003), which propose an open-system environment characterised by multi-step or even continuous fractionation of U and Th. Pedogenic carbonates and silica of clast-rinds were investigated by U-series disequilibrium chronology (Ludwig and Paces 2002; Sharp et al. 2003) and provided reliable ages of the carbonate formation. However, leach-residue techniques using strong acids for separating pedogenic from detrital phases failed, and gave corrupt ages as the chemical treatment fractionates Th from U (Ludwig and Paces 2002). Hence, the choice of reagents for a selective leaching of U and Th is of great importance to avoid any element fractionation during leach experiments. Leach procedures for separating discrete phases in soils and sediments have been proposed by e.g., Schultz et al. (1998) and Leleyter and Probst (1999) who investigated the yield of trace elements and the selectivity for each treatment. Yokoyama et al. (1999) provide a modified method for silica digestion to inhibit co-precipitations of insoluble fluoride complexes that formed with tetravalent cations.

Since U and Th fractionation occurs, the question of whether it is an analytical artefact or a natural effect has to be addressed. As a natural laboratory to do this, we have chosen sites in which the material represents paleosols, for which the pedogenesis was arrested at a known time. The paleosols are over- and underlain by volcanics that are not affected by pedogenetic processes such as, e.g., the formation of secondary minerals due to the penetration of fluids or the reaction with organic material. We followed the sequential extraction technique by Leleyter and Probst (1999), which is credited with separating pedogenic phases for U-series radionuclide analyses in combination with the modified silicate digestion method by Yokoyama et al. (1999) for the silicate residuum. In addition to measuring U and Th by mass spectrometry, we also document the elements mobilised by laboratory leaching. We qualitatively and quantitatively check each leach step with energy dispersive spectrometry (EDS) analyses to verify the selectivity of the chemical separation.

In the present study five paleosols between ca. 150 ka old ignimbrite layers of the Vico volcanic complex (Northern Latium, Italy) were chemically separated and analysed to unravel the contributions of each fraction to the U and Th budget. To provide a reliable geochronological framework we analysed sanidine separates from all units directly underlying and overlying the investigated paleosols with the Ar-Ar technique. Furthermore we investigated paleosols from two different Quaternary volcanoes to extend our database and to compare paleosols from different environments. The first of these is one baked paleosol from Monte Vulture (SE Italy), expected to yield equilibrated ^{230}Th and ^{234}U because its age is narrowly bracketed by under- and overlying ignimbrites (730 - 740 ka, Villa 1988). Second, five paleosols underlain and overlain by pyroclastics and one paleo-lacustrine sediment embedded between two lava flows from the Nisyros-Yali volcanic system (e.g., DiPaola 1974) in the easternmost section of the Hellenic arc (Greece) were added to the database.

4.2 Geological setting and sample description

Vico is a Quaternary stratovolcano in the central part of Italy and belongs to the potassic alkaline Roman Volcanic Province (RVP). Its volcanic edifice is located on the western shoulder of the NW-SE striking Radicofani-Cimino graben-structure parallel to the Apennine mountain chain (e.g. Barberi et al. 1994). The volcanism of Vico is related to the late to postorogenic tectonic activity between 0.4 and 0.1 Ma (Ar-Ar ages on mineral separates by Laurenzi and Villa 1987) and can be subdivided into four main phases (Bertagnini and Sbrana 1986). In the present study we focus on the third and fourth phases of volcanic activity as their geochronological background is well known (Fig. 1).

Monte Vulture is a Quaternary volcano in the southeastern Apennines in southern Italy. Unlike the large RVP volcanic complexes, which are located west of the Apennines Monte Vulture is located to the east of the main Apenninic chain. Recent studies (e.g., Giannandrea et al. 2004) present a refined volcanostratigraphical profile and provide a detailed subdivision into synthem and subsynthem. The investigated paleosol of Monte Vulture derived from the basal eruptive cycle (Fig. 1). The Quaternary Nisyros-Yali system (Greece) in the easternmost part of the Hellenic Arc was formed between 160 and 35 ka (Smith et al. 1996). Our samples derive from different phases of volcanic activity (Fig. 1).

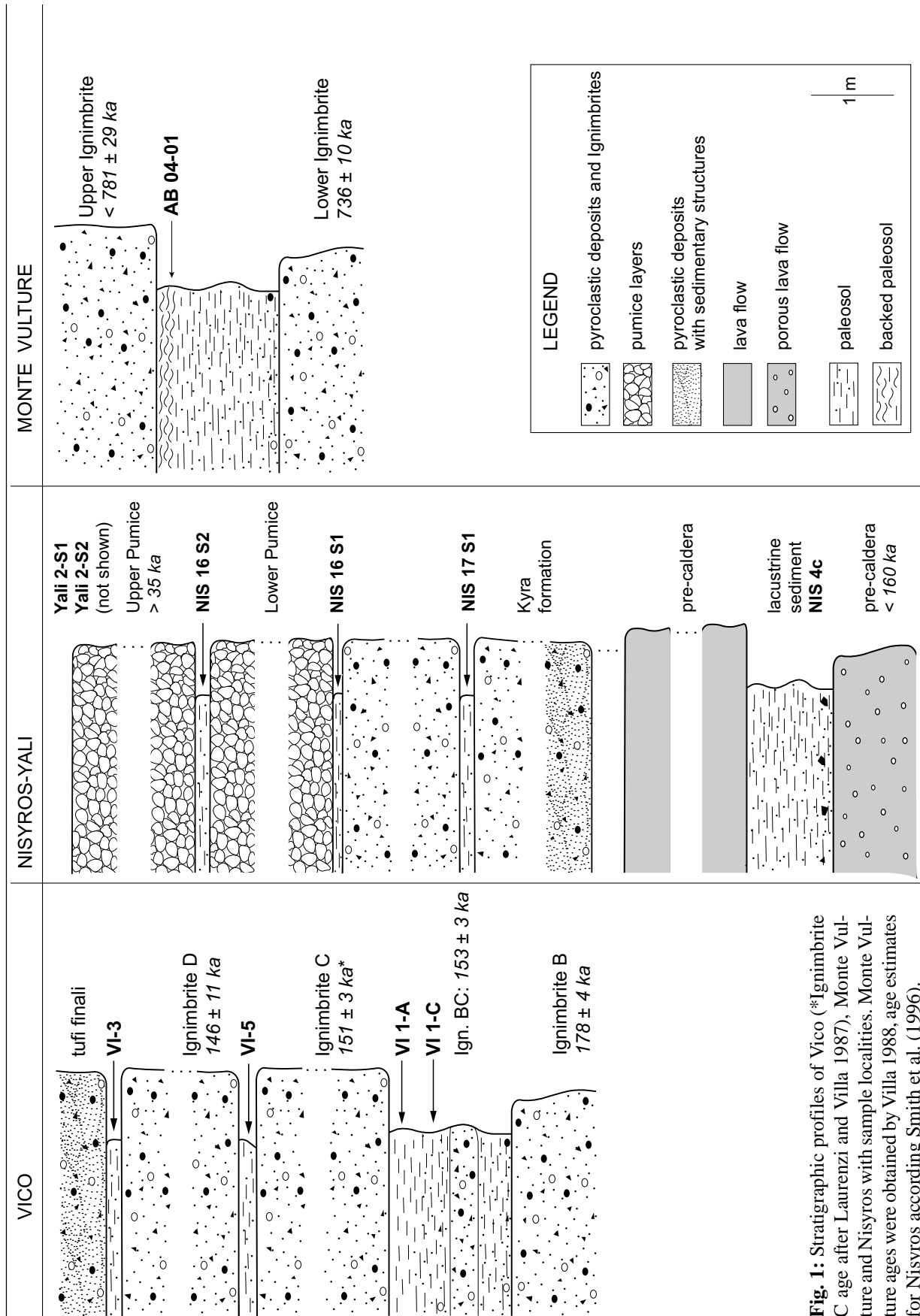


Fig. 1: Stratigraphic profiles of Vico (*Ignimbrite C age after Laurenzi and Villa 1987), Monte Vulture and Nisyros with sample localities. Monte Vulture ages were obtained by Villa 1988, age estimates for Nisyros according Smith et al. (1996).

^{39}Ar - ^{40}Ar analyses were performed on handpicked sanidine separates of the covering Vico ignimbrites. Overall K_2O contents of the sanidine separates are high, varying between 13.5 and 16.6 wt %. The volcanic paleosols are weathering horizons that divide different volcanic units. The time of the development of soils is restricted to the time interval of inactivity between two ignimbrites. Therefore, mainly poorly developed soils without distinguishable A, B and C horizons and limited thicknesses (only a few tens of cm) can be found in such environments.

We define these paleosols according to the paleosol classification of Mack et al. (1993) as Protosols. The investigated Protosols mainly consist of detrital components from the underlying volcanics, of authigenic phases such as amorphous iron oxide coatings, clay minerals and carbonates and of organic matter in different portions depending on the recent and paleo-climatic conditions. We assumed that our paleosol soil-phases can be subdivided into three main groups that mainly influence the U and Th budget: A mobile group including adsorbed U and Th onto different particle surfaces, such as iron oxides, clay minerals and organic chelate complexes. Secondly, the authigenic group of paleosol phases is focussed on carbonates, which are known to be suitable for U-Th investigations provided they formed rapidly and remained chemically closed. The third main group of soil components includes the detrital phases of a paleosol mainly consisting of silicates. The paleo-lacustrine sediment from Nisyros consists mainly of oncolitic carbonates mixed with detrital components from the underlying lava (Fig. 2). We investigated the selected Protosols in two different analytical protocols (see below).

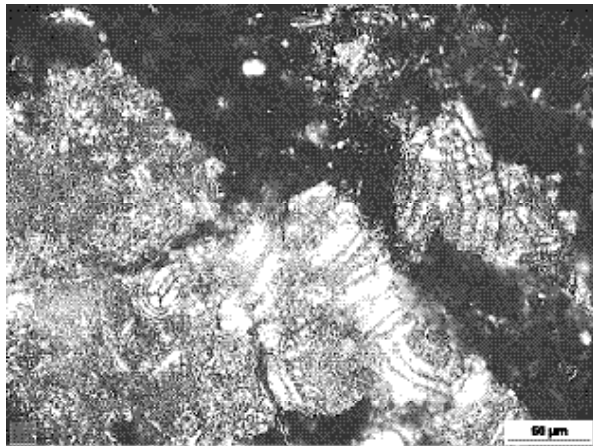


Fig. 2: Microphotograph of oncolitic calcite fragments from the paleo-lacustrine sediment (sample NIS 4c) of Nisyros volcano (Greece).

4.3 Analytical techniques

4.3.1 ^{39}Ar - ^{40}Ar analyses

The sanidine separates were irradiated at the McMasters Research Reactor (Canada) without Cd-shielding. To calculate the J value, sanidine from the Fish Canyon tuff with an assigned age of 28.02 Ma (Renne et al. 1998) was used as irradiation monitor. The ^{39}Ar - ^{40}Ar analyses were performed on a MAPTM 215-50B noble gas mass spectrometer using incremental heating. A detailed description is given in Villa et al. (2000). Ar isotopes were detected in a Faraday collector.

4.3.2 Sequential extraction technique

We applied a five-step sequential extraction procedure that is slightly modified from that of Leleyter and Probst (1999) to separate the three main phases of paleosols, namely the mobile group, the authigenic group and the detrital group. Figure 3 provides a schematic overview of all leaching steps. Between each two steps both the leachate and the residue were completely dried. In the first step, a total of around 0.1 g of the mortar-ground whole soil (WS) aliquot was leached for 2 hours at 20°C with 2 ml of 1 M $\text{Mg}(\text{NO}_3)_2$ -solution to re-mobilise cations that are adsorbed onto solid materials. According to Leleyter and Probst (1999) silicates and carbonates are not attacked during step 1. Centrifuging at 5500 rpm for 10 minutes finally allowed separation of leachates from residues that were subsequently dried. During the step 2, the residue of step 1 was treated for 5 hours with a buffer solution of pH = 4.0 (generated by mixing 1ml of 1M Na-acetate with 1ml 1M acetic acid) at room temperature. According to Leleyter and Probst (1999) the choice of a buffer solution with a pH-value of 4.0 rather than acetic acid guarantees highest yields for the dissolution of carbonates.

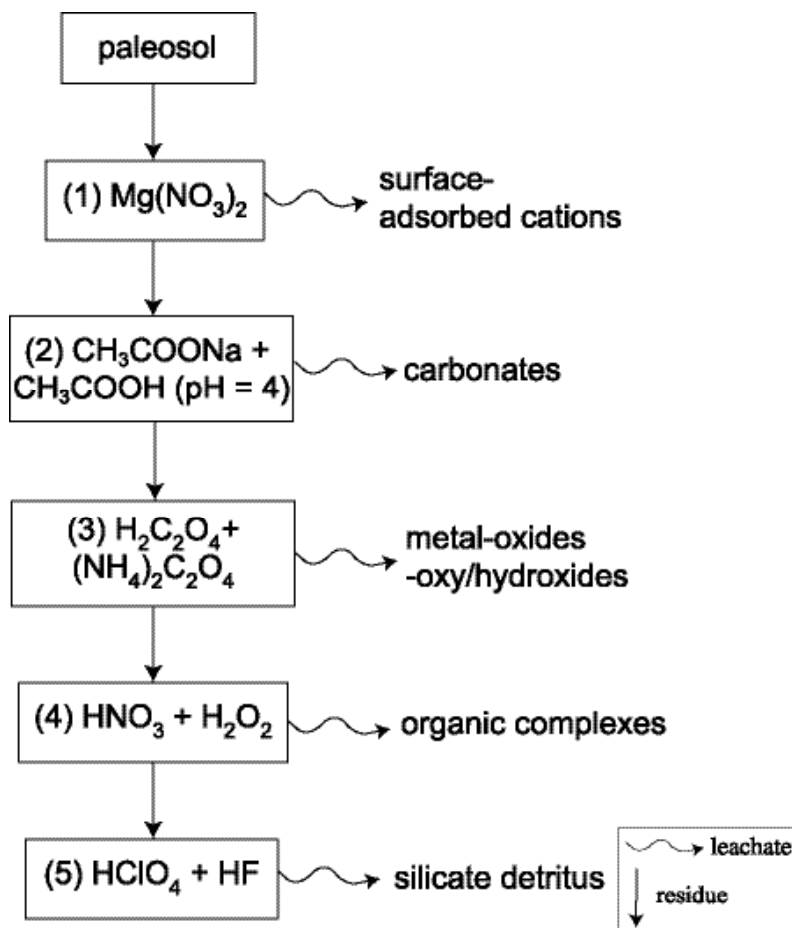


Fig. 3: Schematic illustration of the step leach procedure.

They checked the influence of different pH-values (5.0, 4.5 and 4.0) on the yield of dissolved carbonates and observed an increase from 12 % (pH-value = 5.0) up to 100 % (pH-value = 4.0). During step 3, iron oxides (amorphous and crystalline) were brought into solution by adding 2 ml of a mixture of 0.2 M oxalic acid and 0.2 M ammonium oxalate (Tamm's reagent) to the residue of step 2. The reaction time is 4 hours at room temperature. During step 4 organic matter was oxidised with a mixture of 1 ml H_2O_2 and 1 ml concentrated HNO_3 . The mixture was heated at 80°C for 4 hours allowing a highly effective dissolution of organic components. In the final step (step 5) detrital components (mainly silicates) were dissolved. Commonly, a mixture of highly concentrated HF and HNO_3 is applied for silicate digestion. However, use of that mixture does not completely inhibit the formation of insoluble fluoride complexes containing Th and, therefore, causes elemental fractionation. In contrast to NO_3^- , ClO_4^- is more effective in substituting F bound to Th, forming soluble complexes with Th such as $\text{Th}(\text{ClO}_4)_4$. We, therefore, followed the procedure of Yokoyama et al. (1999) and added 0.5 ml 7 M HClO_4 and 0.5 ml of 28 M HF to the solid residue of step 4. In order to guarantee a complete decomposition of silicates the solution was repeatedly treated in an ultrasonic bath and heated to about 100°C at least for one day (step 5a) and then dried. During step 5b 0.5 ml 7 M HClO_4 were added to remove fluoride complexes completely. The dry perchlorate-residue was dissolved by adding 6 M HCl (step 5c). Finally, the chloride residue was taken up with 1 ml of 4 M HNO_3 to convert chlorides into nitrates for elution of U and Th (step 5d). To evaluate the reliability of the five-step approach presented above, aliquots of selected samples were treated in two steps only, namely with the acetate-buffer (step 2) and HF + HClO_4 digestion (step 5).

4.3.3 SEM analyses

The selectivity of each leach step was checked by analysing the dried eluate with EDS analyses on a scanning electron microscope (SEM) CamScan CS4[®] at the University of Bern. Operation parameters were 2.5 A for the filament current and an acceleration voltage of 20 kV. The beam geometry was set on face modus to allow for homogeneous analyses.

Fresh dried aliquots of the mortar-ground WS aliquot were leached following two protocols, AO and sL. In protocol AO (applied to eight out of the eleven samples) the WS was only treated with 1M Na-acetate/1M acetic acid buffer solution, which was expected to leach only the authigenic carbonates. A second series of three samples was subjected to protocol sL, which included steps 1, 2 and 3 of the sequential extraction described above. A replicate aliquot of one of the paleosol samples was treated with cold 14 M HNO_3 for 10 minutes. This treatment removes exchangeable cations from the clay inter-layer and dissolves hydroxides. Hence, a semi-qualitative classification of the paleosol-phases can be made. Two aliquots of a pure anorganic calcite crystal were leached to compare the yields with that of the paleosols. The first calcite was treated only with the acetate-buffer-solution and the second one with the three step approach of protocol sL (see above). For SEM/EDS analyses the dried residues were loaded onto a gold-carrier. Recoveries were determined by weighing the WS, the residue, and the dried leachate; the sums seldom matched perfectly (Table A-4-1; Appendix A) because anion-complexes of the starting material were substituted by nitrates and acetates.

4.3.4 U and Th separation

Prior to the chemical separation of U and Th all leachates and the dissolved residue were spiked with a mixed ^{229}Th - ^{236}U spike solution ($^{232}\text{Th}/^{229}\text{Th} = 0.0013$, $^{238}\text{U}/^{236}\text{U} = 0.001483$).

Bio-Rad[®] columns with porous frits at the bottom were filled up with around 0.77 ml Dowex[®] anion exchange resin (100 - 200 mesh) and conditioned with 7 N HNO_3 for elution of U and Th. Before Th can be collected (using 0.5 N HNO_3), U and leftover matrix of the sample were collected and evaporated for further separation. For the final U separation the evaporated U+matrix collection has to be converted into chlorides. U is separated from the matrix by using 6 N HCl to wash out the matrix and by collecting U with 1 N HCl. The dried U and Th eluates were taken up with 0.5 N HNO_3 for measurement.

4.3.5 Multi-collector ICP mass spectrometry

Measurements of U and Th isotopes were carried out with a double focusing NU Instruments[®] multi-collector ICP MS at the University of Bern. Samples were additionally oxidised with a H_2O_2 - HNO_3 mixture (Hippler et al. 2004) to remove organics coming from the resin during elution prior to the analyses to avoid a clogging of the capillary that takes up the sample. The samples are nebulised using an APEX-Q[®] nebuliser with an uptake rate of 80 $\mu\text{L}/\text{min}$. U and Th analyses are carried out for a mass range from 229 to 238. Th isotopes were measured in two cycles to measure both ^{229}Th and ^{230}Th with the electron multiplier that has a WARP filter to reduce the ^{232}Th tail to better than 0.01 ppm. Mass fractionation is monitored by adding natural U to the pure Th fraction. U isotopes are analysed separately with ^{234}U and ^{236}U on two electron multipliers. The multiplier gain was calibrated using a NIST U050 standard solution for U. A pristine pre-Pliocene uraninite from Moss (Norway) being in radioactive equilibrium has been used as standard solution for the $^{234}\text{U}/^{238}\text{U}$, $^{230}\text{Th}/^{232}\text{Th}$ and $^{230}\text{Th}/^{234}\text{U}$ ratios. Its known $^{230}\text{Th}/^{232}\text{Th}$ of 0.000156 allows to calibrate the multiplier gain. The external reproducibility of each session ranges between 740 and 180 ‰. Decay constants used in this study for ^{230}Th , ^{234}U and ^{238}U are $9.165 \times 10^{-6}\text{a}^{-1}$, $2.826 \times 10^{-6}\text{a}^{-1}$ and $1.551 \times 10^{-10}\text{a}^{-1}$, respectively (Cheng et al. 2000).

4.4 Results and discussion

4.4.1 ^{39}Ar - ^{40}Ar ages

We analysed four sanidine separates (VI 1E, VI 1P, VI 1TE and VI4). All ^{39}Ar - ^{40}Ar results are listed in Table A-4-2 (Appendix A). A comparison with the results of Laurenzi and Villa (1987) provides a tight chronological frame to assess U-Th systematics in paleosols. Sample VI 1E derives from the Ignimbrite B of the 3rd phase of volcanic activity directly underlying the soil (Fig. 1). A weighted average of chemically homogenous steps provides an age of 178 ± 4 ka (1SD) and an isochron estimate of 180 ± 11 ka with atmospheric $^{40}\text{Ar}/^{36}\text{Ar}$ intercept. Two sanidine separates of the thin BC layer, from a pumice clast (VI 1P) and the tephra (VI 1TE) provide 153 ± 3 ka (VI 1P) and 161 ± 12 ka (VI 1TE). These ages fit with the published age of 151 ± 3 ka for Ignimbrite C (Laurenzi and Villa 1987). Hence, the soil overlying BC must have been formed between 153 ± 3 and 151 ± 3 ka. The sanidine separate of Ignimbrite D gives a hump-shaped spectrum. A weighted average of these isochemical steps provides an age of 146 ± 11 ka that is consistent with the published estimate of 138 ± 2 ka (Laurenzi and Villa 1987).

Note that our sampling locality (road cut in the city of Vetralla) was chosen on account of its high pedogenisation, while those of Laurenzi and Villa (1987) had the opposite aim of avoiding any alteration; still, the sanidine analyses of the present work are satisfactory.

4.4.2 *Selectivity of the sequential extraction technique*

In the following we focus on the selectivity of the acetate leach step, in which Th and U from carbonate phases should have been extracted. Carbonates with the lowest initial ^{230}Th (ideally $\text{Th}_0 = 0$) are the most suitable phase for dating with the U-Th method. Accordingly different leach-experiments were performed in order to compare the qualitative and quantitative yields of step 2 with the AO protocol and the selectivity after the treatment with further reagents following the sL protocol.

The results of the EDS analyses are summarised in Table A-4-1 (Appendix A). In sample VI 5 (reference sample) treated with concentrated HNO_3 , the cation concentrations indicate the presence of essentially Al-Fe-oxides with subordinate alkali and earth-alkali oxides. The Na content of this sample (2.17 wt %, see Table A-4-1) was used as a reference sample-derived amount. Hence, the total Na of our soil samples can be considered as a combination of Na coming from the acetate buffer and the sample (denoted as $\text{Na}_{\text{buffer}}$ and Na_{K} ; Table A-4-1). As the input coming from the acetate buffer can be discriminated, a quantitative estimation based on the sample derived Na can be made.

The resulting Ca yields are low in all of the eight samples analysed with protocol AO. They range from 0.57 wt % (normalised to the total soil-weight) up to 3.31 wt %. Al, Si, Mg and K are low but within their uncertainties not negligible. The AO protocol with pure calcite crystals (sample calc 2) provides an unexpectedly low Ca yield of 0.42 wt %. Moreover, Al is present in a considerable amount. In contrast, the results of protocol sL display a different pattern (see Table A-4-1). The Ca yields for paleosol-samples of the acetate buffer step 2 are negligibly low and show no reproducibility with the AO protocol. The Ca yield remains low also in step 1 and step 3. Pure calcite crystals show a contrasting pattern: Microscope observations reveal a considerable roughening of the crystal surface after the treatment with $\text{Mg}(\text{NO}_3)_2$. A further reaction with the acetate buffer-solution leads to the complete decomposition of the remaining calcite and 28.84 wt % Ca are detectable.

To explain these observations we assume for the paleosols a reaction leading to the incorporation of Ca into a precipitate during the treatment with $\text{Mg}(\text{NO}_3)_2$ -solution that is not re-dissolved during the further chemical treatment until step 5 of the extraction protocol. Schultz et al. (1998) show that cations like Ca readsorb during chemical extraction. A further possible reaction leading to the precipitation of Ca could be the interaction of released Ca with chelate ligands forming chelate-complexes that are inert to the subsequent chemical treatments. Even if chelate ligands are not present as in the pure calcite crystal both the three-step approach of the sL protocol and the AO protocol are not suitable for a complete dissolution of CaCO_3 .

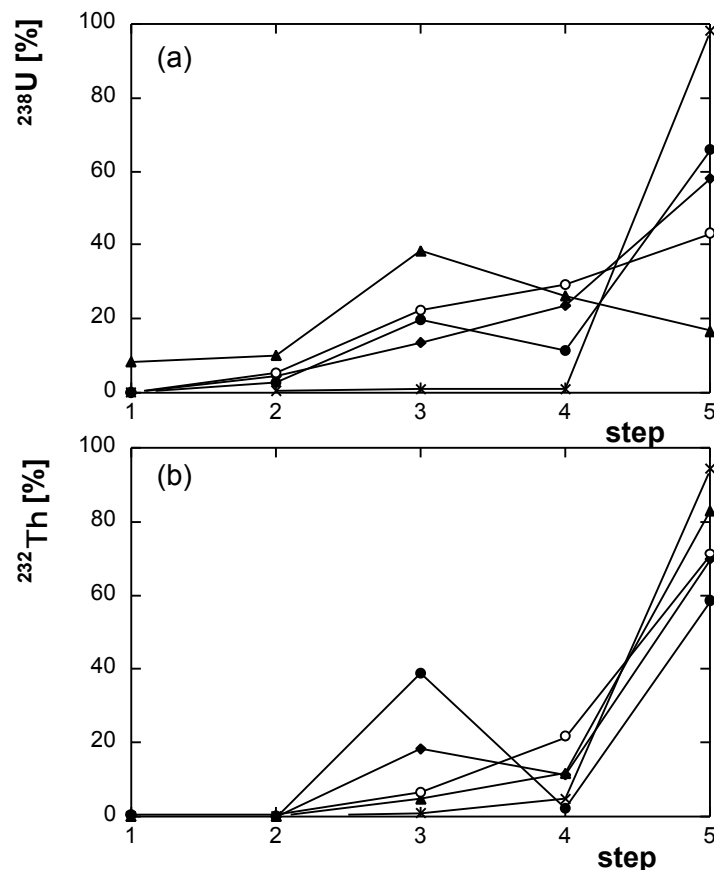
Paleosols attacked only with the acetate buffer-solution (AO protocol) release part of their Ca during this reaction. The high crystallinity of pure calcite suppresses the reaction with the buffer solution and only a negligible amount of Ca is released from the crystal. Sample NIS4c (the paleo-lacustrine sediment from Nisyros) provides a similar pattern as the Ca yield is low compared to the high amount of carbonates (around 14 wt %). Handpicked but still impure carbonate separates of the oncolith-bearing sample NIS4c (NIS4c-L1 and NIS4c-L2; Table A-4-3, Appendix A; Fig. 2) have been leached: one

aliquot according to step 2 and the second one with 7 M HNO₃, which we routinely use to decompose speleothems, and H₂O₂ to eliminate any organic remnants. The comparison of the U-Th results of these two aliquots allows for an estimation of the U and Th yields of the acetate buffer step 2. It is seen that during step 2 a fractionation of U and Th occurs. U is depleted by 13 % and the Th depletion is as high as 81 % compared to the HNO₃-H₂O₂ leached aliquot. Step 2 seems to attack micritic Ca-bearing phases rather than crystalline calcite. A combination of both the presence of complex-building ligands and the sample crystallinity has a great influence on yield and selectivity of step 2 of the chemical separation procedure. However, following the unexpected behaviour of Ca we suspect that the treatment with the acetate buffer solution at a pH of 4.0 causes elemental fractionation of U and Th and is, therefore, not suitable for U-Th disequilibrium dating.

4.4.3 U-Th results

Table A-4-3 summarises the measured U-Th results. All ²³⁴U/²³⁸U isotope ratios scatter narrowly around the natural value of 5.48×10^{-5} whereby the Vulture-paleosol exhibits the highest variations (4.87×10^{-5} for the third leach-step up to 7×10^{-5} for the second step). ²³⁰Th/²³⁸U ratios scatter non-systematically between 4×10^{-8} and 2×10^{-5} . Finally, ²³⁸U/²³²Th ratios vary between 0.16 and 247 being lowest in the HF-HClO₄ leach steps 5 and highest for the acetate-buffer leach steps 2.

Fig. 4: The yield of ²³⁸U (a) and ²³²Th (b) for each leach step, VI 1C, ○ VI 1A, ▲ VI 3 (Vico); ● AB 04-1 (Vulture); × NIS 16S2 (Nisyros volcano). The humine-rich Vico soil (VI 3) releases around 40 % of its U during step 3, while the majority of paleosols retracts U until step 5. Th provides a similar trend. Only the Vulture soil (AB 04-1) shows an exceptional behaviour in releasing around 40 % Th during step 3.



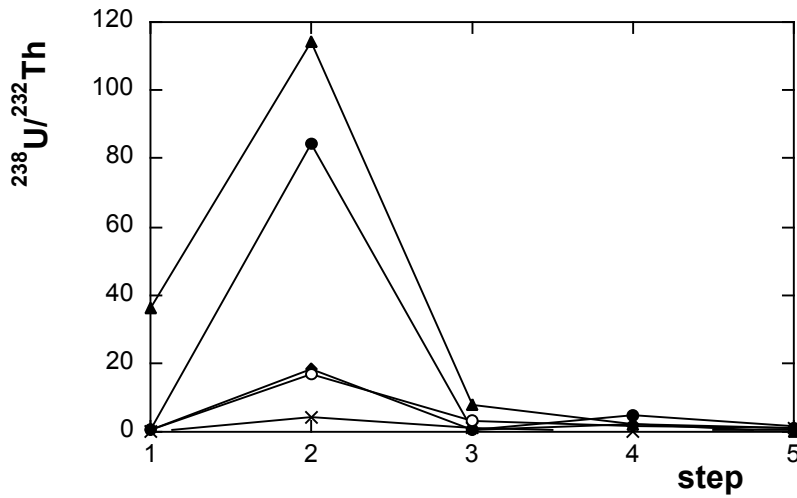


Fig. 5: U/Th ratios for all leach steps show peaks for step 2 suggesting both the presence of detritus-free carbonate or the re-adsorption of Th in this step (symbols as in Fig. 4).

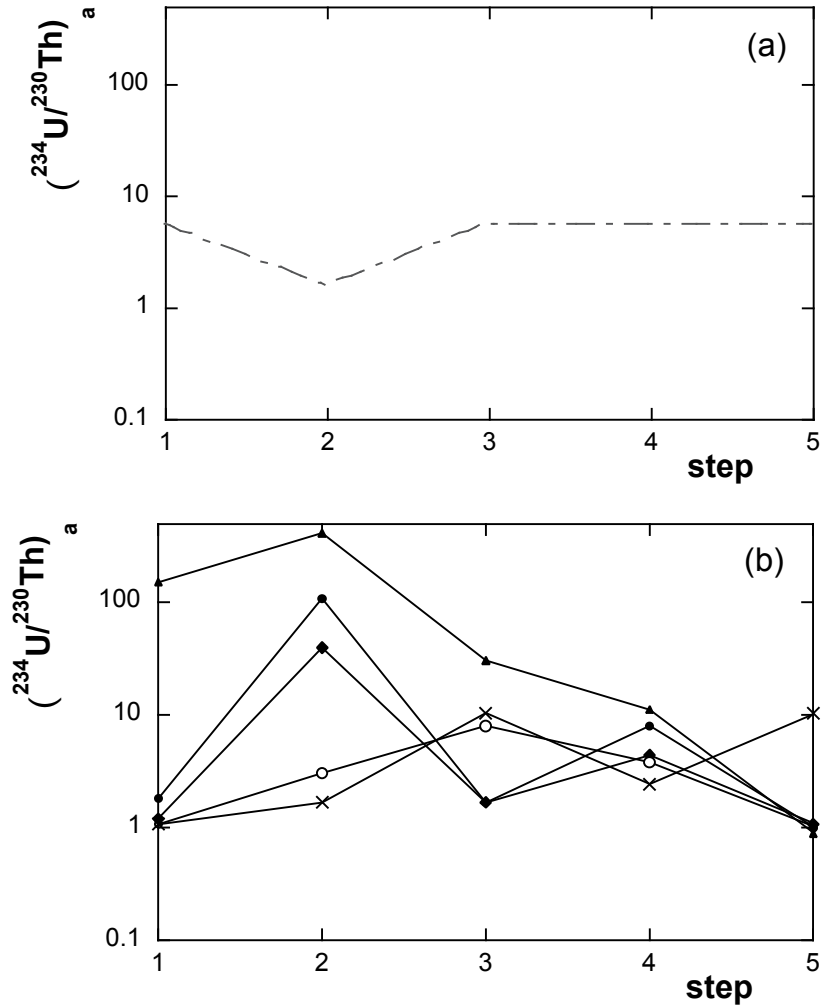


Fig. 6: (a) Theoretical evolution of $(^{234}\text{U}/^{230}\text{Th})_a$ activity ratio for authigenic carbonates that are not affected by multi-stage processes causing U-Th fractionation. (b) $(^{234}\text{U}/^{230}\text{Th})_a$ results. The positive peaks suggest secondary processes led to U-gain (symbols as in Fig. 4).

In the following considerations all isotope ratios are expressed as activity ratios. Figure 4 shows the percentage distribution of U and Th for each leach step. All samples release their main portion of U and Th during step 5 (HF + HClO₄). An exception to this general trend is the humine-rich paleosol from Vico (sample VI 3), which shows an U peak of around 39 % for step 3. We ascribe this pattern to the enhanced abundance of metal-oxides in this soil layer and a rather small amount of detrital components compared to the other paleosols. The majority of Th is retained until step 5. When attacked with the highly oxidising reactants (step 3) only two samples (AB 04-1, VI 1C) reveal Th peaks of around 39 % and 18 %, respectively, while the majority of Th is re-adsorbed during this step. Figure 5 exhibits an apparent detritus free step 2 which would allow for dating the authigenic carbonates. This assumption failed with reference to the (²³⁴U/²³⁰Th) ratios (Fig. 6 a). (²³⁴U/²³⁰Th) ratios, uncorrected for detrital Th, is shown for the five leach steps (Fig. 6 b). High (²³⁴U/²³⁰Th) ratios correspond to low ages, low detrital input, or both. If a pure, detritus-free carbonate is formed during the pedogenesis, one would expect a behaviour such as in Fig. 6 a, in which authigenic carbonates have lower (²³⁴U/²³⁰Th) ratios than secondary alteration phases (oxides, humines). Clearly, our samples contradict this, probably due to both to secondary U⁶⁺ mobility in water and to detrital Th. The data furthermore exhibit a small spread in (²³⁴U/²³⁸U) ratios (for Vico, Vulture and Nisyros-Yali: between 0.933 - 1.125, 0.888 - 1.276 and 0.939 - 1.108, respectively) scattering around equilibrium, with analytically significant, but non-systematic, small deviations from unity (Fig. 7). The (²³⁰Th/²³⁸U) ratios of samples from Vico and Nisyros-Yali show large variations (0.003 - 1.372, 0.073 - 1.642). Th/U element ratios of the overlying and underlying ignimbrites of Vico are significantly high between 5 and 11. According to Locardi (1965) anomalous high Th (up to 260 ppm) and U (up to 32 ppm) contents are associated with secondary CO₂ and H₂S exhalations. These enrichments are not restricted to a certain stratigraphic unit or lithology.

(²³⁰Th/²³⁸U) ratios of the residue steps of some Vico samples (Fig. 7 a) plot in the "forbidden zone" of the evolution plot in which (²³⁰Th/²³⁸U) > (²³⁴U/²³⁸U). Consequently, none of our Vico data fit on isochrons (Fig. 8 a). Even assuming laboratory fractionation artefacts are excluded when calculated bulk activity ratios for steps 1 to 4 (denoted as mobile fraction - M in Fig. 8 a). The mobile fraction and the corresponding residue step 5 result in negative slopes, which forbid the calculation of an internal isochron. Maximum model (²³⁰Th/²³⁴U) ages can be calculated for the M-fraction as well as the bulk sample, with a minimum possible initial of 0; all are younger than the present stratigraphy (Table A-4-3).

In contradiction to the present work, U-Th analyses on whole rock samples from the Vico volcanic complex have been used by Villemant and Fléhoc (1989) to calculate an age of 93 ± 11 ka (roughly summarised on one isochron, with an unspecified, high MSWD value) for the Ignimbrites A, B, C and D that all plot on one isochron. Our results emphasise that whole rocks violate the assumptions of a single-stage evolution and should not be regressed in an isochron.

U-Th systematics on paleosols from Nisyros are likewise not suitable for geochronological investigations. Again, the M-fractions and the corresponding residues of step 5 define negative slopes in Fig. 8 b, which do not allow internal isochron calculations. However, the model ages given by the residue steps 5 of some samples do not contradict the bulk age estimations (Table A-4-3). These ages cannot be considered as "true" ages as the assumption that the initial ²³⁰Th = 0 is only a minimum limit. Present day (²³⁰Th/²³⁴U) ratio which results in a "false" age (Villa 1992) can be due to the secondary input of unsupported ²³⁰Th by e.g., fluids.

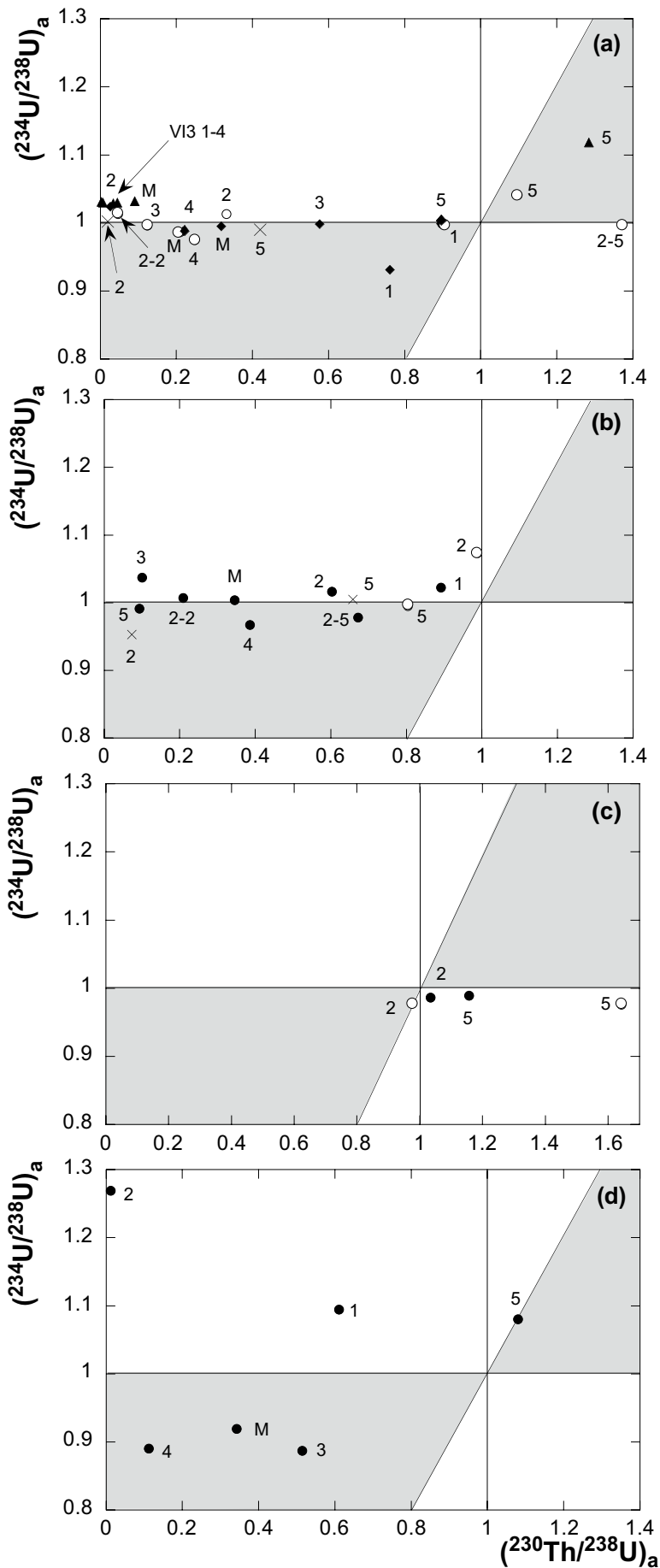


Fig. 7: $(^{230}\text{Th}/^{238}\text{U})$ vs $(^{234}\text{U}/^{238}\text{U})$ evolution diagrams. The leach steps are denoted with the corresponding numbers (see text). (a) Vico paleosol-samples: \circ VI1A; \blacklozenge VI1C; \blacktriangle VI3; \times VI5. (b) Nisyros paleosol-samples: \bullet NIS16-S2, step-numbers with the suffix “2-” refer to the two-step approach; \circ NIS17-S1; \times NIS16-S1. (c) Yali paleosols: \circ Yali 2-S1; \bullet Yali2-S2. (d) Vulture paleosol: AB 04-1. The gray shaded areas refer to the “forbidden” zones of the evolution plot which can only be reached during a multi-stage evolution of U and Th.

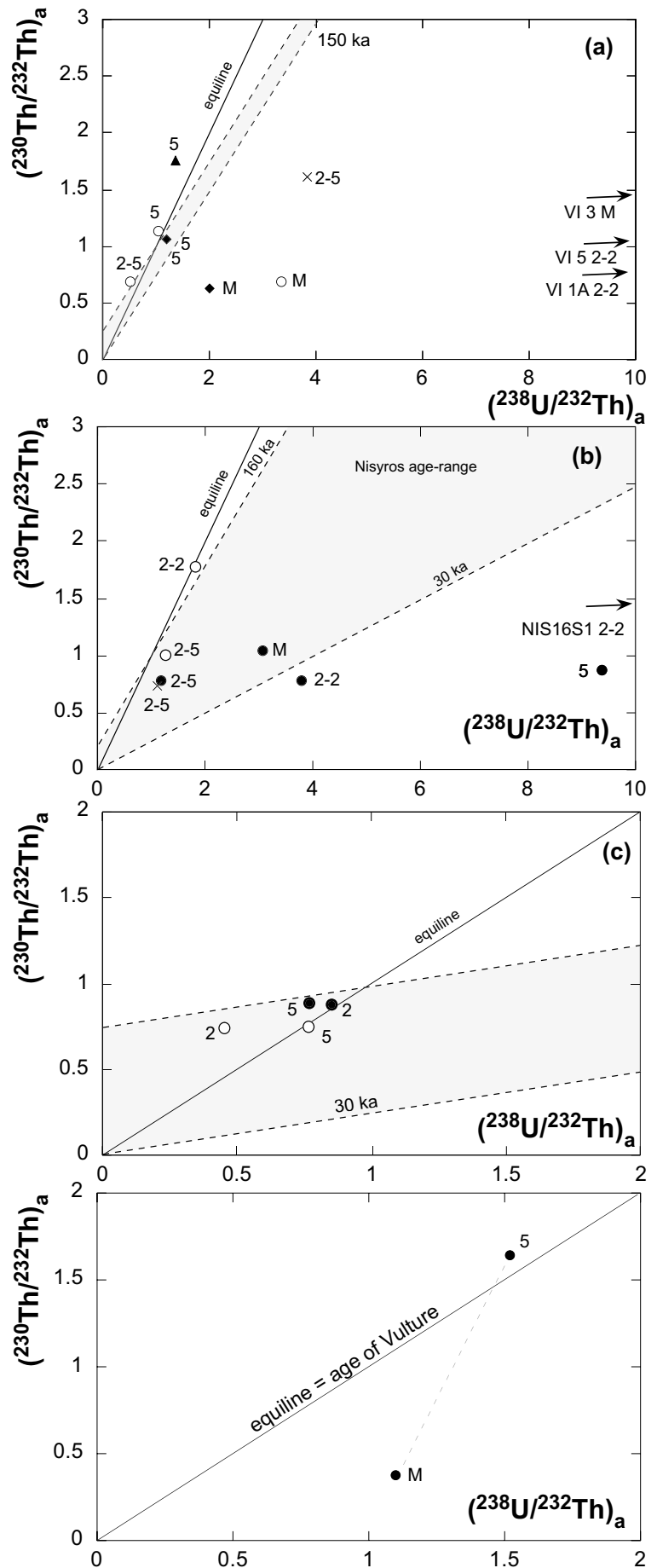


Fig. 8: $(^{238}\text{U}/^{232}\text{Th})_a$ vs $(^{230}\text{Th}/^{232}\text{Th})_a$ diagrams. All leach steps are denoted with the corresponding numbers. Samples that are leached in only two steps have the suffix “2-”. The mobile fraction (M) is the calculated bulk of steps 1 to 4. Grey shaded areas mark the age constraints of the volcanic systems. (a) Vico paleo-sols; (b) Nisyros paleosols; (c) Yali paleosols and (d) Vulture paleosol (symbols as in Fig. 7).

All leach steps of paleosol-samples from Yali are characterised by Th-excess. Similar to Vico the underlying and overlying pumices of Yali show high Th/U element ratios (averaging between 18 and 23; Buettner et al. *subm.*) resulting in $(^{230}\text{Th}/^{238}\text{U})$ ratios > 1 (see Table A-4-3) and hence plot in the "forbidden zone" of the $(^{234}\text{U}/^{238}\text{U})$ vs $(^{230}\text{Th}/^{238}\text{U})$ evolution diagram (Fig. 7 c). As a result of the high Th/U ratios, the $(^{230}\text{Th}/^{232}\text{Th})$ vs $(^{238}\text{U}/^{232}\text{Th})$ plot of the two Yali paleosols (Fig. 8 c) shows a slope of 0.

Finally, the leach steps of the paleosol from Monte Vulture (known to be much older than the datable range of U-Th) provide $(^{234}\text{U}/^{230}\text{Th})$ ages, which are again too young (175 ± 6 ka for the bulk sample and 50.9 ± 1.4 ka for the M-fraction). The $(^{230}\text{Th}/^{234}\text{U})$ ratio of the residue-step, however, is in equilibrium (0.995 ± 0.016 ; Fig. 7 d).

All leach steps appear to be affected by laboratory fractionation. However, bulk calculations of the M-fraction (summarising steps 1-4) overcomes this effect. We observe that the analysed paleosols must have been open for secondary processes which have a strong influence on the U-Th budget as all calculated bulk ages are discordant to the given age constraints. Interestingly, this M-fraction shows $(^{234}\text{U}/^{238}\text{U})$ within error of unity for all samples, and a $(^{230}\text{Th}/^{234}\text{U}) \ll 1$ for all except Yali paleosols. As Th is normally immobile in the surface environment, this means that U has been added to the soils after their formation.

4.5 Conclusions

U-Th systematics in paleosols, in which maturation is very low and pedogenic processes have supposedly been arrested by blanketing, reveal instead that major chemical exchanges are ongoing. Even in paleosols whose known age should long have achieved $(^{230}\text{Th}/^{234}\text{U})$ equilibrium apparent ages are in the hundreds to thousands of years range; whole rock samples display a deficit of ^{230}Th or an excess of ^{234}U . In order to unravel the distribution of U and Th amongst the soil phases, we applied sequential leaching protocols from the literature. These protocols do not provide the chronological results approaching the independently known paleosol ages. A chemical investigation of the main cations released during the sequential leaching demonstrates an unsurmountable complexity.

Acknowledgements

We are indebted to Alessandro Sbrana, University of Pisa (Italy) for the helpful guidance in the field. Marco Herwegh, University of Bern (Switzerland) is thanked for supporting at the SEM. The present work was funded by the Swiss National Science Foundation (grant No21-63866.00).

References

- Barberi, F., Buonasorte, G., Cioni, R., Fiordelisi, A., Foresi, L., Iaccarino, S., Laurenzi, M.A., Sbrana, A., Vernia, L., Villa, I.M. (1994). Plio-Pleistocene geological evolution of the geothermal area of Tuscany and Latium. *Memorie descrittive della carta geologica d'Italia*, 49, pp. 133.
- Bertagnini, A., Sbrana, A. (1986). Il vulcano di Vico: Stratigrafia del complesso vulcanico e sequenze eruttive delle formazioni piroclastiche. *Mem. Soc. Geol. It.*, 35, 699-713.
- Buettner, A., Kleinhanns, I.C., Rufer, D., Hunziker, J.C., Villa, I.M. (submitted). Magma generation at the easternmost section of the Hellenic Arc: Hf, Nd, Pb and Sr isotope geochemistry of Nisyros and Yali volcanoes (Greece).
- Chabaux, F., Riotte, J., Dequincey, O. (2003). U-Th-Ra fractionation during weathering and river transport. In: Bourdon, B., Henderson, G.M., Lundstrom, C.C., Turner, S.P., Uranium-series geochemistry. *Reviews in Mineralogy & Geochemistry*, 52, 533-576.
- Cheng, H., Edwards, R.L., Hoff, J., Gallup, C.D., Richards, D.A., Asmerom, Y. (2000). The half-lives of uranium-234 and thorium-230. *Chemical Geology*, 169, 17-33.
- Dequincey, O., Chabaux, F., Clauer, N., Liewig, N., Muller, J.P. (1999). Dating weathering profiles by radioactive disequilibria: contribution of the study of authigenic mineral fractions. *Earth and Planetary Sciences*, 328, 679-685.
- Dequincey, O., Chabaux, F., Clauer, N., Sigmarsson, O., Liewig, N., Leprun, J.C. (2002). Chemical mobilizations in laterites: Evidence from trace elements and ^{238}U - ^{234}U - ^{230}Th disequilibria. *Geochimica et Cosmochimica Acta*, 66 (7), 1197-1210.
- DiPaola, G.M. 1974. Volcanology and petrology of Nisyros Island (Dodecanese, Greece). *Bulletin of Volcanology*, 38, 944-987.
- Giannandrea, P., La Volpe, L., Principe, C., Schiattarella, M. (2004). Geological map of Monte Vulture. *Soc. Geol. It.*
- Hippler, D., Villa, I.M., Nägler, T.F., Kramers, J.D. (2004). A ghost haunts mass spectrometry: Real isotope fractionation or analytical paradox? *International Goldschmidt Conference 2004*, Abstract A215.
- Laurenzi, M.A., Villa, I.M. (1987). $^{40}\text{Ar}/^{39}\text{Ar}$ chronostratigraphy of Vico ignimbrites. *Per. Mineral.*, 56, 285-293.
- Leleyter, L., Probst, J.L. (1999). A new sequential extraction procedure for the speciation of particulate trace elements in river sediments. *International Journal of Environmental Analytical Chemistry*, 73 (2), 109-128.
- Locardi, E. (1965). Tipi di ignimbriti di magmi mediterranei. Le ignimbriti del vulcano di Vico. *Atti Soc. Tosc. Sci. Nat.*, 72, 55-173.
- Ludwig, K.R. (2002). Isoplot ver. 2.49n.

- Ludwig, K.R., Paces, J.B. (2002). Uranium-series dating of pedogenic silica and carbonate, Crater Flat, Nevada. *Geochimica et Cosmochimica Acta*, 66 (3), 487-506.
- Mack, G.H., James, W.C., Monger, H.C. (1993). Classification of paleosols. *Geological Society of America Bulletin*, 105, 129-136.
- Mathieu, D., Bernat, M., Nahon, D. (1995). Short-lived U and Th isotope distribution in a tropical laterite derived from granite (Pitinga river basin, Amazonia, Brazil): Application to assessment of weathering rate. *Earth and Planetary Science Letters*, 136, 703-714.
- Reiller, P., Moulin, V., Casanova, F., Dautel, C. (2002). Retention behaviour of humic substances onto mineral surfaces and consequences upon thorium (IV) mobility: case of iron oxides. *Applied Geochemistry*, 17, 1551-1562.
- Renne, P.R., Swisher, C.C., Deino, A.L., Karner, D.B., Owens, T.L., DePaolo, D.J. (1998). Intercalibration of standards, absolute ages and uncertainties in $^{40}\text{Ar}/^{39}\text{Ar}$ dating. *Chemical Geology*, 145, 117-152.
- Schultz, M., Burnett, W.C., Inn, K.G.W. (1998). Evaluation of a Sequential Extraction Method for Determining Actinide Fractionation in Soils and Sediments. *Journal of Environmental Radioactivity*, 40 (2), 155-174.
- Sharp, W.D., Ludwig, K.R., Chadwick, O.A., Amundson, R., Glaser, L.L. (2003). Dating fluvial terraces by $^{230}\text{Th}/\text{U}$ on pedogenic carbonate, Wind River Basin, Wyoming. *Quaternary Research*, 59, 139-150.
- Smith, P.E., York, D., Chen, Y., Evensen, N.M., 1996. Single crystal ^{40}Ar - ^{39}Ar dating of a Late Quaternary paroxysm on Kos, Greece: Concordance of terrestrial and marine ages. *Geophysical Research Letters*, 23(21), 3047-3050.
- Stoppa, F., Principe, C. (1997). Eruption style and petrology of a new carbonatitic suite from the Mt. Vulture Southern Italy: The Monticchio Lakes Formation. *Journal of volcanology and geothermal research*, 78, 251-265.
- Villa, I.M. (1988). Excess Ar in K-rich volcanites: the role of fluids. *Rendiconti della Società di Mineralogia e Petrologia*, 43, 95-104.
- Villa, I.M. (1992). Datability of Quaternary volcanic rocks: an $^{40}\text{Ar}/^{39}\text{Ar}$ perspective on age conflicts in lavas from the Alban Hills, Italy. *European Journal of Mineralogy*, 4, 369-383.
- Villa, I.M., Hermann, J., Müntener, O., Trommsdorff, V. (2000). ^{39}Ar - ^{40}Ar dating of multiply zoned amphibole generations (Malenco, Italian Alps). *Contribution to Mineralogy and Petrology*, 140, 363-381.
- Villemant, B., Fléhoc, C. (1989). U-Th fractionation by fluids in K-rich magma genesis: the Vico volcano, Central Italy. *Earth and Planetary Science Letters*, 91, 312-326.
- Yokoyama, T., Makishima, A., Nakamura, E. (1999). Evaluation of the coprecipitation of incompatible trace elements with fluoride during silicate rock dissolution by acid digestion. *Chemical Geology*, 157, 175-187.

Appendices

Table A-1-1: Sample description and stratigraphical position of Nikia and Yali units following the nomenclature of several studies (*DiPaola 1974; **Vougioukalakis 1993; ***Allen et al. 2000)

<i>Sample</i>	<i>Locality</i>	<i>Description</i>	<i>Stratigraphy</i>
Y 4	E part of Yali	pumice	
Y 2a+	quarry island of Yali	pumice	phreatomagmatic event post obsidianic-flow
Y 2	quarry island of Yali	pumice	Yali fallout (subaerial)***
Y 1	quarry island of Yali	pumice	Yali pumice breccia (submarine)***
			Yali pumice breccia (submarine)***
NIS 9c	Trapezina	lava	post-caldera domes**
NIS 11a	Loutra	pumice	Upper pumice**
NIS 11c	Loutra	pumice	Upper pumice**
NIS 8	S caldera rim	pumice	Upper pumice**
NIS 19	S Thermiani	pumice	Upper pumice**
NIS 2a	NE Nikia	pumice	Upper pumice**
NIS 2	NE Nikia	pumice	Upper pumice**
NIS 1	E Nikia	lava flow	Nikia lava**
NIS 1B	N Nikia	enclave in lava flow	Nikia lava**
NIS 1c	Theologos Monastery	lava flow	Nikia lava**
NIS 11	Loutra	pumice	Lower pumice**
UNT.B.	W flank - cape Kanoni	pumice	Lower pumice**
			<i>caldera-causing unit</i>
NIS 12	cape Katsuni	pumice	
NIS 14	S flank	scoriae	unit 5* (pyroclastic deposits)
LD	NE caldera rim	lava flow	unit 6* (glassy lava flow)
NIS 4, 4a	NE caldera rim	lava flow and bomb	unit 8* (subaerial basic pyroclastics)
NIS 4c	road to Lakki Plain	lacustrine sediment	
NIS 10A	W of Mandraki	pillow lava	unit 10* (submarine basic)

Table A-1-2: Major- and trace element data of Nisyros, Yali and Ios.

	Pre-caldera units				Post-caldera-units										Yali			Ios		
	NIS 4	NIS10A	LD	NIS4A	NIS 14	NIS 1B	NIS 1I	NIS 1I	NIS 1	NIS 1C	NIS11C	NIS 9C	Y 1	Y 2	Y 2A+	Y 4	IOS 1	IOS 2	IOS 3	
<i>Major Elements [wt %]</i>																				
SiO ₂	53.5	58.1	55.1	58.1	53.4	53.1	60.4	68.9	69.4	68.0	68.2	73.2	71.8	67.8	75.6	73.06	69.25	76.57		
TiO ₂	0.94	1.12	0.79	1.12	0.93	0.94	0.75	0.40	0.35	0.36	0.34	0.12	0.16	0.32	0.13	0.16	0.36	0.07		
Al ₂ O ₃	17.8	17.1	18.3	17.1	18.5	18.1	16.3	15.2	14.9	15.0	14.8	11.8	12.2	13.6	12.1	14.16	14.98	11.66		
Fe ₂ O ₃	7.02	7.27	6.60	7.27	7.20	8.13	5.29	3.14	2.79	2.90	2.67	1.10	1.38	2.09	1.09	0.74	2.65	0.52		
MnO	0.13	0.13	0.12	0.13	0.12	0.14	0.09	0.07	0.08	0.07	0.06	0.04	0.05	0.07	0.04	0.01	0.03	0.01		
MgO	3.93	2.77	4.05	2.77	4.34	4.34	2.60	1.44	0.83	1.04	1.00	0.16	0.39	0.82	0.24	0.16	0.58	0.16		
CaO	9.46	6.59	8.80	6.59	9.19	8.27	5.20	3.50	2.54	2.92	3.12	0.74	1.51	2.47	0.74	0.34	1.59	0.23		
Na ₂ O	3.46	4.06	3.59	4.06	3.44	3.35	3.65	3.87	4.51	3.98	4.16	3.32	3.35	3.86	3.53	2.85	3.11	2.35		
K ₂ O	1.30	1.81	1.21	1.81	0.97	1.54	2.04	3.00	3.13	2.95	3.11	4.54	4.26	3.76	4.41	5.63	3.97	5.73		
P ₂ O ₅	0.19	0.25	0.22	0.25	0.22	0.21	0.15	0.10	0.09	0.10	0.09	0.02	0.03	0.08	0.02	0.15	0.01	0.05		
L.O.I.	1.49	0.07	0.29	0.04	1.31	1.26	3.26	0.06	0.38	2.61	1.44	4.22	4.46	4.84	2.15	1.04	1.64	0.85		
Sum	99.2	99.2	99.0	99.2	99.6	99.4	99.8	99.7	99.1	99.9	99.0	99.2	99.6	99.7	100	98.36	98.33	98.29		
<i>Trace Elements [ppm]</i>																				
Cs	2.75	0.38	0.18	0.41	0.15	0.50	0.99	1.53	7.21	9.17	9.10	13.9	13.3	12.0	15.5	2.38	2.24	1.49		
Rb	196	170	50.2	139	51.0	91.5	40.0	59.0	390	483	450	880	947	553	893	205	175	157		
Ba	261	399	321	396	283	298	462	677	797	735	721	879	831	676	845	324	1973	886		
Th	12.63	11.62	8.15	13.61	8.21	6.82	8.32	10.02	25.00	33.13	27.74	51.55	53.22	37.58	53.68	9.26	33.6	17.2		
U	1.24	1.66	1.09	1.72	0.92	0.85	1.68	1.76	3.14	3.00	3.37	5.02	4.87	4.02	5.18	2.21	3.07	3.81		
Ta	2.22	1.48	0.54	0.84	0.66	0.45	0.92	0.82	2.75	1.02	2.13	1.66	1.58	1.66	1.62	1.85	1.31	0.94		
Nb	11.8	14.8	10.2	14.8	12.0	9.84	15.3	12.3	19.1	14.5	16.1	20.9	20.1	23.3	19.8	15.4	20.6	6.46		
La	25.4	33.1	28.2	31.1	26.9	22.5	20.7	23.5	41.5	43.8	42.0	54.9	56.9	41.4	51.0	16.0	129	41.0		

...continued

	<i>Pre-caldera units</i>										<i>Post-caldera-units</i>					<i>Yali</i>				<i>Ios</i>		
	NIS 4	NIS10A	LD	NIS 4A	NIS 14	NIS 1B	NIS 11	NIS 1	NIS 1C	NIS11C	NIS 9C	Y 1	Y 2	Y 2A+	Y 4	IOS 1	IOS 2	IOS 3				
Ce	42.1	56.6	46.7	55.3	44.0	42.2	42.1	38.4	68.3	63.6	62.0	81.0	81.2	64.1	76.7	34.4	253	87.0				
Pr	4.66	5.86	5.11	5.73	5.03	4.48	3.68	3.22	5.61	5.91	5.45	6.89	7.57	5.72	6.36	3.89	26.7	9.66				
Pb	5.38	8.95	7.67	8.50	4.52	14.8	8.61	8.73	12.0	11.8	12.7	15.5	16.3	11.1	15.7	12.8	23.6	21.8				
Mo	2.60	2.06	1.80	2.16	0.77	1.10	2.81	1.67	4.62	3.39	4.03	5.58	5.46	3.98	5.56	0.74	3.22	0.86				
Nd	19.7	24.1	21.0	23.3	20.4	19.2	14.5	11.6	19.2	20.2	18.3	22.1	25.2	20.4	20.9	15.7	103	38.9				
Sr	568	335	442	329	412	581	276	420	247	270	322	65.4	130	172	58.7	33.0	183	53.0				
Zr	125	167	132	164	127	107	136	91.5	78.5	61.6	91.3	104	105	180	97.7	8.07	11.6	14.9				
Hf	3.18	4.10	3.34	4.16	3.23	2.75	3.48	1.75	3.72	2.67	2.64	3.42	3.57	4.84	3.28	0.24	0.44	0.68				
Sm	4.22	4.81	4.06	4.77	4.18	3.78	3.07	1.92	3.06	3.19	2.91	3.29	3.66	3.37	3.04	4.07	16.8	7.13				
Eu	1.23	1.26	1.17	1.27	1.18	1.17	0.85	0.79	0.71	0.77	0.71	0.42	0.52	0.72	0.39	0.36	2.14	0.79				
Gd	4.21	4.71	3.87	4.81	4.10	3.59	3.11	1.79	2.85	2.94	2.66	2.98	3.23	3.07	2.74	3.30	13.6	5.30				
Li	10.4	6.58	0.98	5.83	3.40	15.9	16.3	39.5	42.5	35.4	40.3	40.3	32.1	39.1	63.4	3.72	16.6	3.63				
Dy	4.17	4.66	3.75	4.74	3.97	3.44	3.18	1.66	2.66	2.68	2.39	2.81	2.99	2.93	2.57	2.07	8.58	3.43				
Y	36.1	35.5	27.6	35.8	29.7	25.7	22.4	11.7	21.2	22.3	19.1	24.9	26.1	24.0	22.3	8.31	41.5	14.6				
Ho	0.90	1.01	0.81	1.03	0.86	0.74	0.71	0.36	0.59	0.58	0.52	0.62	0.65	0.64	0.57	0.28	1.49	0.56				
Yb	2.55	2.92	2.35	3.01	2.41	2.12	2.22	1.18	2.12	2.03	1.78	2.39	2.44	2.33	2.20	0.33	2.58	1.03				
Lu	0.39	0.45	0.36	0.47	0.37	0.32	0.35	0.19	0.34	0.33	0.29	0.39	0.39	0.38	0.36	0.04	0.35	0.14				
Cr	14.5	8.65	73.7	9.42	52.1	1.33	74.9	4.94	3.33	3.03	3.47	0.27	1.76	2.69	0.92	5.07	26.4	5.75				
Co	63.9	16.8	19.5	16.8	21.0	22.7	13.2	6.39	29.0	3.89	33.29	0.55	1.65	2.31	0.67	1.05	10.6	0.70				
Ni	29.9	8.20	38.0	8.81	34.4	6.00	26.6	6.87	2.44	4.99	4.06	3.32	3.82	4.74	1.91	3.14	13.3	3.43				

Table A-1-3: Isotope data. Sm-Nd and Lu-Hf mantle extraction ages (t_{Nd} and t_{Hf}) are presented in Ga, Rb-Sr model ages (t_{Sr}) in Ma. Uncertainties are given as 2 S.D. to the last significant digits. *Isotope data of lower crustal xenoliths after Kempton et al. (1997). LCX1-3 correspond to samples Szg 3017, Szg 3004 and Szg 3006, respectively.

Sample	$^{143}Nd/^{144}Nd$	$\epsilon(Nd)$	$^{147}Sm/^{144}Nd$	t_{Nd}	$^{176}Hf/^{177}Hf$	$\epsilon(Hf)$	$^{176}Lu/^{177}Hf$	t_{Hf}	$^{87}Sr/^{86}Sr$	t_{Sr}	$^{206}Pb/^{204}Pb$	$^{207}Pb/^{204}Pb$	$^{208}Pb/^{204}Pb$
NIS 4	0.512675±2	0.73	0.1356±4	0.880	0.282915±5	5.06	0.0146±4	0.748	0.704618±22	52.96	18.713±1	15.644±1	38.649±2
NIS 10A	0.512632±5	-0.12	0.1258±4	0.859	0.282935±7	5.76	0.0163±4	0.741	0.704521±21	79.29	18.698±1	15.629±1	38.576±2
LD	0.512668±7	0.58	0.1224±4	0.777	0.282929±5	5.56	0.0161±4	0.755	0.704278±21	0	18.647±1	15.645±1	38.502±2
NIS 4A	0.512632±5	-0.12	0.1285±4	0.862	0.282937±7	5.85	0.0164±4	0.751	0.704616±18	54.87	18.710±1	15.642±1	38.650±1
NIS 14	0.512622±6	-0.31	0.1262±4	0.878	0.282914±6	5.02	0.0157±4	0.773	0.704547±20	102.08	18.690±1	15.634±1	38.589±2
NIS 11	0.512628±5	-0.19	0.1217±4	0.830	0.282890±6	4.16	0.0133±4	0.754	0.704510±17	27.11	18.738±1	15.643±1	38.646±2
NIS 1B	0.512747±7	2.12	0.1257±7	0.679	0.282961±7	6.69	0.0165±7	0.697	0.703648±19	0	18.709±2	15.639±2	38.618±4
NIS 1	0.512572±7	-1.29	0.0989±5	0.747	0.282817±1	1.58	0.0111±5	0.827	0.704194±48	24.05	18.743±1	15.646±1	38.687±1
NIS 1C	0.512589±4	-0.96	0.0991±5	0.727	0.282874±7	3.61	0.0112±4	0.730					
NIS 11C	0.512576±6	-1.21	0.0977±4	0.735	0.282835±8	2.21	0.0119±4	0.817	0.704384±18	22.14	18.779±1	15.652±1	38.720±2
NIS 9C	0.512572±5	-1.28	0.0983±4	0.743	0.282838±6	2.33	0.0107±4	0.780	0.704312±32	19.19	18.753±1	15.643±1	38.689±1
Yali 1	0.512607±6	-0.61	0.0937±6	0.676	0.282917±6	5.12	0.0146±4	0.735	0.704701±11	6.63	18.742±1	15.649±1	38.676±3
Yali 2A+	0.512553±4	-1.66	0.1026±4	0.794	0.282794±5	0.77	0.0107±4	0.856	0.704847±20	32.19	18.785±1	15.658±1	38.749±1
Yali 4	0.512571±5	-1.31	0.1036±9	0.777	0.282827±6	1.93	0.0142±4	0.900	0.704461±14	4.21	18.756±1	15.651±1	38.708±2
IOS 1	0.512049±7	-11.49	0.1583±4	2.715	0.282366±12	-14.3	0.0050±8	1.339	0.766346±19	215.85	18.821±1	15.740±1	38.895±1
IOS 2	0.512038±4	-11.7	0.0989±4	1.397	0.282462±8	-11	0.0116±8	1.462	0.722314±17	196.53			
IOS 3	0.512051±5	-11.45	0.1121±4	1.546	0.282409±18	-12.9	0.0091±5	1.436	0.739004±19	196.53	18.688±1	15.716±1	39.094±2
<i>lower crustal xenoliths*</i>													
LCX1	0.512583								0.707200		18.738	15.664	38.808
LCX2	0.512390								0.708350		18.685	15.703	38.809
LCX3	0.512853								0.706994		19.040	15.777	39.197

Table A-2-1: Summary of published age estimations on different units of the Nisyros-Yali volcanic system.

Stratigraphy	Di Paola (1974)	Wagner (1976)	Federman & Carey (1980)	Barberi et al. (1988)	Rehren (1988)	Keller et al. (1990)	Limburg & Varenkamp (1991)	Vougioukalakis (1993)	Smith et al. (1996)
Yali units									
Yali Obsidiane		24 ± 10 ka (fission track)							
Yali pumice			31 ka (O-isotope)	neolithic (< 14 ka)				< 10 ka	
post-caldera				110 ka			> 44 ka (fission track)		
pre-caldera									
Kyra - paleosol					24 ka (¹⁴ C)				
Kyra formation					38 ± 20 ka (K/Ar)				
Argos lava						66 ± 2 ka (K/Ar)			
Submarine lava		200 ± 50 ka (K/Ar – WR)						145 ka	
KPT (Kos Plateau Tuff)					145 ± 5 ka (K/Ar)				161 ± 1 ka (Ar-Ar)

Table A-2-2: ^{39}Ar - ^{40}Ar data of Nisyros plagioclase separates and volcanic glasses. Isotope data are given in nL.

step	T[°C]	$^{40}\text{Ar}_{\text{tot}}$	^{39}Ar	^{38}Ar	^{37}Ar	^{36}Ar	Age[Ma]
<i>NIS 12 (plag) (100.6 mg; $K_2O = 0.34$ wt%, $Cl = 108$ ppm; $J = 0.000515$; values are given in nL; errors are 1σ)</i>							
1	530	4.377±0.007	0.102±0.001	0.033±0.001	0.034±0.001	0.0143±0.0003	1.317±0.710
2	880	1.866±0.001	0.057±0.001	0.019±0.001	0.036±0.001	0.0062±0.0003	0.359±1.200
3	950	1.345±0.003	0.075±0.001	0.022±0.001	0.101±0.001	0.0038±0.0003	2.943±1.100
4	1015	1.571±0.001	0.076±0.001	0.017±0.001	0.142±0.001	0.0045±0.0003	2.946±0.880
5	1180	0.990±0.002	0.105±0.001	0.013±0.001	0.301±0.001	0.0029±0.0002	1.293±0.590
6	1420	1.731±0.002	0.191±0.001	0.009±0.001	0.704±0.002	0.0054±0.0003	0.848±0.370
<i>NIS 19 (glass) (99.4 mg; $K_2O = 0.7$ wt %, $Cl = 251$ ppm; $J = 0.000515$)</i>							
1	521	22.452±0.022	0.373±0.001	0.1578±0.0004	0.134±0.001	0.0761±0.0004	neg. value
2	741	5.109±0.002	0.230±0.001	0.0687±0.0002	0.368±0.002	0.0176±0.0002	neg. value
3	887	0.770±0.001	0.145±0.001	0.0159±0.0002	0.509±0.002	0.0028±0.0002	neg. value
4	1009	0.379±0.001	0.129±0.001	0.0082±0.0001	0.517±0.002	0.0017±0.0002	neg. value
5	1128	0.323±0.001	0.153±0.001	0.0068±0.0002	0.604±0.002	neg. value	neg. value
6	1420	0.270±0.002	0.207±0.001	0.0065±0.0001	0.842±0.003	0.0015±0.0002	neg. value
<i>NIS 11 (102.5 mg; $K_2O = 0.58$ wt %, $Cl = 136$ ppm; $J = 0.000515$)</i>							
1	530	9.621±0.006	0.213±0.001	0.0854±0.004	0.089±0.001	0.0335±0.0002	neg. value
2	740	1.383±0.003	0.173±0.001	0.0383±0.0003	0.324±0.001	0.0044±0.0002	6.475±2.500
3	885	0.337±0.001	0.111±0.001	0.0060±0.0002	0.390±0.001	0.0020±0.0001	neg. value
4	1005	0.419±0.003	0.164±0.001	0.0043±0.0002	0.593±0.002	0.0010±0.0001	10.316±1.600
5	1190	0.422±0.001	0.196±0.001	0.0088±0.0002	0.684±0.002	0.0025±0.0001	neg. value
6	1415	0.499±0.001	0.189±0.001	0.0070±0.0002	0.674±0.002	0.0012±0.0002	9.659±2.300
<i>NIS 2 (100.6 mg; $K_2O = 0.5$ wt %, $Cl = 142$ ppm; $J = 0.000515$)</i>							
1	535	12.284±0.041	0.158±0.001	0.0552±0.0003	0.049±0.001	0.0385±0.0003	5.294±0.520
2	740	8.842±0.014	0.240±0.001	0.075±0.0003	0.281±0.001	0.0275±0.0012	2.886±0.310
3	890	1.328±0.003	0.069±0.001	0.0100±0.0002	0.183±0.001	0.0033±0.0002	4.824±0.940
4	1011	1.158±0.002	0.115±0.001	0.0064±0.0003	0.391±0.001	0.0030±0.0003	2.362±0.570
5	1180	0.908±0.001	0.120±0.001	0.0037±0.0002	0.423±0.002	0.0017±0.0003	3.454±0.570
6	1415	1.364±0.002	0.197±0.001	0.0074±0.0001	0.699±0.003	0.0046±0.0003	0.277±0.350
<i>NIS 2a (108.6 mg; $K_2O = 0.9$ wt %, $Cl = 340$ ppm; $J = 0.000515$)</i>							
1	525	14.653±0.081	0.211±0.002	0.0755±0.0010	0.043±0.001	0.0443±0.0002	6.860±0.270
2	744	6.287±0.160	0.173±0.004	0.0681±0.0021	0.055±0.002	0.0171±0.0004	6.596±0.590
3	887	7.748±0.002	0.611±0.001	0.1835±0.0004	0.837±0.003	0.0264±0.0002	neg. value
4	1010	1.168±0.001	0.292±0.001	0.0320±0.0002	0.911±0.003	0.0040±0.0002	0.129±0.180
5	1180	0.495±0.001	0.167±0.001	0.0097±0.0001	0.560±0.002	0.0014±0.0002	0.702±0.270
6	1420	0.528±0.001	0.215±0.001	0.0098±0.0002	0.816±0.003	0.0020±0.0002	0.047±0.180

...continued

step	T[°C]	⁴⁰ Ar _{tot}	³⁹ Ar	³⁸ Ar	³⁷ Ar	³⁶ Ar	Age [Ma]
<i>NIS 8 (plag.) (94.9 mg; K₂O = 0.7 wt %, Cl = 311 ppm; J = 0.00132)</i>							
1	525	54.488±0.160	0.462±0.004	0.2058±0.0019	0.127±0.001	0.1755±0.0008	5.304±0.450
2	621	3.617±0.002	0.102±0.001	0.0382±0.0001	0.074±0.001	0.0115±0.0002	2.055±0.510
3	738	1.256±0.002	0.154±0.001	0.0387±0.0001	0.327±0.001	0.0042±0.0002	0.265±0.330
4	884	0.675±0.002	0.133±0.001	0.0094±0.0001	0.546±0.002	0.0042±0.0002	neg. value
5	1008	0.443±0.001	0.133±0.001	0.0083±0.0002	0.578±0.002	0.0017±0.0002	neg. value
6	1179	0.413±0.001	0.138±0.001	0.0124±0.0001	0.581±0.002	0.0017±0.0002	neg. value
7	1420	0.418±0.001	0.130±0.001	0.0125±0.0002	0.572±0.002	0.0014±0.0002	0.373±0.370
<i>NIS 8 (glass) (29.3 mg; K₂O = 2.6 wt %, Cl = 173 ‰; J = 0.00132; values are given in nL; errors are 1σ)</i>							
1	489	121.00±0.67	1.190±0.003	0.469±0.002	0.155±0.002	0.387±0.002	10.269±0.940
2	623	47.30±0.02	1.270±0.001	0.508±0.001	0.128±0.001	0.157±0.001	1.269±0.230
3	712	10.10±0.01	0.666±0.001	0.267±0.001	0.090±0.001	0.031±0.001	2.148±0.140
4	789	6.17±0.01	0.132±0.001	0.053±0.001	0.046±0.001	0.021±0.001	neg. value
5	886	3.03±0.01	0.036±0.001	0.013±0.001	0.035±0.001	0.009±0.001	22.685±2.400
6	969	5.55±0.01	0.066±0.001	0.025±0.001	0.060±0.001	0.018±0.001	5.407±0.980
7	1432	4.28±0.01	0.062±0.001	0.025±0.001	0.051±0.001	0.014±0.001	6.956±1.100
<i>UNT.B. (plag.) (6.8 mg; K₂O = 0.6 wt %, Cl = 205 ppm; J = 0.000515)</i>							
1	528	27.658±0.039	0.183±0.001	0.0898±0.0007	0.063±0.001	0.0935±0.0004	0.103±0.570
2	740	3.143±0.015	0.124±0.001	0.0410±0.0002	0.176±0.001	0.0106±0.0002	0.114±0.430
3	884	0.670±0.002	0.074±0.001	0.0106±0.0002	0.236±0.001	0.0015±0.0002	3.528±0.670
4	1006	0.748±0.001	0.094±0.001	0.0059±0.0001	0.389±0.002	0.0034±0.0002	neg. value
5	1181	0.655±0.001	0.105±0.001	0.0042±0.0002	0.449±0.002	0.0025±0.0002	neg. value
6	1313	0.529±0.001	0.067±0.001	0.0034±0.0002	0.297±0.001	0.0025±0.0002	neg. value
7	1420	0.440±0.001	0.059±0.001	0.0033±0.0001	0.258±0.001	0.0011±0.0002	2.139±0.780

Table A-2-3: U-Th data of Nisyros post-caldera volcanites. Errors are given in 2SD (gm refers to groundmass). The ages are calculated using ISOPLOT ver. 2.49n (Ludwig 2002) assuming an initial $^{230}\text{Th}/^{234}\text{U}$ of 0.

sample	phase	U [ppb]	Th [ppb]	$^{230}\text{Th}/^{238}\text{U}$	$^{234}\text{U}/^{238}\text{U}$	$^{238}\text{U}/^{232}\text{Th}$	age [ka]*	$(^{234}\text{U}/^{238}\text{U})_i$
<i>post-caldera series</i>								
NIS 1	glass	121±13	574±5	1.689±0.183	1.011±0.004	0.637±0.068	n.d.	
NIS 1	WR	2122±227	7596±127	1.048±0.114	1.006±0.003	0.843±0.091	n.d.	
NIS 1	gm	2371±6	9425±65	1.132±0.009	0.993±0.001	0.759±0.006	n.d.	
NIS 1	mag	779±2	2797±46	1.070±0.019	1.005±0.004	0.840±0.014	n.d.	
NIS 1	mag	2876±7	11631±65	1.154±0.007	0.992±0.001	0.746±0.005	n.d.	
NIS 2a	plag	568±1	1996±28	1.123 ±0.013	0.990±0.002	0.859±0.012	n.d.	
NIS 2a	gm	294±1	1196±25	1.201±0.035	0.983±0.004	0.742±0.016	n.d.	
NIS 2a	mag	915±2	4060±23	1.204±0.007	0.997±0.002	0.680±0.004	n.d.	
NIS 9c	WR	2246±11	459±40	0.241±0.013	1.002±0.005	14.775±1.292	30.0±1.8	1.003±0.005
NIS 9c	glass	169±1	395±26	1.696±0.124	0.992±0.007	1.294±0.084	n.d.	
NIS 9c	mag	600±2	1973±41	0.987±0.012	1.009±0.006	0.918±0.019	401±63	1.029±0.017

Table A-3-1: Unconformity Bounded Stratigraphic Unit (UBSU) in Monte Vulture volcanic sequence. ^{39}Ar - ^{40}Ar ages in ka from (A) Bonadonna et al. (1998), (B) Brocchini (1993), (C) Villa (1985*, 1988**, 1991***). In bold, ages recalculated in this work based on isochemical reservoirs and updated monitor age. Primary ages are presented in parentheses.

Supersynthem	Synthem	Subsynthem	ages		
			A	B	C
Monticchio	Laghi di Monticchio	Serra di Braida			
		Lago Piccolo		(176±19)	
		Lago Grande		160±17	
		Piano Comune			
		Casa Rossa			
	Valle dei Greggi-Fosso del Corbo	Meseria di Cuscito			
		Imbandina			
		Case Lopes		(435±6)	
			494±5		
Monte Vulture	Melfi	Piano di Croce			
		Castello di Melfi	(557±7)		565±4***
		Piano di Gaudio	573±4		
	Barile	Ventaruolo		(654±33)	
				670±24	
				(659±33)	
				671±13	
		Vulture San-Michele		(600±7)	590*
			611±6		
	Foggianello	Rionero	(612±19)	630±20	660**
			(654±11)	672±6	
Toppo San Paolo					
Fara d'Olivo				(731±40*)	
			742±22		
	Campanile				
	Spinoritola	(674±7)	698±8		

Table A-3-2: Location, description, stratigraphical position and phases separated from samples analysed in the present work.

Synthem	Subsynthem	Sample	Locality	Description	Mineral phase
Monticchio		VUT 0004 PG 3	Ripe del Cavallo (Upp.) Ripe del Cavallo (Low)	Alloctonous tephra Alloctonous tephra	san. san.
	Laghi di Monticchio	VUT 0008	Ripacandida	Tuffisitic lapilli	bio., phl.
		VUT 251	SS dei Laghi di Monticchio	Tuffisitic lapilli	bio.
		VUT 0001	Mulino Vecchio	Diatremic breccia	bio., phl.
Valle dei Greggi - Fosso del Corbo		VUT 168	Ciaulino quarry	Scoriae deposit	bio.
		VU 1523	Melfi (Normann quarry)	Hauynophyre lava flow	nos.
Melfi		VUT 9923	Fontana dei giumentari	Dyke	bio., phl.
		VUT 9919	Fontana dei Preti	Dyke	bio.
Barile		VUT 9918	Fontana dei preti	Lava flow	phl.
		VU 1907	Madonna di Costantinopoli quarry	Lava flow	lc.
		VUT 0002	Sant' Antonio quarry (marker M3)	Pumice fall	san.
		VU 1680	Masseria Boccaglie (marker M3)	Pumice fall	san.
Monte Vulture		VU 1813	Piana di Croce	Upper Ignimbrite	san.
		VUT 9905 PG5	Piana di Croce	Upper Ignimbrite	san. (selected pumices)
		VU 1809	La Cupa (Atella)	Lower Ignimbrite	san. and phl. (selected pumices)
			Piana di Croce	Lower Ignimbrite	san. (from whole rock)
Foggianello		VUT 110	Rupe di Gallo	Dyke	san.
		VUG1	Rupe di Gallo	Dyke	san.

Table A-3-3: ^{39}Ar - ^{40}Ar data. All isotopes are in nL. Steps marked with an asterisk were used for isochron and/or average calculations, as their relatively uniform Ca/K and/or Cl/K ratios represent an isochemical reservoir.

step	T[°C]	$^{40}\text{Ar}_{\text{tot}}$	^{39}Ar	^{38}Ar	^{37}Ar	^{36}Ar	Age[ka]
<i>VUT 0004-san (115mg; $K_2O = 12.11\text{wt}\%$, $Cl = 21\text{ppm}$; $J = 0.001032$; values are given in nl; errors are 1σ)</i>							
1	525	3.481±0.073	0.616±0.02	0.022±0.044	0.051±0.004	0.0127±0.0003	786±266
2	634	1.123±0.002	1.271±0.002	0.019±0.017	0.021±0.002	0.0026±0.0002	515±70
3*	695	1.714±0.002	10.658±0.001	0.135±0.003	0.182±0.006	0.0053±0.0002	27±5
4*	747	1.152±0.001	11.848±0.001	0.148±0.004	0.191±0.006	0.0033±0.0002	28±5
5*	798	1.297±0.001	14.348±0.001	0.179±0.004	0.238±0.006	0.0034±0.0002	37±4
6*	845	1.224±0.001	9.905±0.009	0.122±0.003	0.142±0.008	0.0032±0.0001	50±4
7	916	0.758±0.001	4.075±0.004	0.050±0.017	0.049±0.005	0.0019±0.0002	89±18
8	1058	1.451±0.001	5.369±0.005	0.067±0.022	0.076±0.004	0.0042±0.0002	70±12
9	1194	1.444±0.001	3.575±0.004	0.046±0.014	0.074±0.008	0.0039±0.0002	155±25
10	1320	0.788±0.003	1.445±0.002	0.019±0.012	0.002±0.001	0.0013±0.0002	500±54
11	1417	0.507±0.001	0.551±0.007	0.007±0.001	0.007±0.006	0.0011±0.0002	583±156
<i>PG 3 - san (30.2mg; $K_2O = 13.7\text{wt}\%$; $Cl = 7\text{ppm}$; $J = 0.000469$)</i>							
1	546	156.819±0.370	2.625±0.004	0.415±0.001	0.763±0.009	0.576±0.002	neg. value
2	585	34.7844±0.030	6.269±0.018	0.281±0.001	0.573±0.010	0.117±0.001	23±14
3	656	156.628±0.061	16.277±0.018	0.386±0.001	0.469±0.003	0.549±0.002	neg. value
4*	716	23.555±0.021	25.630±0.027	0.362±0.001	0.620±0.004	0.078±0.001	15±3
5	770	12.846±0.070	23.066±0.023	0.317±0.001	0.602±0.003	0.026±0.001	193±5
6*	819	15.882±0.085	32.302±0.030	0.432±0.001	0.735±0.006	0.052±0.001	14±3
7*	868	15.170±0.032	40.250±0.048	0.525±0.001	0.847±0.008	0.047±0.001	27±2
8*	910	11.201±0.026	39.859±0.038	0.521±0.001	0.920±0.008	0.035±0.001	17±1
9*	955	10.153±0.016	38.822±0.038	0.496±0.002	0.808±0.005	0.031±0.001	20±1
10	991	12.210±0.045	22.359±0.039	0.300±0.001	0.560±0.004	0.045±0.001	neg. value
11*	1034	26.629±0.016	57.431±0.062	0.753±0.002	1.172±0.010	0.084±0.001	neg. value
12*	1069	18.034±0.029	28.098±0.038	0.368±0.002	0.640±0.004	0.060±0.001	7±3
13*	1123	17.816±0.017	37.372±0.066	0.498±0.001	0.751±0.004	0.057±0.001	22±2
<i>VUT 0008-phl (38.1mg, $K_2O = 6.15\text{wt}\%$, $Cl = 86\text{ppm}$; $J = 0.001031$)</i>							
1	490	56.734±0.046	1.647±0.002	0.068±0.002	0.008±0.001	0.1895±0.0007	821±226
2*	598	23.403±0.061	1.697±0.002	0.046±0.002	0.006±0.001	0.0760±0.0003	1041±96
3*	689	9.281±0.002	0.983±0.001	0.020±0.002	0.011±0.002	0.0299±0.0002	823±94
4*	767	14.770±0.001	1.626±0.002	0.036±0.001	neg. value	0.0472±0.0003	936±81
5*	838	12.442±0.003	1.091±0.001	0.026±0.002	neg. value	0.0406±0.0002	767±106
6*	883	10.659±0.002	0.979±0.001	0.022±0.001	0.007±0.001	0.0337±0.0002	1309±106
7*	977	18.676±0.004	1.849±0.002	0.043±0.003	0.003±0.001	0.0597±0.0003	1032±72
8*	1051	5.350±0.014	0.583±0.001	0.013±0.001	0.005±0.002	0.0166±0.0002	1400±146
9*	1192	2.462±0.004	0.229±0.001	0.006±0.002	0.010±0.001	0.0078±0.0001	1298±256
10	1420	2.080±0.005	0.018±0.001	0.001±0.001	0.009±0.002	0.0067±0.0001	10774±4096
<i>VUT 0008 - bio small (26.3mg; $K_2O = 5.3\text{wt}\%$, $Cl = 33\text{ppm}$; $J = 0.000463$)</i>							
1	551	11.494±0.002	0.053±0.001	0.0065±0.0002	0.0118±0.0011	0.0396±0.0002	neg. value
2	623	17.117±0.630	0.142±0.001	0.0015±0.0006	neg. value	0.0432±0.0004	25392±1196
3*	687	36.863±0.051	0.255±0.001	0.0321±0.0002	0.0018±0.0007	0.1249±0.0005	neg. value
4*	770	29.289±0.005	0.541±0.001	0.0281±0.0002	0.0047±0.0002	0.0963±0.0004	1276±166
5*	870	13.398±0.004	0.508±0.001	0.0175±0.0001	0.0003±0.0001	0.0431±0.0002	1078±96
6	998	9.521±0.004	0.464±0.001	0.0145±0.0001	0.0081±0.0008	0.0305±0.0002	908±88
7*	1077	4.458±0.004	0.194±0.001	0.0060±0.0001	0.0142±0.0009	0.0138±0.0001	1621±91
8*	1216	36.729±0.003	0.045±0.001	0.0233±0.0001	0.0005±0.0001	0.1226±0.0005	9425±2496
9	1445	2.113±0.004	0.002±0.001	0.0013±0.0001	0.0054±0.0007	0.0054±0.0001	242506±20999

...continued

step	T[°C]	⁴⁰ Ar _{tot}	³⁹ Ar	³⁸ Ar	³⁷ Ar	³⁶ Ar	Age[ka]
<i>VUT 0008 - bio large (32.6mg; K₂O = 4.7wt%, Cl = 37ppm; J = 0.000465; values are given in nl; errors are 1σ)</i>							
1	560	0.064±0.005	0.001±0.001	neg. value	0.0114±0.0017	0.0002±0.0001	11917±3596
2*	629	10.009±0.210	0.386±0.002	0.0069±0.0002	0.0065±0.0002	0.0364±0.0009	neg. value
3*	690	3.903±0.003	0.183±0.001	0.0055±0.0003	0.0041±0.0001	0.0118±0.0002	1963±226
4*	772	7.126±0.006	0.641±0.001	0.0155±0.0001	0.0076±0.0007	0.0227±0.0001	561±47
5*	870	6.528±0.004	0.527±0.001	0.0170±0.0001	0.0090±0.0009	0.0205±0.0002	722±83
6*	917	5.823±0.002	0.319±0.001	0.0084±0.0001	0.0032±0.0008	0.0184±0.0002	1028±126
7*	1000	10.519±0.002	0.754±0.001	0.0183±0.0001	0.0213±0.0014	0.0317±0.0002	1294±70
8*	1078	2.499±0.001	0.253±0.001	0.0057±0.0001	0.0059±0.0002	0.0065±0.0002	1874±176
9*	1213	0.687±0.001	0.058±0.001	0.0025±0.0002	0.0035±0.0011	0.0023±0.0002	neg. value
10	1440	0.794±0.001	0.003±0.001	neg. value	0.0072±0.0011	0.0047±0.0002	neg. value
<i>VUT 251 - bio (28mg; K₂O = 2.7wt.%, Cl = 411ppm; J = 0.000468)</i>							
1	510	2.594±0.006	0.008±0.001	0.0037±0.0001	0.0103±0.0003	0.0089±0.0001	1658±1996
2	623	5.811±0.003	0.035±0.001	0.0054±0.0001	0.0262±0.0001	0.0168±0.0003	23566±846
3	673	12.015±0.016	0.239±0.003	0.0150±0.0001	0.0204±0.0001	0.0405±0.0002	431±280
4	713	14.526±0.003	0.578±0.005	0.0223±0.0001	0.0090±0.0001	0.0478±0.0001	618±96
5	743	86.860±0.020	3.343±0.004	0.0024±0.0001	0.0014±0.0001	0.2930±0.0012	82±9
6	796	13.881±0.003	0.930±0.001	0.0286±0.0006	0.0111±0.0001	0.0457±0.0002	389±51
7	820	9.301±0.004	0.476±0.001	0.0168±0.0004	0.0075±0.0001	0.0294±0.0001	1136±65
8	867	8.870±0.002	0.526±0.001	0.0172±0.0005	0.0090±0.0001	0.0294±0.0002	354±71
9*	910	7.031±0.001	0.631±0.001	0.0176±0.0004	0.0096±0.0001	0.0235±0.0001	117±33
10*	951	2.751±0.001	0.306±0.001	0.0084±0.0002	0.0071±0.0001	0.0092±0.0001	122±27
11	1005	1.609±0.004	0.076±0.001	0.0027±0.0001	0.0033±0.0001	0.0061±0.0001	neg. value
12*	1036	2.396±0.003	0.339±0.002	0.0090±0.0002	0.0244±0.0001	0.0080±0.0001	113±23
13	1065	2.204±0.004	0.262±0.001	0.0079±0.0002	0.0575±0.0002	0.0075±0.0001	6±3
14	1197	2.035±0.005	0.194±0.001	0.0065±0.0001	0.1414±0.0005	0.0069±0.0001	5±5
15	1442	1.564±0.002	0.018±0.001	0.0016±0.0001	0.0406±0.0002	0.0053±0.0001	214±36
<i>VUT 0001-phl (66.1mg, K₂O = 8wt%, Cl = 278ppm; J = 0.001031)</i>							
1	492	13.439±0.001	0.159±0.007	0.023±0.002	neg. value	0.0445±0.0002	3401±776
2	598	3.576±0.004	0.613±0.007	0.022±0.001	neg. value	0.0102±0.0002	1723±156
3	689	2.551±0.001	2.219±0.001	0.059±0.002	neg. value	0.0058±0.0002	690±35
4	762	7.352±0.001	8.312±0.007	0.213±0.005	neg. value	0.0133±0.0002	759±7
5	849	5.220±0.002	4.192±0.004	0.108±0.002	0.005±0.002	0.0118±0.0002	771±18
6	896	5.248±0.002	2.814±0.003	0.073±0.002	neg. value	0.0140±0.0001	727±24
7	973	11.851±0.003	3.716±0.003	0.099±0.003	neg. value	0.0355±0.0003	679±35
8	1053	6.653±0.002	1.382±0.001	0.039±0.002	neg. value	0.0196±0.0002	1141±76
9	1196	3.327±0.001	0.620±0.007	0.017±0.002	0.008±0.001	0.0104±0.0002	766±136
10	1430	1.410±0.001	0.074±0.002	0.002±0.001	0.006±0.002	0.0042±0.0002	4599±1096
<i>VUT 0001 - bio (28.1mg; K₂O = 7.7wt.%, Cl = 202ppm; J = 0.000468)</i>							
1	500	1.310±0.018	0.011±0.001	0.0016±0.0002	0.0027±0.0002	0.0045±0.0002	neg. value
2	616	3.543±0.001	0.095±0.001	0.0040±0.0001	0.0223±0.0003	0.0106±0.0002	3723±426
3	703	4.498±0.002	0.801±0.001	0.0209±0.0002	0.0056±0.0003	0.0106±0.0001	1440±36
4	795	0.723±0.003	0.193±0.001	0.0054±0.0002	0.0006±0.0001	0.0010±0.0002	1867±246
5	866	5.380±0.002	1.059±0.001	0.0300±0.0001	neg. value	0.0148±0.0002	797±32
6	908	6.116±0.003	0.872±0.001	0.0237±0.0002	0.0014±0.0004	0.0177±0.0002	864±47
7	990	7.542±0.003	0.899±0.001	0.0265±0.0002	0.0021±0.0003	0.0228±0.0002	748±47
8	1060	5.703±0.002	0.435±0.001	0.0150±0.0001	0.0058±0.0002	0.0177±0.0002	933±91
9	1202	3.623±0.001	0.137±0.003	0.0062±0.0002	0.0332±0.0003	0.0117±0.0001	986±256
10	1445	3.709±0.002	0.010±0.001	0.0032±0.0001	0.0274±0.0005	0.0119±0.0002	17533±4596

...continued

step	T[°C]	⁴⁰ Ar _{tot}	³⁹ Ar	³⁸ Ar	³⁷ Ar	³⁶ Ar	Age[ka]
<i>VUT 168 - bio (23.9mg; K₂O = 7.8wt.%, Cl = 113ppm; J = 0.000465; values are given in nl; errors are 1σ)</i>							
1	556	0.767±0.002	0.003±0.001	0.0007±0.0001	0.0302±0.0020	0.0033±0.0001	neg. value
2	624	2.842±0.008	0.126±0.001	neg. value	0.0136±0.0017	0.0046±0.0002	9815±336
3	715	3.052±0.008	0.353±0.001	0.0081±0.0001	0.0116±0.0015	0.0081±0.0004	1587±266
4*	771	1.295±0.001	0.469±0.001	0.0103±0.0001	0.0032±0.0016	0.0034±0.0002	498±96
5*	868	5.024±0.002	1.424±0.001	0.0349±0.0003	0.0061±0.0012	0.0139±0.0001	532±20
6	914	3.724±0.001	0.676±0.001	0.0149±0.0001	neg. value	0.0109±0.0002	627±61
7	997	4.210±0.003	0.359±0.001	0.0094±0.0001	0.0249±0.0015	0.0133±0.0002	622±96
8	1072	4.615±0.003	0.311±0.001	0.0083±0.0001	0.0018±0.0006	0.0142±0.0002	1152±146
9	1208	2.688±0.002	0.121±0.001	0.0041±0.0001	neg. value	0.0089±0.0001	472±266
10	1440	12.657±0.017	0.013±0.001	0.0077±0.0003	0.0128±0.0012	0.0440±0.0003	neg. value
<i>VU 1523 - noesane (6.6mg; K₂O = 3wt.%, Cl = 11 ppm; J = 0.000468)</i>							
1	185	82.859±0.011	0.501±0.001	0.084±0.001	0.264±0.004	0.227±0.001	26501±406
2	251	34.133±0.058	0.839±0.002	0.054±0.001	0.270±0.002	0.077±0.001	11445±176
3	302	25.656±0.034	2.572±0.005	0.080±0.001	0.261±0.003	0.107±0.001	neg. value
4	355	43.595±0.035	5.345±0.006	0.155±0.003	0.228±0.001	0.145±0.001	117±26
5	395	43.092±0.011	4.114±0.004	0.259±0.005	1.372±0.004	0.145±0.001	56±26
6	439	34.048±0.140	1.973±0.011	0.182±0.018	1.376±0.004	0.094±0.025	2701±336
7	480	27.767±0.044	1.574±0.004	0.113±0.004	1.386±0.007	0.091±0.001	580±66
8	523	0.735±0.001	0.031±0.001	0.195±0.005	6.954±0.033	0.002±0.001	17316±116
9	622	100.476±0.028	0.250±0.001	0.111±0.003	7.843±0.031	0.350±0.001	neg. value
10	826	113.522±0.011	1.875±0.002	0.921±0.002	122.926±0.394	0.422±0.002	neg. value
11	1431	97.810±0.015	2.295±0.002	0.800±0.002	11.284±0.032	0.305±0.001	3137±116
<i>VUT 9923-phl (60mg; K₂O = 8.13wt.%, Cl = 284ppm; J = 0.001030)</i>							
1	495	12.074±0.003	0.098±0.001	0.016±0.001	neg. value	0.0397±0.0002	6401±1196
2	602	2.075±0.001	0.166±0.002	0.004±0.001	neg. value	0.0057±0.0002	4422±55
3	693	2.511±0.001	1.321±0.001	0.035±0.001	neg. value	0.0056±0.0002	1181±67
4	770	5.547±0.001	3.376±0.003	0.091±0.003	0.0076±0.0001	0.0144±0.0001	711±18
5	844	5.820±0.001	3.316±0.003	0.088±0.002	neg. value	0.0157±0.0002	659±22
6	888	5.444±0.001	2.882±0.003	0.077±0.002	neg. value	0.0144±0.0002	754±31
7	967	13.190±0.003	4.140±0.004	0.113±0.003	0.0009±0.0001	0.0389±0.0002	755±24
8	1052	11.593±0.001	4.286±0.004	0.115±0.003	neg. value	0.0343±0.0002	632±21
9	1194	7.796±0.001	2.50±0.002	0.071±0.002	neg. value	0.0227±0.0002	802±30
10	1415	1.968±0.001	0.178±0.003	0.005±0.001	neg. value	0.0065±0.0001	561±33
<i>VUT 9923 - bio (28mg; K₂O = 7wt.%, Cl = 188ppm; J = 0.000466)</i>							
1	554	0.884±0.002	0.009±0.001	0.0001±0.0001	0.0082±0.0012	0.0033±0.0001	neg. value
2	625	1.315±0.002	0.061±0.003	0.0001±0.0001	0.0065±0.00012	0.0037±0.0001	2935±576
3	677	1.020±0.002	0.106±0.002	0.0002±0.0001	0.0038±0.00012	0.0026±0.0001	2018±316
4	769	3.234±0.002	0.827±0.008	0.0024±0.0001	0.0004±0.0002	0.0092±0.0001	533±32
5	870	4.483±0.002	1.105±0.011	0.0032±0.0001	0.0110±0.0011	0.0124±0.0001	615±25
6	914	2.776±0.002	0.536±0.006	0.0014±0.0002	0.0077±0.0013	0.0084±0.0001	478±35
7	997	10.025±0.001	0.880±0.008	0.0029±0.0001	0.0117±0.0011	0.0310±0.0002	820±38
8	1075	4.680±0.002	0.303±0.004	0.0010±0.0001	0.0051±0.0010	0.0145±0.0001	1102±96
9	1212	3.365±0.002	0.225±0.003	0.0008±0.0001	0.0030±0.0006	0.0118±0.0001	neg. value
10	1444	0.741±0.001	0.013±0.001	0.0002±0.0001	neg. value	0.0026±0.0001	neg. value

...continued

step	T[°C]	⁴⁰ Ar _{tot}	³⁹ Ar	³⁸ Ar	³⁷ Ar	³⁶ Ar	Age[ka]
<i>VUT 9919 - bio (21.6mg; K₂O = 7.1wt%, Cl = 249ppm; J = 0.000464; values are given in nl; errors are 1σ)</i>							
1	527	5.974±0.003	0.004±0.001	0.0024±0.0002	0.0038±0.0005	0.0204±0.0001	neg. value
2	629	0.573±0.002	0.020±0.001	neg. value	0.0061±0.0013	0.0018±0.0001	2258±996
3	719	1.007±0.002	0.251±0.001	0.0084±0.0001	neg. value	0.0030±0.0001	433±89
4	797	1.376±0.001	0.760±0.001	0.0234±0.0002	0.0069±0.0009	0.0025±0.0001	691±32
5	870	1.808±0.001	0.922±0.001	0.0290±0.0001	0.0021±0.0013	0.0038±0.0001	614±27
6	913	1.153±0.001	0.478±0.001	0.0162±0.0001	0.0018±0.0008	0.0033±0.0001	299±66
7	1000	1.897±0.001	0.431±0.001	0.0154±0.0001	0.0003±0.0001	0.0051±0.0001	734±43
8	1074	2.047±0.002	0.201±0.001	0.0057±0.0002	neg. value	0.0048±0.0001	2560±106
9	1214	0.975±0.004	0.055±0.001	0.0026±0.0001	0.0054±0.0012	0.0014±0.0003	8386±1096
10	1445	0.927±0.001	0.014±0.001	0.0011±0.0001	0.0102±0.0011	0.0036±0.0001	neg. value
<i>VUT 9918-phl (70mg; K₂O = 8.29wt%, Cl = 265ppm; J = 0.001029)</i>							
1	488	2.558±0.003	0.063±0.004	0.009±0.002	neg. value	0.0076±0.0002	9016±1396
2	593	2.166±0.001	0.316±0.004	0.009±0.001	neg. value	0.0078±0.0002	neg. value
3	689	3.315±0.001	2.072±0.002	0.053±0.002	0.0061±0.0001	0.0084±0.0002	748±43
4*	766	10.593±0.001	4.887±0.004	0.127±0.003	neg. value	0.0297±0.0003	691±25
5*	841	14.531±0.002	5.627±0.005	0.146±0.004	0.0007±0.0001	0.0419±0.0002	704±19
6*	886	20.684±0.002	4.927±0.004	0.131±0.003	neg. value	0.0633±0.0003	744±28
7*	968	55.963±0.003	5.204±0.005	0.160±0.003	neg. value	0.1818±0.0007	796±68
8	1044	36.923±0.006	2.525±0.002	0.085±0.002	neg. value	0.1195±0.0005	1173±106
9	1190	13.524±0.003	0.740±0.007	0.028±0.001	0.0076±0.0001	0.0432±0.0003	1936±206
10	1424	5.043±0.001	0.092±0.001	0.005±0.001	neg. value	0.0162±0.0002	5414±1196
<i>VU 1907 A - lc (36.1mg; K₂O = 20wt%, Cl = 90ppm; J = 0.000468)</i>							
1	189	13.822±0.006	0.206±0.001	0.0133±0.0001	0.0038±0.0001	0.0456±0.0002	1175±236
2*	249	3.106±0.022	0.687±0.002	0.0131±0.0003	0.0057±0.0001	0.0097±0.0001	241±30
3*	300	2.292±0.002	1.138±0.002	0.0177±0.0001	0.0033±0.0001	0.0054±0.0001	428±12
4*	347	3.401±0.002	2.401±0.003	0.0364±0.0002	0.0037±0.0001	0.0073±0.0001	362±7
5*	427	4.890±0.002	4.709±0.004	0.0692±0.0001	0.0045±0.0001	0.0057±0.0001	479±6
6*	468	4.337±0.001	3.955±0.005	0.0592±0.0004	0.0035±0.0001	0.0045±0.0001	536±5
7	500	3.201±0.005	2.461±0.003	0.0389±0.0001	0.0032±0.0001	0.0035±0.0001	617±7
8	543	1.766±0.001	1.044±0.001	0.0167±0.0001	0.0019±0.0001	0.0033±0.0001	540±11
9*	585	1.488±0.002	0.685±0.001	0.0114±0.0001	0.0018±0.0001	0.0037±0.0001	395±39
10*	615	2.332±0.004	0.475±0.001	0.0094±0.0001	0.0019±0.0001	0.0072±0.0002	319±66
11*	645	0.771±0.002	0.135±0.001	0.0025±0.0001	0.0007±0.0001	0.1651±0.0006	neg. value
12	720	7.981±0.003	0.120±0.001	0.0101±0.0001	0.0046±0.0001	0.0268±0.0001	316±226
13	817	2.865±0.001	0.0125±0.001	0.0046±0.0001	0.0048±0.0001	0.0088±0.0001	15009±1696
<i>VUT 0002-san (102mg; K₂O = 10.36wt%, Cl = 38ppm; J = 0.001032)</i>							
1	532	5.519±0.001	9.943±0.009	0.143±0.003	0.371±0.044	0.0070±0.0002	645±7
2*	685	5.946±0.001	13.183±0.001	0.167±0.003	0.095±0.004	0.0031±0.0002	707±5
3*	822	4.648±0.002	10.038±0.001	0.126±0.004	0.067±0.006	0.0029±0.0002	699±6
4*	868	2.321±0.001	4.343±0.004	0.054±0.001	neg. value	0.0017±0.0002	770±17
5*	911	1.704±0.001	2.859±0.003	0.035±0.001	0.031±0.005	0.0018±0.0003	756±53
6	952	1.362±0.001	1.912±0.002	0.023±0.001	0.018±0.006	0.0015±0.0002	885±40
7	1054	1.500±0.001	1.990±0.002	0.025±0.002	neg. value	0.0030±0.0002	578±39
8	1127	1.574±0.002	1.866±0.002	0.026±0.002	0.024±0.003	0.0021±0.0002	941±49
9	1192	1.265±0.001	1.290±0.002	0.021±0.002	0.060±0.005	0.0028±0.0002	621±85
10	1268	0.795±0.001	0.629±0.001	0.017±0.001	0.090±0.006	0.0017±0.0002	843±166
11	1420	0.995±0.001	0.291±0.001	0.009±0.001	neg. value	0.0022±0.0002	2120±336

...continued

step	T[°C]	⁴⁰ Ar _{tot}	³⁹ Ar	³⁸ Ar	³⁷ Ar	³⁶ Ar	Age[ka]
<i>VU 1680 A - san (30.4mg; K₂O = 13.1 wt %, Cl = 710ppm; J = 0.000468; values are given in nl; errors are 1σ)</i>							
1	543	0.905±0.002	0.168±0.003	0.0148±0.0015	0.0078±0.0003	0.0027±0.0002	604±260
2	650	2.507±0.001	1.027±0.001	0.0250±0.0001	0.0273±0.0002	0.0047±0.0002	910±37
3*	709	1.969±0.001	1.385±0.001	0.0216±0.0001	0.0246±0.0002	0.0027±0.0002	717±30
4	760	1.642±0.001	1.170±0.002	0.0168±0.0001	0.0228±0.0002	0.0019±0.0001	780±27
5	817	2.628±0.001	1.738±0.002	0.0289±0.0002	0.0352±0.0003	0.0034±0.0002	789±25
6	868	1.019±0.001	0.482±0.001	0.0101±0.0002	0.0112±0.0004	0.0023±0.0001	605±100
7	931	1.329±0.001	0.637±0.001	0.0147±0.0002	0.0156±0.0003	0.0023±0.0001	842±77
8	1122	2.347±0.001	1.192±0.002	0.1635±0.0003	0.1262±0.0005	0.0049±0.0002	633±40
9	1330	1.972±0.001	0.474±0.001	0.0382±0.0001	0.1310±0.0005	0.0047±0.0002	1058±100
10	1427	1.160±0.001	0.030±0.001	0.0063±0.0001	0.0312±0.0002	0.0033±0.0002	5036±1600
<i>VU 1813 A - san (50.5mg; K₂O = 12.95wt%, Cl = 20.5ppm; J = 0.000468)</i>							
1	543	1.210±0.002	0.193±0.001	0.0033±0.0002	0.0027±0.0002	0.0319±0.0014	1174±176
2	647	2.208±0.001	0.708±0.001	0.0098±0.0002	0.0073±0.0001	0.0616±0.0011	459±36
3*	705	1.928±0.001	1.181±0.002	0.0142±0.0002	0.0126±0.0003	0.0242±0.0017	863±33
4*	769	3.582±0.001	2.170±0.002	0.0285±0.0002	0.0264±0.0003	0.0525±0.0018	787±16
5*	819	1.386±0.001	0.757±0.001	0.0085±0.0002	0.0084±0.0003	0.0204±0.0014	871±43
6*	866	1.711±0.001	0.940±0.001	0.0099±0.0002	0.0103±0.0003	0.0262±0.0015	839±37
7	932	1.993±0.001	1.317±0.001	0.0176±0.0002	0.0144±0.0002	0.0317±0.0019	674±31
8*	1120	4.894±0.002	3.933±0.004	0.0496±0.0002	0.0492±0.0003	0.0397±0.0024	795±11
9*	1332	3.488±0.001	2.225±0.002	0.0281±0.0002	0.0265±0.0001	0.0455±0.0014	810±12
10	1431	1.719±0.001	0.247±0.005	0.0030±0.0001	0.0049±0.0003	0.0510±0.0015	718±146
<i>VUT 9905-san (110mg; K₂O = 9.96wt%, Cl = 40ppm; J = 0.001031)</i>							
1*	530	1.780±0.001	1.374±0.001	0.042±0.002	0.001±0.001	0.0035±0.0002	983±58
2*	630	2.420±0.001	3.393±0.003	0.045±0.002	0.075±0.006	0.0032±0.0001	777±17
3*	690	2.984±0.001	5.944±0.005	0.075±0.002	0.066±0.007	0.0015±0.0001	772±8
4*	730	2.621±0.001	5.282±0.005	0.066±0.002	0.031±0.009	0.0014±0.0002	748±12
5*	770	3.508±0.001	7.053±0.006	0.087±0.002	0.074±0.005	0.0017±0.0002	767±11
6*	820	3.460±0.001	6.717±0.006	0.083±0.002	0.080±0.005	0.0024±0.0002	738±10
7*	870	1.682±0.001	2.823±0.003	0.034±0.002	0.004±0.002	0.0009±0.0002	905±25
8*	930	3.262±0.003	5.564±0.005	0.069±0.003	0.036±0.005	0.0028±0.0001	790±9
9*	1050	2.699±0.001	4.482±0.004	0.055±0.002	0.024±0.005	0.0026±0.0001	778±12
10*	1190	3.874±0.001	6.039±0.005	0.076±0.002	0.061±0.011	0.0035±0.0002	850±11
<i>PG5-phl (96.4mg; K₂O = 8.3wt%, Cl = 219ppm; J = 0.001030)</i>							
1	480	3.080±0.002	0.031±0.001	0.003±0.001	0.041±0.012	0.010±0.001	7632±1996
2	560	2.042±0.001	0.101±0.002	0.005±0.001	neg.value	0.006±0.001	5205±706
3	627	1.513±0.012	0.284±0.003	0.009±0.001	neg.value	0.004±0.001	2209±266
4*	690	1.660±0.001	0.760±0.007	0.018±0.002	neg.value	0.005±0.002	696±126
5*	770	11.295±0.010	4.660±0.004	0.111±0.003	0.006±0.002	0.032±0.001	675±22
6*	840	11.723±0.010	7.212±0.006	0.168±0.003	neg.value	0.030±0.001	725±11
7*	884	8.896±0.001	6.000±0.005	0.138±0.003	neg.value	0.022±0.001	755±16
8*	969	16.956±0.002	8.852±0.008	0.206±0.005	neg.value	0.045±0.001	747±14
9*	1051	9.188±0.002	6.593±0.006	0.150±0.003	0.005±0.001	0.022±0.001	765±9
10	1187	4.308±0.001	1.903±0.002	0.045±0.002	neg.value	0.011±0.001	971±38
11	1414	6.574±0.002	0.258±0.003	0.010±0.001	neg.value	0.021±0.001	1818±376

...continued

step	T[°C]	⁴⁰ Ar _{tot}	³⁹ Ar	³⁸ Ar	³⁷ Ar	³⁶ Ar	Age[ka]
<i>PG5-san (112.7mg; K₂O = 10.76wt%, Cl = 32ppm; J = 0.001030; values are given in nl; errors are 1σ)</i>							
1	527	0.757±0.004	0.157±0.003	0.007±0.001	neg. value	0.0016±0.0002	3269±356
2	624	0.708±0.009	0.377±0.010	0.006±0.001	neg. value	0.0028±0.0002	660±316
3	685	0.641±0.010	0.641±0.008	0.008±0.001	neg. value	0.0014±0.0002	630±166
4	738	0.771±0.004	1.041±0.001	0.013±0.001	neg. value	0.0010±0.0002	861±106
5	798	0.914±0.005	1.243±0.001	0.016±0.002	0.015±0.007	0.0006±0.0002	1080±90
6	838	9.019±0.005	20.294±0.002	0.255±0.005	0.208±0.005	0.0054±0.0001	676±4
7*	905	4.697±0.010	10.568±0.009	0.131±0.003	0.063±0.008	0.0016±0.0002	738±8
8*	1101	5.467±0.012	10.737±0.001	0.151±0.003	0.184±0.009	0.0043±0.0002	723±6
9*	1309	4.015±0.011	7.449±0.006	0.099±0.001	0.030±0.010	0.0034±0.0002	750±9
10	1411	1.666±0.003	2.844±0.003	0.036±0.002	0.020±0.007	0.0020±0.0002	695±28
<i>VU 1809 - san (380mg; K₂O = 13.6wt%; J = 0.0001175)</i>							
1	650	2.243±0.078	0.272±0.001			0.0684±0.0003	1718±59
2	750	1.953±0.088	0.518±0.001			0.0595±0.0003	800±30
3	800	1.700±0.034	0.646±0.001			0.0500±0.0002	724±16
4*	850	3.360±0.091	1.576±0.003			0.0942±0.0004	770±12
5*	900	2.017±0.075	1.085±0.003			0.0549±0.0002	768±10
6*	950	1.776±0.059	1.171±0.002			0.0467±0.0002	715±7
7*	1000	2.657±0.140	1.486±0.003			0.0721±0.0003	749±8
8*	1100	2.609±0.026	1.876±0.002			0.0664±0.0003	727±6
9*	1200	2.689±0.042	1.447±0.002			0.0665±0.0003	733±8
10	1300	2.773±0.031	1.027±0.001			0.0796±0.0003	864±16
11	1450	4.523±0.100	0.453±0.001			0.1451±0.0006	1091±82
12	1600	11.202±0.160	0.374±0.002			0.3613±0.0014	2972±226
<i>VU 110 A -san (16.9mg; K₂O = 8.86wt%, Cl = 161ppm; J = 0.0010325)</i>							
1	525	1.302±0.060	0.232±0.003	0.013±0.003	0.0072±0.0017	0.0040±0.0001	1028±326
2*	622	0.894±0.001	0.697±0.001	0.016±0.001	0.0009±0.0001	0.0020±0.0001	845±96
3*	685	1.439±0.001	2.277±0.002	0.037±0.001	0.0365±0.0003	0.0017±0.0001	756±26
4*	748	0.680±0.001	0.844±0.001	0.013±0.001	neg. value	0.0009±0.0001	882±79
5*	798	0.427±0.001	0.379±0.001	0.007±0.001	0.1214±0.0004	0.0006±0.0001	1210±176
6*	896	0.665±0.001	0.335±0.001	0.007±0.001	neg. value	0.0015±0.0001	1230±206
7*	1060	1.398±0.001	1.193±0.001	0.019±0.001	0.0079±0.0002	0.0029±0.0001	853±55
8*	1198	0.994±0.001	0.639±0.001	0.009±0.001	neg. value	0.0022±0.0001	1032±106
9	1424	0.510±0.001	0.254±0.001	0.003±0.001	neg. value	0.0009±0.0001	1665±266
<i>VU 110L - san (K₂O = 17.5wt.%; J = 0.00046)</i>							
1*	700	7.714±0.154	0.487±0.007			0.248±0.005	696±40
2*	800	1.843±0.037	0.688±0.010			0.044±0.001	657±8
3*	900	1.564±0.031	1.312±0.020			0.016±0.001	684±3
4*	1000	1.163±0.023	0.739±0.011			0.019±0.001	667±5
5	1100	0.729±0.015	0.160±0.002			0.022±0.001	451±21
6	1200	0.002±0.001	0.048±0.001			0.022±0.001	neg. value
7	1700	7.313±0.146	0.127±0.002			0.243±0.005	846±166

...continued

step	T[°C]	⁴⁰ Ar _{tot}	³⁹ Ar	³⁸ Ar	³⁷ Ar	³⁶ Ar	Age[ka]
VUG 1 - san (28.9mg; K ₂ O = 9.2wt.%, Cl = 29ppm; J = 0.000468; values are given in nl; errors are 1_)							
1	549	203.131±1.8	16.442±0.019	1.381±0.011	0.479±0.003	0.065±0.001	578±100
2	651	191.980±0.044	80.983±0.079	2.287±0.010	0.699±0.003	0.045±0.001	617±24
3*	711	99.077±0.012	57.145±0.068	1.0886±0.940	0.203±0.002	0.018±0.001	699±30
4*	765	63.961±0.022	34.726±0.035	0.664±0.009	0.114±0.003	0.012±0.001	697±46
5	813	109.262±0.054	48.722±0.046	1.169±0.008	0.181±0.002	0.028±0.001	481±33
6	865	49.179±0.011	11.630±0.016	0.037±0.001	0.046±0.002	0.013±0.001	701±23
7	910	80.742±0.034	18.428±0.017	0.061±0.001	0.063±0.002	0.022±0.001	661±17
8	930	36.759±0.024	5.651±0.009	0.020±0.001	0.020±0.001	0.011±0.001	533±45
9	956	22.964±0.034	2.631±0.003	0.001±0.001	0.011±0.001	0.007±0.001	491±97
10	978	29.021±0.026	4.026±0.006	0.013±0.001	0.017±0.001	0.009±0.001	553±63
11	1009	115.765±0.038	13.207±0.019	0.042±0.001	0.055±0.002	0.036±0.001	617±30
12	1048	71.450±0.027	6.307±0.006	0.016±0.001	0.026±0.001	0.023±0.001	594±55
13	1116	124.562±0.005	17.924±0.019	0.037±0.001	0.067±0.002	0.038±0.001	555±23
14	1484	113.650±0.034	26.170±0.025	0.048±0.001	0.084±0.003	0.031±0.001	710±14

Table A-3-4: Chronostratigraphy of Monte Vulture volcano. Each accepted age refers to one single sample (indicating the weighted average or the most reliable assignment where duplicate analyses were performed). Multiple ages for some subsynthem refer to stratigraphically distinct units (n.r. denotes unreliable ages). Recalculated ages from Brocchini et al. (1994) and Bonadonna et al. (1998).

Supersynthem	Synthem	Subsynthem	Accepted ages [ka]	
Vesuvius		Ripe del Cavallo upp.	16±6 23±5	
		Ripe del Cavallo low.	38±9	
Monticchio	Laghi di Monticchio	Serra di Braida	n.r.	
		Lago Piccolo	141±11	
		Lago Grande		
		Piano Comune		
		Casa Rossa	n.r.	
	Valle dei Greggi-Fosso del Corbo	Meseria di Cuscito		
		Imbandina		
		Case Lopes	530±22	
Monte Vulture	Melfi	Piano di Croce		
		Castello di Melfi	573±4	
		Piano di Gaudio		
	Barile	Ventaruolo		670±24 671±13
			Vulture San-Michele	590±12 n.r.
		Rionero		626±20 668±6 710±18 < 720±30
			Toppo San Paolo	
		Foggianello	Fara d'Olivo	
	Campanile			
	Spinoritola		694±8 678±9 698±25	

Table A-4-1: EDS results of selected samples (errors as 1SD). Cations are presented as wt %. Step numbers for protocol sL and the reference calcites are denoted in brackets. NaK was calculated by subtracting Na-concentrations of in the reference sample from the Na-concentration of the acetate-buffer. The results are presented as % of the whole soil weight.

sample	Al [wt %]	Ca [wt %]	Si [wt %]	Cl [wt %]	Fe [wt %]	Mg [wt %]	K [wt %]	Na _{tot} [wt%]	Na _k [wt%]
<i>protocol AO</i>									
NIS 4c	0.87±0.14	1.08±0.06		0.02±0.02			0.03±0.03	71.81±0.31	0.01
NIS4c LL	2.21±0.31	5.12±0.21	2.09±0.45		0.28±0.28		0.26±0.16	90.04±0.44	0.10
Nis 16 S2	0.39±0.33	4.82±0.20	4.71±0.47		0.63±0.40	0.80±0.57	0.75±0.16	87.90±0.54	0.28
AB04-2	1.81±0.31	8.80±0.27			0.65±0.45	4.65±0.59	2.47±0.19	81.62±0.50	0.93
AB04-1	1.09±0.31	5.39±0.45	0.18±0.18			1.06±0.58	3.22±0.20	89.06±0.48	1.22
VI 1A	1.15±0.28	7.78±0.45	0.46±0.21			0.04±0.04	0.45±0.04	88.66±0.28	0.17
VI 1C	0.63±0.08	4.04±0.07	1.04±0.12				0.48±0.05	67.03±0.27	0.18
VI 3	1.11±0.08	4.38±0.07		1.42±0.10			0.61±0.05	66.47±0.31	0.23
VI 5	1.06±0.08	3.67±0.07		0.15±0.05			1.22±0.05	67.69±0.31	0.46
<i>protocol sL</i>									
VI 1A - (1)	0.62±0.13	0.37±0.05	1.12±0.13	0.03±0.06		57.48±0.28	0.22±0.05	0.23±0.08	
VI 1A - (2)	1.03±0.17	0.05±0.05	0.70±0.17	0.26±0.08	0.30±0.18	7.23±0.56	0.08±0.07	62.11±0.42	0.03
VI 1A - (3)	13.46±0.17	0.18±0.09	4.37±0.12	11.71±0.23	7.41±0.23	10.04±0.35	1.54±0.09	17.92±0.22	
NIS 16 S2 (1)	0.54±0.14	0.33±0.06	0.91±0.14	0.61±0.07	0.11±0.11	57.11±0.30	0.07±0.06	0.74±0.10	
NIS 16 S2 (2)	0.25±0.13	0.09±0.06	0.18±0.08	0.93±0.07	0.10±0.10	11.32±0.45		58.72±0.36	0
NIS 16 S2 (3)	4.60±0.14	0.32±0.10	2.51±0.18	31.19±0.28	2.82±0.37	18.92±0.19	0.56±0.10	13.52±0.28	
VI 1C - (1)	0.25±0.12	0.41±0.05	1.09±0.12	0.08±0.05	0.02±0.02	57.60±0.28	0.28±0.05	0.48±0.08	
VI 1C - (2)	0.42±0.14		0.18±0.08	4.00±0.09		6.55±0.47	0.12±0.06	62.19±0.37	0.05
VI 1C - (3)	14.58±0.34	0.19±0.08	1.52±0.12	8.90±0.21	5.22±0.20	14.08±0.35	0.97±0.09	20.82±0.21	
<i>reference sample</i>									
VI 5*	29.12±0.16	7.74±0.08	0.38±0.06	0.15±0.04	12.93±0.25	2.93±0.09	5.74±0.12	2.17±0.14	
<i>reference calcites</i>									
calc 1 - (1)	2.60±0.67	0.30±0.28	5.45±0.76		0.34±0.34	91.30±0.49			
calc 1 - (2)	1.43±0.28	8.45±0.24	0.39±0.22				0.23±0.17	89.44±0.45	0.09
calc 2 - (2)	1.96±0.53	0.44±0.34	0.55±0.41		1.24±0.77		0.10±0.10	95.71±0.63	0.04

...continued

sample	Al [%]	Ca [%]	Si [%]	Cl [%]	Fe [%]	Mg [%]	K [%]	NaK [%]
<i>protocol AO</i>								
NIS 4c	0.46	0.57	0	0.01	0	0	0.01	0
NIS4c LL	1.07	2.49	1.02	0	0.14	0	0.13	0.05
Nis 16 S2	0.15	1.82	1.78	0	0.24	0.30	0.28	0.11
AB04-2	0.68	3.31	0	0	0.24	1.75	0.93	0.35
AB04-1	0.40	1.99	0.07	0	0	0.39	1.19	0.45
VI 1A	0.45	3.04	0.18	0	0	0	0.18	0.07
VI 1C	0.24	1.56	0.40	0	0	0	0.19	0.07
VI 3	0.53	2.08	0	0.67	0	0	0.29	0.11
VI 5	0.65	2.24	0	0.09	0	0	0.75	0.28
<i>protocol sL</i>								
VI 1A - (1)								
VI 1A - (2)	0.57	0.03	0.39	0.15	0.17	4.04	0	0
VI 1A - (3)								
NIS16S2 (1)								
NIS16S2 (2)	0.11	0.04	0.08	0.41	0	5.02	0	0
NIS16S2 (3)								
VI 1C - (1)								
VI 1C - (2)	0.19	0	0.08	1.77	0	2.89	0	0
VI 1C - (3)								
<i>reference sample</i>								
VI 5*								
<i>reference calcites</i>								
calc 1 - (1)								
calc 1 - (2)	4.88	28.84	1.33	0	0	0	0.79	0.30
calc 2 - (2)	1.86	0.42	0.52	0	1.18	0	0.09	0

Table A-4-2: ^{39}Ar - ^{40}Ar results of mineral separates. All isotopes are in nL.

step	T[°C]	$^{40}\text{Ar}_{\text{tot}}$	^{39}Ar	^{38}Ar	^{37}Ar	^{36}Ar	Age[ka]
<i>VI 4 sanidine (m = 25.3 mg, J = 0.000479, K₂O = 13.5 wt %, Cl = 3.4 ppm)</i>							
1	549	68.505±0.020	12.127±0.018	0.241±0.001	0.752±0.005	0.239±0.001	145±19
2	586	42.114±0.048	15.127±0.014	0.244±0.001	0.526±0.004	0.140±0.001	45±10
3	644	25.302±0.007	26.442±0.030	0.367±0.001	0.598±0.005	0.072±0.001	129±3
4	711	36.612±0.034	59.763±0.060	0.787±0.002	1.091±0.005	0.093±0.001	133±2
5	769	22.592±0.019	35.221±0.037	0.466±0.001	0.678±0.004	0.054±0.001	166±2
6	820	26.674±0.022	42.651±0.038	0.557±0.001	0.807±0.006	0.064±0.001	160±2
7	868	22.868±0.014	35.297±0.045	0.463±0.002	0.682±0.006	0.056±0.001	157±3
8	912	30.153±0.005	46.082±0.058	0.598±0.001	0.806±0.006	0.079±0.001	131±2
9	931	15.260±0.059	17.134±0.028	0.226±0.001	0.431±0.003	0.042±0.001	146±3
10	953	14.188±0.058	12.435±0.020	0.169±0.001	0.322±0.004	0.044±0.001	93±6
11	975	17.929±0.033	9.617±0.013	0.135±0.001	0.245±0.003	0.056±0.001	130±8
12	1041	19.740±0.006	11.817±0.028	0.161±0.001	0.321±0.003	0.060±0.001	141±7
13	1070	23.356±0.056	24.263±0.045	0.325±0.001	0.511±0.005	0.064±0.001	157±3
14	1122	20.467±0.051	14.659±0.019	0.204±0.001	0.404±0.004	0.063±0.001	107±5
15	1443	29.745±0.065	14.502±0.026	0.219±0.001	0.509±0.010	0.096±0.001	81±8
<i>VI 1P sanidine (m = 34.6 mg, J = 0.000477, K₂O = 14.23 wt %, Cl = 2.89 ppm)</i>							
1	552	76.078±0.029	15.838±0.017	0.271±0.001	0.764±0.005	0.247±0.001	174±15
2	586	36.050±0.023	17.099±0.027	0.256±0.001	0.789±0.004	0.114±0.001	126±6
3	651	30.580±0.011	23.163±0.027	0.314±0.001	0.942±0.004	0.090±0.001	151±4
4	714	37.362±0.023	45.583±0.061	0.602±0.001	1.548±0.011	0.099±0.001	156±2
5	768	25.833±0.015	44.433±0.048	0.578±0.001	1.317±0.007	0.062±0.001	145±2
6	817	22.613±0.006	49.940±0.049	0.640±0.002	1.399±0.007	0.051±0.001	131±2
7	864	33.544±0.012	89.133±0.084	1.135±0.002	1.989±0.008	0.060±0.001	155±1
8	908	29.776±0.027	79.646±0.075	1.011±0.002	1.769±0.013	0.055±0.001	146±1
9	931	23.527±0.032	45.093±0.044	0.583±0.001	1.028±0.007	0.057±0.001	129±2
10	950	24.547±0.064	33.325±0.039	0.452±0.001	0.846±0.007	0.067±0.001	123±3
11	979	29.721±0.035	18.577±0.028	0.253±0.001	0.435±0.003	0.090±0.001	141±5
12	1013	20.426±0.024	32.829±0.059	0.427±0.001	0.787±0.005	0.048±0.001	161±2
13	1052	16.266±0.021	19.327±0.030	0.256±0.001	0.548±0.004	0.047±0.001	113±3
14	1122	18.945±0.023	24.247±0.048	0.322±0.001	0.618±0.004	0.051±0.001	136±4
15	1429	65.485±0.020	14.056±0.017	0.236±0.001	0.860±0.005	0.225±0.001	62±15
<i>VI 11 tephra sanidine (m = 41.4 mg, J = 0.000485, K₂O = 11.6 wt %, Cl = 2.66 ppm)</i>							
1	552	370.185±0.250	6.438±0.026	0.310±0.001	n.d.	1.165±0.005	3519±190
2	605	62.659±0.017	15.924±0.015	0.239±0.001	n.d.	0.202±0.001	165±13
3	667	134.694±0.043	18.222±0.018	0.321±0.001	n.d.	0.455±0.002	12±24
4	727	22.976±0.025	24.356±0.036	0.331±0.001	n.d.	0.064±0.001	147±3
5	780	169.088±0.170	52.735±0.054	0.779±0.001	n.d.	0.555±0.002	85±10
6	828	19.860±0.067	17.864±0.019	0.238±0.001	n.d.	0.055±0.001	183±5
7	875	16.614±0.032	24.416±0.025	0.317±0.001	n.d.	0.039±0.001	182±3
8	920	15.9186±0.085	35.382±0.038	0.462±0.001	n.d.	0.035±0.001	136±3
9	962	21.605±0.099	31.838±0.034	0.404±0.001	n.d.	0.057±0.001	127±4
10	1001	26.217±0.054	28.335±0.032	0.371±0.001	n.d.	0.073±0.001	145±3
11	1037	22.742±0.062	23.958±0.024	0.319±0.001	n.d.	0.068±0.001	100±3
12	1125	27.970±0.071	26.407±0.035	0.348±0.001	n.d.	0.083±0.001	116±4
13	1446	101.139±0.034	19.963±0.019	0.316±0.001	n.d.	0.332±0.001	137±16

...continued

	T[°C]	$^{40}\text{Ar}_{\text{tot}}$	^{39}Ar	^{38}Ar	^{37}Ar	^{36}Ar	Age[ka]
<i>VI IE sanidine (m = 35 mg, J = 0.000482, K₂O = 16.6 wt %)</i>							
1	717	368.946±0.073	265.104±0.260	3.831±0.008	12.882±0.045	0.914±0.003	317±3
2	744	72.004±0.650	103.720±0.100	1.346±0.004	2.989±0.011	0.169±0.003	183±7
3	796	28.199±0.019	31.575±0.037	0.419±0.001	1.116±0.006	0.075±0.001	163±3
4	844	29.013±0.040	37.425±0.035	0.503±0.001	1.277±0.010	0.073±0.001	172±2
5	891	20.752±0.007	29.756±0.042	0.392±0.001	0.922±0.005	0.049±0.001	178±2
6	933	48.446±0.029	40.130±0.047	0.539±0.001	1.222±0.005	0.136±0.001	178±4
7	954	24.716±0.031	20.628±0.022	0.276±0.001	0.737±0.005	0.069±0.001	182±4
8	988	27.115±0.018	6.025±0.009	0.093±0.001	0.258±0.002	0.089±0.001	126±14
9	1018	21.778±0.027	25.669±0.026	0.343±0.001	0.805±0.005	0.055±0.001	180±3
10	1053	23.420±0.020	21.694±0.027	0.295±0.001	0.764±0.008	0.062±0.001	205±4
11	1121	61.293±0.084	57.185±0.061	0.773±0.002	1.678±0.012	0.166±0.001	183±3
12	1448	237.953±0.130	18.688±0.022	0.395±0.001	1.513±0.007	0.818±0.003	167±45

Table A-4-3: U-Th results. Isotope ratios are expressed as activity ratios. * Ages calculated using Isoplot version 2.49n (Ludwig 2002).

sample	step	^{238}U [%]	^{232}Th [%]	$^{230}\text{Th}/^{238}\text{U}$	$^{234}\text{U}/^{238}\text{U}$	$^{238}\text{U}/^{232}\text{Th}$	age [ka]*	$(^{234}\text{U}/^{238}\text{U})_i$
<i>Vico</i>								
VI 3	1	8.21	0.23	0.007±0.001	1.030±0.001	245.259±1.497	0.72±0.02	1.030±0.001
VI 3	2	10.06	0.09	0.003±0.001	1.031±0.002	768.887±4.513	0.27±0.01	1.031±0.002
VI 3	3	38.54	4.87	0.034±0.001	1.029±0.001	53.343±0.720	3.60±0.06	1.029±0.001
VI 3	4	26.34	11.70	0.091±0.002	1.032±0.001	15.167±0.360	10.02±0.23	1.033±0.001
VI 3	5	16.85	83.11	1.285±0.019	1.118±0.001	1.366±0.020	n.d.	
VI 3 mobiles				0.045±0.001	1.030±0.001	33.187±1.772	4.884±0.072	1.032±0.001
VI 3 bulk				0.254±0.004	1.045±0.001	6.740±1.422	30.16±0.60	1.052±0.002
VI 5 carb	2	37.98	1.92	0.020±0.001	1.002±0.001	120.356±0.689	2.23±0.01	1.002±0.001
VI 5	5	62.02	98.08	0.420±0.008	0.990±0.001	3.841±0.069	60.10±1.50	0.988±0.001
VI 5 bulk				0.268±0.004	0.994±0.001	6.075±0.379	34.02±0.58	0.998±0.001
VI1A	1	0.17	0.40	0.899±0.014	0.999±0.018	0.714±0.005	250.00±27.00	0.999±0.037
VI1A	2	5.16	0.30	0.332±0.068	1.013±0.004	28.825±0.197	43.00±11.00	1.015±0.004
VI1A	3	22.08	6.64	0.124±0.001	0.996±0.001	5.653±0.047	14.46±0.13	0.996±0.001
VI1A	4	29.27	21.55	0.248±0.006	0.975±0.001	2.308±0.052	32.01±0.85	0.972±0.001
VI1A	5	43.32	71.11	1.097±0.010	1.041±0.001	1.035±0.009	n.d.	
VI1A mobiles				0.209±0.022	0.986±0.006	3.333±0.076	25.90±3.10	0.987±0.006
VI1A bulk				0.594±0.020	1.010±0.005	1.699±0.062	n.d.	
VI 1A	2	20.73	0.74	0.047±0.001	1.013±0.003	17.581±0.108	5.18±0.04	1.013±0.003
VI 1A	5	79.27	99.26	1.372±0.086	0.997±0.001	0.502±0.032	n.d.	
VI 1A bulk				1.097±0.043	1.001±0.003	0.629±0.070	95.60±5.10	1.018±0.006
VI1C	1	0.21	0.32	0.761±0.014	0.931±0.024	0.933±0.010	193.00±21.00	0.881±0.048
VI1C	2	4.38	0.24	0.026±0.001	1.024±0.010	26.217±0.201	2.81±0.05	1.024±0.010
VI1C	3	13.73	18.17	0.577±0.008	0.998±0.001	1.077±0.011	94.00±2.00	0.998±0.001
VI1C	4	23.55	11.23	0.218±0.003	0.988±0.001	2.990±0.034	27.10±0.36	0.987±0.001
VI1C	5	58.13	70.04	0.896±0.011	0.999±0.001	1.184±0.014	248.00±12.00	0.998±0.002
VI1C mobiles				0.318±0.006	0.995±0.009	1.993±0.064	41.90±1.10	0.995±0.010
VI1C bulk				0.654±0.007	0.997±0.007	1.426±0.054	115.20±2.80	1.002±0.010
<i>Monte Vulture</i>								
AB 04-1	1	0.19	0.33	0.611±0.014	1.094±0.039	0.772±0.008	87.00±6.00	1.121±0.048
AB 04-1	2	2.67	0.03	0.012±0.001	1.269±0.008	113.781±0.735	0.99±0.06	1.270±0.008
AB 04-1	3	19.84	38.81	0.515±0.005	0.887±0.001	0.687±0.006	97.00±1.50	0.852±0.001
AB 04-1	4	11.31	2.45	0.112±0.001	0.890±0.004	6.211±0.049	14.61±0.14	0.886±0.004
AB 04-1	5	65.99	58.37	1.080±0.011	1.080±0.001	1.520±0.013	399.00±39.00	1.247±0.027
AB 04-1 mobiles				0.342±0.005	0.919±0.013	1.099±0.200	50.90±1.40	0.908±0.015
AB 04-1 bulk				0.829±0.006	1.026±0.010	1.344±0.162	175.20±6.20	1.049±0.016

...continued

sample	step	^{238}U [%]	^{232}Th [%]	$^{230}\text{Th}/^{238}\text{U}$	$^{234}\text{U}/^{238}\text{U}$	$^{238}\text{U}/^{232}\text{Th}$	age [ka]*	$(^{234}\text{U}/^{238}\text{U})_i$
<i>Nisyros-Yali</i>								
Yali 2 S1	2	3.91	6.48	1.642±0.029	0.978±0.038	0.450±0.008	n.d.	
Yali 2 S1	5	96.09	93.52	0.977±0.023	0.976±0.003	0.766±0.007	n.d.	
Yali 2 S1 bulk				1.003±0.026	0.976±0.020	0.746±0.008	n.d.	
Yali 2 S2	2	3.69	4.07	1.157±0.029	0.986±0.056	0.767±0.019	n.d.	
Yali 2 S2	5	96.31	95.93	1.035±0.010	0.989±0.002	0.851±0.007	n.d.	
Yali 2 S2 bulk				0.606±0.020	0.989±0.029	0.847±0.013	102.60±7.90	0.991±0.039
NIS 16 S2	1	0.06	0.23	0.892±0.098	1.022±0.113	2.190±0.061	220.00±120.0	1.040±0.200
NIS 16 S2	2	0.40	0.10	0.603±0.152	1.016±0.012	35.745±0.289	98.00±40.00	1.021±0.016
NIS 16 S2	3	0.68	0.73	0.100±0.002	1.037±0.009	8.394±0.073	10.98±0.25	1.038±0.009
NIS 16 S2	4	0.80	4.67	0.386±0.003	0.967±0.005	1.540±0.011	55.56±0.73	0.962±0.006
NIS 16 S2	5	98.06	94.27	0.094±0.001	0.991±0.002	9.362±0.121	10.88±0.17	0.991±0.002
NIS 16 S2 mobiles				0.345±0.064	1.004±0.035	3.049±0.109	46.00±11.00	1.005±0.040
NIS 16 S2 bulk				0.099±0.051	0.991±0.028	9.000±0.111	11.40±6.20	0.997±0.029
NIS 16 S2	2	14.24	4.88	0.209±0.003	1.007±0.005	3.791±0.026	25.22±0.42	1.008±0.005
NIS 16 S2	5	85.76	95.12	0.672±0.008	0.978±0.002	1.171±0.011	127.20±2.90	0.969±0.003
NIS 16 S2 bulk				0.606±0.005	0.983±0.003	1.299±0.018	103.90±1.70	0.983±0.005
NIS 16 S1	2	11.00	0.94	0.073±0.001	0.953±0.012	14.623±0.121	8.63±0.18	0.952±0.013
NIS 16 S1	5	89.00	99.06	0.658±0.008	1.005±0.003	1.118±0.010	115.50±2.50	1.007±0.005
NIS 16 S1 bulk				0.594±0.004	0.999±0.008	1.244±0.066	97.30±1.80	1.004±0.010
NIS 17 S1	2	2.32	1.62	0.988±0.012	1.073±0.019	1.799±0.019	254.00±24.00	1.150±0.030
NIS 17 S1	5	97.68	98.38	0.804±0.006	0.995±0.002	1.248±0.009	179.90±3.70	0.992±0.003
NIS 17 S1 bulk				0.808±0.009	0.997±0.010	1.257±0.014	178.90±7.70	1.002±0.017
NIS 4c	2	10.50	2.88	0.535±0.007	1.108±0.016	4.318±0.056	71.00±2.00	1.132±0.019
NIS 4c	5	89.50	97.12	0.704±0.005	0.935±0.005	1.090±0.008	156.70±3.70	0.898±0.009
NIS 4c bulk				0.686±0.006	0.953±0.011	1.183±0.032	139.60±4.60	0.936±0.017

CURRICULUM VITAE

Name: Büttner
First Name: Annett
Date of Birth: 24/09/1970
Place of Birth: Jena, Germany
Marital Status: single
Nationality: German

Scholar Education:

1977 – 1987 Polytechnische Oberschule, Pörsneck (former GDR)
1987 – 1989 Erweiterte Oberschule, Pörsneck (former GDR)
Degree: Abitur

Working Experience:

1989 – 1992 Professional training
Profession: typesetter
1992 – 1995 employee at an advertising agency, Göttingen (Germany)

University Education:

1995 – 2000 study of Geology/Palaeontology at University of Göttingen, Germany
1997 Vordiplom-Degree
2000 Diploma-Degree
2000-2004 Dissertation at the University of Bern, Switzerland